Nakazaki, Eiji

BOTTOM SHEAR STRESS, WAVE HEIGHT AND WAVE SET-UP UNDER WAVE TRANSFORMATION

University of Hawaii

PH.D. 1985

BOTTOM SHEAR STRESS, WAVE HEIGHT AND WAVE SET-UP UNDER WAVE TRANSFORMATION

A DISSERTATION SUBMITTED TO THE GRADUATE DIVISION OF
THE UNIVERSITY OF HAWAII IN PARTIAL FULFILLMENT
OF THE REQUIREMENTS FOR THE DEGREE OF

DOCTOR OF PHILOSOPHY

IN OCEAN ENGINEERING

AUGUST 1985

BY

Eiji Nakazaki

Dissertation Committee:

Hans J. Krock, Chairman
Frans Gerritsen
Harold G. Loomis
Charles L. Bretschneider
Brent Gallagher

ACKNOWLEDGEMENTS

The author wishes to thank the members of his committee: Dr. Hans J. Krock for his guidance, support and his unselfish giving of his time and energy in ensuring the successful completion of this study; Dr. Frans Gerritsen for his initial suggestion of this research work and his valuable discussion sessions and guidance; Dr. Charles L. Bretschneider for not only his valuable assistance in this study but also his long-time support and encouragement during this author's graduate school years; Dr. Harold Loomis for his willing assistance in solving problems and for his concern and encouragement; and Dr. Brent Gallagher for his kind service as a committee member and for his assistance, even during the period of his leave of absence from school.

The author also wishes to thank the late Dr. Theodore Lee for his valuable assistance until the very last moment when he passed away in March 1985. Dr. Lee's dedication to scientific research and his efforts to ensure opportunities for student research are greatly appreciated.

The author would like to acknowledge Mr. Chien Chu Ma, visiting colleague from China to the Department of Ocean Engineering, and Mr. George Weber for their assistance in the laboratory work.

Thanks are extended to Tar-Zen, Dayananda and Mauro for their discussion sessions about this project and for their close friendship through the years.

Thanks are also extended to Edith, secretary of the Department of Ocean Engineering, Doreen, secretary of the J.K.K. Look Laboratory, and Henry, mechanical technician, for their valuable assistance to students.

The author is grateful to the National Science Foundation for the partial support of this study.

The author is also grateful to Professor Brebner at Queen's University in Canada for lending us a shear plate.

Finally, the author must thank his wife, Jolaine, who kept him going during the daily ups and downs of study and patiently shared the hardships with him.

ABSTRACT

This study is concerned with the influence of wave transformation and bed shear stress on wave height and wave set-up. The ultimate goal is the prediction of wave height and mean water level in the nearshore zone. In order to develop such a predictive model, relevant empirical relationships were determined based on data measured during a two-dimensional hydraulic model study with a scale of 1:12 representing the Ala Moana reef on the south shore of Oahu.

For predicting the wave height from deep water to inside the breaker zone, a new empirical relationship is obtained for the parameters, H/η_{rms}, and $P_a = H_a/L_a \coth^2(D/L_a)$. The relationship is based on data from this experiment and from Hansen and Svendsen (1979). The hydraulic model used in this study had a compound slope of roughly 0, 1:80, 1:32 and 1:20, while Hansen and Svendsen used a plane slope of 1:34.

The bed shear stress was determined by direct measurements of wave forces on the bed and of fluid velocities near the bed under breaking waves and other highly nonlinear waves. The resulting friction factors are compared with the existing friction factor curve by Jonsson (1964), which was established under sinusoidal wave conditions.

Under the assumption that the dominant factors for the dissipation of energy are bottom friction and the wave breaking phenomenon, the energy dissipation is determined based on linear wave theory for the friction loss and on bore similarity for the breaking loss. Correction factors to these theoretical dissipations are empirically obtained.

The effect of the mean shear stress on wave set-up is examined by comparing measured mean water levels with results calculated using the computational procedure developed in this study.

It is concluded that the new curve for wave height prediction is applicable in the entire nearshore region, even in the breaking zone, at least for slopes ranging from 0 to 1:34. The Jonsson's friction factor curve for rough turbulence, developed from linear waves, accurately predicts friction factors for highly nonlinear waves, provided that an appropriate particle amplitude at the bed is used. The mean shear stress, which is usually considered to be negligible, is important in the calculation of wave set-up.

TABLE OF CONTENTS

Page

Page

LIST OF TABLES

LIST OF FIGURES

Figure Page

Figure Page

LIST OF SYMBOLS

Symbols

a_δ Wave particle amplitude at the bed

$a_{\delta 1}$ Wave particle amplitude at the bed defined in linear wave theory

A Wave amplitude

$\bar{A}$ Mean wave amplitude over a distance increment

A_e Area of front or back edge of shear plate

A_p Area of shear plate

A_ε Dissipation coefficient in breaking waves

b Flume width

C Wave velocity

C_a Wave velocity defined in linear wave theory

C_b Breaking wave velocity

C_f Friction factor defined by instantaneous shear stress and particle velocity at the bed

C_{fm} Friction factor defined by Kajiura as twice the f_w

D Mean water depth

D_{90} Roughness diameter corresponding to 90% of the cumulative distribution

E Mean wave energy per unit area

E_1 Energy available in hydraulic jump per unit width

E_b Energy dissipation due to wave breaking

E_d Energy dissipation due to bed friction

Symbols

E_{dc} "Current" dissipation due to bed friction

E_{dl} Energy dissipation calculated using linear wave theory

E_{dmn} Minimum limit of energy dissipation due to bed shear stress

E_{dw} "Wave" dissipation due to bed friction

E_t Total energy dissipation

E_v Viscous dissipation on side walls

f Frequency

f_w Friction factor defined by maximum shear stress and particle velocity at the bed

F Mean energy flux

F_i Inertial force per unit length

F_I Inertial force

F_{IP} Force combined inertial force and pressure gradient force

F_P Pressure gradient force

F_r Froude number

F_{rl} Froude number defined by wave velocities

F_S Shear force

F_s Shear force per unit length

F_T Total wave force on the shear plate

g Gravitational acceleration

h Still water depth

h_1 Water depth before jump

h_2 Water depth after jump

Symbols

H	Wave height
H_a	Wave height defined by: $H_a = \sqrt{8}\,\eta_{rms}$
H_b	Breaking wave height
H_o	Deep water wave height
ΔH	Change in energy level
I	Imaginary part of frequency components
k	Wave number
k_a	Wave number defined in linear wave theory
K_s	Nikuradse roughness
ℓ	Shear plate length
L	Wave length
L_a	Wave length defined in linear wave theory
L_b	Breaking wave length
L_m	Model length
L_o	Deep water wave length
L_p	Prototype length
L_r	The ratio of model length to prototype length
m	Added mass
M	Mass
n	The ratio of wave group velocity to wave velocity
P	Total pressure
P_a	Wave nonlinearity parameter
P_n	Wave nonlinearity parameter
P_o	Wave nonlinearity parameter
P_c	Steady component of the total pressure

Symbols

P_w Unsteady component of the total pressure

P_1 Pressures acting on front edge of shear plate

P_2 Pressures acting on back edge of shear plate

q Discharge per unit width

R Real part of frequency components

RE Amplitude Reynolds number

s Bottom slope

S_p Slope parameter

S_{xx} Radiation stress in x-direction

S_* Modified slope parameter

t Time

t_1 Time spent by a wave over shear plate

t_2 Time lag between data of particle velocity at the bed and wave force data

T Wave period

T_r The ratio of model time to prototype time

u Horizontal wave particle velocity

u_δ Wave particle velocity at the bed

$u_{\delta m}$ Maximum particle velocity at the bed

U_{fm} Friction velocity

U Current velocity

$\overline{U}$ Depth averaged current velocity

U_r Ursell's parameter

V Total particle velocity

V_δ Total particle velocity at the bed

Symbols

$\dot{V}_\delta$ Time derivative of total particle velocity at the bed

V_r The ratio of model velocity to prototype velocity

w Vertical particle velocity

X_V Square of total particle velocity at the bed in the same direction of the velocity

Y_V Integrated value of X_V with respect to time

α Empirical constant ratio of mean water depth to water depth at the trough ($\alpha = 1.22$)

δ Boundary layer thickness

ε Eddy viscosity (Chapter 4)

ε Similarity parameter (Chapter 5)

ε_0 Similarity parameter in terms of deep water wave steepness

η Water surface elevation

$\bar{\eta}$ Difference of mean water depth from still water depth; i.e., wave set-up

η_c Water surface elevation at the crest

η_{rms} Root-mean-square surface elevation

η_t Water surface elevation at the trough

ν Kinematic viscosity

ν_r The ratio of model kinematic viscosity to prototype kinematic viscosity

ρ Water density

σ_t Surface tension

τ Shear stress

Symbols

$\bar{\tau}$ Mean shear stress

τ_b Shear stress at the bed

τ_{bm} Maximum shear stress at the bed

τ_m Maximum shear stress

$\tau_{\delta m}$ Maximum shear stress at the level, δ

CHAPTER 1
INTRODUCTION

1.1 Overview

Waves transform in the process of propagation from deep water through the breaking region to the shore. The primary transformations are in wave height, energy density, celerity, steepness, asymmetry, bed shear stress, breaking and energy dissipation. The consequent common phenomena are mass transport, reflection, refraction, defraction and wave set-up. It is common knowledge in the field of ocean engineering that linear wave theory no longer gives accurate values of nonlinear wave characteristics in this region. In order to obtain reasonably accurate values for these nonlinear wave characteristics, several nonlinear wave theories have been developed, such as Stoke's nonlinear wave theory, cnoidal wave theory, nonlinear long wave theory, Dean's stream function theory and Cokelet's wave theory. It is, however, still common in coastal engineering practice to use linear wave theory to estimate values of wave characteristics in the nearshore zone. The reasons for this practice are that it is difficult to use these nonlinear wave theories and that these theories are applicable only in limited water regions. None of these wave theories are applicable in the breaking region and predictions in this area presently depend on empirical rules.

1.2 Purpose

The purpose of this study is to conduct a hydraulic scale model investigation and establish empirical rules describing wave transformations for nearshore areas. Wave characteristics of primary concern are wave height, bed shear stress, wave breaking, energy dissipation and wave set-up.

1.3 Arrangement of Dissertation

This two-dimensional hydraulic model study was initially conducted as a portion of the National Science Foundation project entitled, "Effect of Wave Induced Resultant Bottom Shear Stress on Wave Set-up". A 1:12 scale hydraulic model of Ala Moana reef was constructed in the wave flume at the J.K.K. Look Laboratory of the University of Hawaii. Among the parameters measured were water surface elevations and mean water levels as indicated by hydrostatic pressure. A unique aspect of this experiment was the direct measurement of wave forces on the bed under highly nonlinear wave and breaking wave conditions as well as measurements of fluid velocity near the bed. All time series quantities were obtained using the zero up-crossing method and were defined as the mean values of the highest one-third. The details of experiments are shown in Chapter 2.

For wave height calculations an empirical curve was obtained as a function of a nonlinearity parameter. The

idea of the nonlinearity parameter was originally proposed by Goda (1983). This parameter combines wave steepness and Ursell's parameter using a hyperbolic cotangent function, so that the parameter can cover an entire region from deep water to shallow water. The applicability of this approach was examined using data from this experiment and from Hansen and Svendsen (1979). The parameter was applied to wave height and wave celerity. The results are shown in Chapter 3.

The data for bed wave forces were analyzed in the frequency domain along with the data of fluid velocities near the bed. This analysis was aimed at obtaining friction factors under highly nonlinear waves by implicitly including a phase difference between bed shear stress and fluid velocity near the bed. The resulting friction factor was used to determine energy loss due to bed shear stress for nonlinear waves. The analysis and results are shown in Chapter 4.

Chapter 5 is concerned with breaking waves. Wave breaking is an important phenomenon when dealing with waves in shallow water. In the experiments, the location of breaking and the end points of broken waves were observed. In some cases, however, it is difficult to determine the breaking points; especially in case of a plunging breaker. For this reason, a general breaking criterion was obtained based on data from other sources. The energy dissipation

from wave breaking was obtained based on the assumption of similarity to a bore. The correction factor to the dissipation from a bore was determined in a way that used all available experimental information including energy dissipation by bottom friction, wave breaking points, wave height and wave set-up. The energy levels were calculated using numerical integration, as discussed in Chapter 7. Using an iterative process, the correction factor was determined from the best fit to the experimental energy levels. These energy levels were determined from variance of the water surface elevation.

In Chapter 6 wave set-up is discussed. Radiation stress was obtained from linear wave theory, as defined by Longuet-Higgins and Stewart (1964). Radiation stress values calculated using linear wave theory were compared with values based on measurements by Stive (1982) in the wave breaking zone. In the wave set-up calculation, the mean shear stress was usually considered to be negligible in the momentum balance equation. This assumption was examined using experimental values of mean shear stress and mean water levels.

In Chapter 7 a computational procedure for two-dimensional cases is developed based on the energy flux equation and the momentum balance equation. In this procedure all experimental relationships obtained in this study are applied. The primary predicted values are wave

energy level, wave height and mean water level in the area from deep water to inside the wave breaking zone.

CHAPTER 2

EXPERIMENTS

2.1 Introduction

A 1:12 scale hydraulic model investigation of Ala Moana reef was conducted in the flume at the J.K.K. Look Laboratory of the Department of Ocean Engineering. There were four objectives in this investigation:

(a) discription of wave height deformation in the propagation process.

(b) determination of friction factor under nonlinear waves.

(c) calculation of energy dissipation from bed shear stress and from breaking waves.

(d) determination of wave set-up on the reef.

For these purposes the following measurements were made:

(a) water surface elevation at six stations.

(b) wave forces on the bed and fluid velocities near the bed at two stations.

(c) mean water levels at thirteen stations.

Figure 2.1 shows the experimental set-up. All data were electronically stored on floppy disks except mean water levels, which were manually recorded. For the electronically recorded data the sampling interval was 0.1 seconds and 4923 data points were recorded for each test.

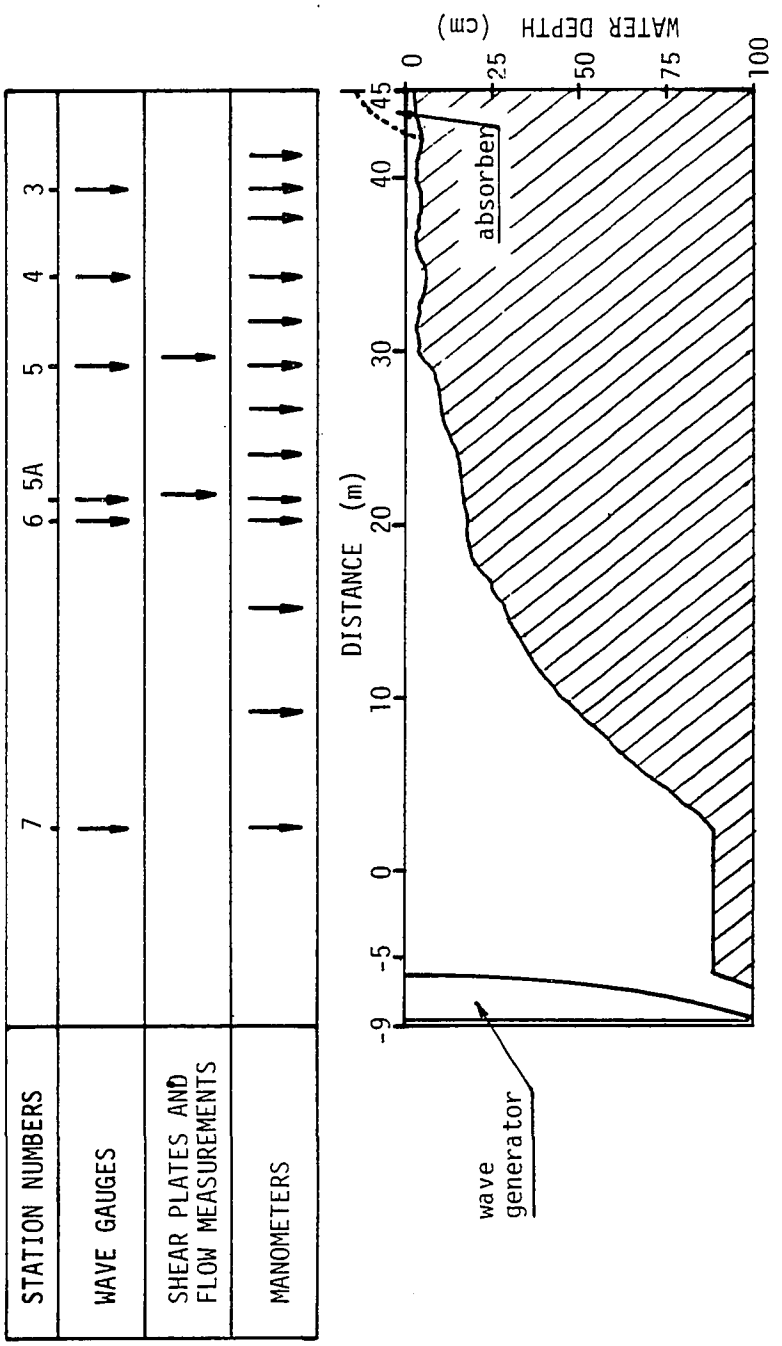

Figure 2.1 Experimental set-up.

2.2 Facilities and Equipment

2.2.1 Flume

The flume is 54 m long and 1.22 m wide. For the 1:12 scale hydraulic model the maximum water depth in the flume is 89 cm at the deep horizontal portion of the bottom profile, and the minimum is 3 cm on the reef at the mean lower low water level (MLLW). A wave absorber was placed at the shoreward end of the flume. This absorber consists of PVC shavings with a wire mesh cover. The flume is covered in order to avoid wind influence on generated waves. A parabolic plunger wave generator, which produces monochromatic waves, is located at the seaward end of the model flume. See Figure 2.1.

2.2.2 Water level measurements in waves

Water surface elevations were measured with capacitance probes of 3.5 mm diameter. In the begining stage of experiments floater wave gauges were also used in the shallow water area. It was, however, realized that the use of these floater gauges were limited to the small waves, and they were not used in the later experiments.

2.2.3 Shear Plates

Two shear plates were used to directly measure the wave force at the bed. One of the shear plates was 25.1 cm wide and 39.4 cm long. The other was 29.9 cm wide and 30.5 cm

long. These shear plates as well as the rest of the model bottom were covered with two types of surfaces, a smooth surface and a rough surface. The smooth surface in the model bottom consisted of a concrete surface. It was estimated that this surface roughness corresponded to the roughness obtained by a surface covered by sand with a diameter between 0.71 mm to 0.83 mm. To obtain this surface on the shear plates varnish was thinly applied on a vinyl adhesive paper, and appropriately sized sand was sprinkled onto the varnish until the surface was completely covered. After the varnish was dry, any excess sand was removed.

For the rough surface, sieved gravel was selected with sizes between 1.3 cm and 2.5 cm and glued to the concrete model bottom. In order to make the gravel surface on the shear plates neutrally buoyant, the gravel was mixed with lighter fiber-glass elements of similar shape and size and attached to the shear plates using vinyl adhesive paper and marine plastic resin glue.

2.2.4 Flow Measurements

A miniature propeller flowmeter, model WSM-01 manufactured by the Delft Hydraulic Laboratory, was used to measure fluid velocities above the shear plates. The propeller is 15 mm in diameter with 4 blades. A ring on the propeller with 60 holes generates 60 pulses per revolution, so that fast fluctuations can be detected. The center of

the propeller was placed 1.5 cm above the bed in the case of the concrete bed and 3 cm above the concrete datum for the gravel surface, so that measured velocities approximately represent fluid velocities just above the boundary layer.

2.2.5 Mean Water Levels

Gerritsen (1981) reported that mean water levels obtained by averaging the water levels measured with capacitance probes were inaccurate due to water run-up and depression around the probes. Based on Gerritsen's report mean water levels in this study were obtained by measuring the hydrostatic pressure using manometers. The manometer design involved a 1.5 foot long tygon level indicator tube with a 0.5 inch inner diameter with a reading scale inside. The indicator section was connected to a flexible tube of 0.5 inch in diameter which extended below the water level of the flume. The water end of the flexible tube was equipped with a sand filter. This filter 3/8 inch inner diameter tube filled with thickness of the sand was determined to be 2.5 cm. The grain size ranged from 0.71 mm to 0.83 mm.

2.3 Procedure

Test-runs were carried out for four incident wave heights ranging from 2.5 cm to 15 cm. For each wave height, 3 or 4 wave periods ranging from 1 to 4 seconds were tested. These various wave conditions were repeated for 3 different

still water levels. These were 3 cm, 6 cm and 9 cm above MLLW. The overall experiment was conducted for 2 types of bed roughness. One roughness was a concrete surface and the other was a surface covered with gravel. The total number of runs tested was 87.

2.4 Modeling and Scale Effects

If the model and the prototype are perfectly similar geometrically, kinematically and dynamically, the model results can exactly predict the prototype properties. In geometrically similar models, kinematic similarity is assured when there is dynamic similarity (Hudson and Keulegan, 1979). However, in practice perfect dynamic similarity between the model and the prototype practically cannot be achieved since several forces cannot be scaled. These forces are the gravitational force, the fluid frictional resistance of adjoining particles and the surface tension.

The Froude number is defined as the ratio of the inertial force to the gravitational force and it is given by $F_r = V/(gL)^{1/2}$, where L is a characteristic length. The length scale is defined as the ratio of the model length to prototype length by $L_r = L_m/L_p$. Subsequently, the velocity ratio and time ratio in the Froude number model are $V_r = L_r^{1/2}$ and $T_r = L_r^{1/2}$, respectively. The ratio of pressure is L_r since the ratio of g is unity. The ratio of shear stress

is also L_r similar to the pressure. The ratio of force is shear stress times area; i.e., L_r^3. The Reynolds number is the ratio of the inertial force to the viscous force and it is given by LV/ν, where ν is the kinematic viscosity. When the surface tension is important the Weber number is considered which is the ratio of the inertial force to the surface tention. It is given by $V/(\sigma_t/\rho L)^{1/2}$, where σ_t is the surface tension. For an air-water interface σ_t is 74 dynes/cm at $20^{\circ}C$.

Froude number and Reynolds number similitude is possible only if the viscosity of the model fluid is scaled according to the relationship of $\nu_r = L_r^{3/2}$. In reality the same fluid water is used in the model and in the prototype, and hence the model Reynolds number is $L_r^{3/2}$ times the prototype Reynolds number.

In general practice the dominant forces in the phenomenon to be studied is determined and the model is scaled according to the dominant force similitude. For example, hydraulic models are usually scaled according to the Froude number similitude considering the inertial and gravitational forces as dominant while the viscous force and the surface tension are neglected. When these secondary forces are not negligible such as in the case of bottom friction with a low Reynolds number, the model results show some disagreement with the prototype behavior. These discrepancies are called scale effects. In cases of fully

turbulent flows the shear stress is proportional to the square of the velocity; i.e., the dominant force is similar to the inertial force. The ratio of the shear force in fully turbulent flows to the gravitational force is also the Froude number. In breaking waves flows are also very turbulent and the dissipation of energy is mostly due to turbulent fluctuations. Le Méhauté (1976) suggested based on rather experience that the scale effect is negligible in breaking waves where the breaker heights are greater than 5 cm. In these cases it is reasonable to neglect the viscous effect. However, in a small-scale model fully turbulent flow frequently cannot be produced. In this data analysis it was found that all flows over the concrete bed formed boundary layers of transition from the smooth turbulent flow to the rough turbulent. In these flow conditions some viscous effects were expected although the relative viscous forces were still small. In the case of the gravel bed all flows belonged to the rough turbulent conditions. These judgements were based on the velosity measurements at two stations on the reef.

The effect of surface tension also increases in the small-scale model. Fan and Le Méhauté (1969) examined the capillary effects and found that the surface tension effects on the wave length is less than 1 % when the wave period is larger than 0.35 seconds and the water depth is greater than 2 cm.

In flume experiments the viscous energy dissipation on the side walls should also be considered. From linear wave theory Hunt (1952) found the viscous energy dissipation on a side wall in one wave period, T, in a region Δx. It is given by:

$$\pi\rho\sqrt{\nu/2\omega}\cdot g^2\bar{A}^2 k/\omega^2\cdot\Delta x \tanh kh \ , \qquad (2.1)$$

where $\bar{A}$ is the mean wave amplitude in Δx. From (2.1) the corresponding energy flux change can be obtained. This equation (2.1) corresponds to the mean energy flux change, $b\Delta FT$, in one wave period in the region Δx, where b is the flume width and ΔF is the mean energy flux change due to a side wall per unit of time. Equating the mean energy flux change to (2.1) and re-arranging the equation, the gradient of the energy flux is given by:

$$\Delta F/\Delta x = \sqrt{\nu/2\omega}\ /b\cdot\rho g\bar{A}^2/2\cdot kg/\omega\cdot\tanh kh \ . \qquad (2.2)$$

Linear wave theory gives:

$$\omega^2 = kg \tanh kh \ , \qquad (2.3)$$

and

$$E = \rho g A^2/2 \ . \qquad (2.4)$$

Inserting (2.3) and (2.4) into (2.2) the rate of change of the energy flux by a side wall yield:

$$\Delta F/\Delta x = E/b\cdot\sqrt{\nu\omega/2} \ .$$

For two side walls this relationship is:

$$\Delta F/\Delta x = E/b\cdot\sqrt{2\nu\omega} \ . \qquad (2.5)$$

CHAPTER 3

TRANSFORMATIONS OF WAVE HEIGHT AND CELERITY

3.1 Introduction

As waves approach the shore from deep water there are changes in several characteristic parameters such as wave height, celerity, steepness, asymmetry, bed shear stress, and energy dissipation. During this approach, waves are transformed from a rather linear condition to a nonlinear one. Consequently, values for parameters which are calculated for the nearshore area using linear wave theory exhibit large deviations from experimental data. The discussion in this chapter is concerned primarily with transformations in wave height and wave celerity. Later chapters will cover the other parameters.

3.2 Wave Height

In coastal engineering practice it is common to use linear wave theory to estimate wave height. It is, however, common knowledge in the field that linear theory underestimates wave height in shallow water regions, where waves are highly nonlinear. In order to calculate nonlinear wave height, several methods based on nonlinear wave theories have been proposed. Sakai and Battjes (1980) used Cokelet's wave theory. Shuto (1974) used nonlinear long wave theory, and Svendsen and Brink-Kjaer (1972) used

cnoidal waves. James (1974) applied a combination of Stoke's waves and third order hyperbolic waves in specified regions. All of these approaches showed that nonlinear wave theories do a good job in predicting nonlinear wave height. There are, however, two significant disadvantages in the use of nonlinear wave theories. First, it is mathematically difficult to use these theories. Second, they are applicable only in limited water regions. For example, Svendsen and Brink-Kjaer used cnoidal waves in the region of $D/L_0 < 0.1$, and James used Stoke's waves for the region $U_r=HL_0^2/D^3 \leq 68$ and third order hyperbolic waves for $U_r>68$. None of these theories are applicable in the breaking region.

For these reasons it was decided in this study to establish an empirical approach for estimating wave heights for all of the water regions of interest. Goda (1983) originally proposed a nonlinearity parameter which smoothly connects the two most familiar wave parameters using a hyperbolic cotangent function. These parameters are the wave steepness, H/L, in the deep water region and Ursell's parameter, U_r, for the shallow water. The proposed nonlinearity parameter by Goda is;

$$\Pi = (H/L_a) \coth^3 k_a h$$

where,

$$\omega^2 = (2\pi/T)^2 = g k_a \tanh k_a h$$

and,

$$k_a = 2\pi/L_a \ .$$

The subscript "a" is used to denote the quantity calculated by linear wave theory. The parameter Π is easily shown to approach H/L_a in deep water and $(2\pi)^{-3}HL_a^2/h^3$ in the extreme of $k_a h \to 0$. For convenience in calculation and ease in definition a new expression can be written in place of Π by using L_a instead of k_a. This new parameter designated P_0.

In order to relate wave height to wave energy the ratio of wave height to the root-mean-aquare surface elevation was chosen as a wave parameter. This is based on the fact that wave energy is proportional to the variance of the water surface elevation. In this study wave energy is defined as:

$$E = \rho g \, \eta_{rms}^2 \ . \qquad (3.1)$$

The change in the wave parameter with respect to the wave nonlinearity parameter, p_0, was examined and is shown in Figure 3.1. It is evident from Figure 3.1 that H/η_{rms} increases with the nonlinearity parameter; i.e., the ratio of wave height to root-mean-square surface elevation is not a constant value of $\sqrt{8}$ as predicted by linear wave theory. In this figure numbers denote rounded wave periods. H is the mean value of the largest one-third of the wave heights as obtained by using the zero up-crossing method. This significant wave height was used because the experimental wave data included secondary waves.

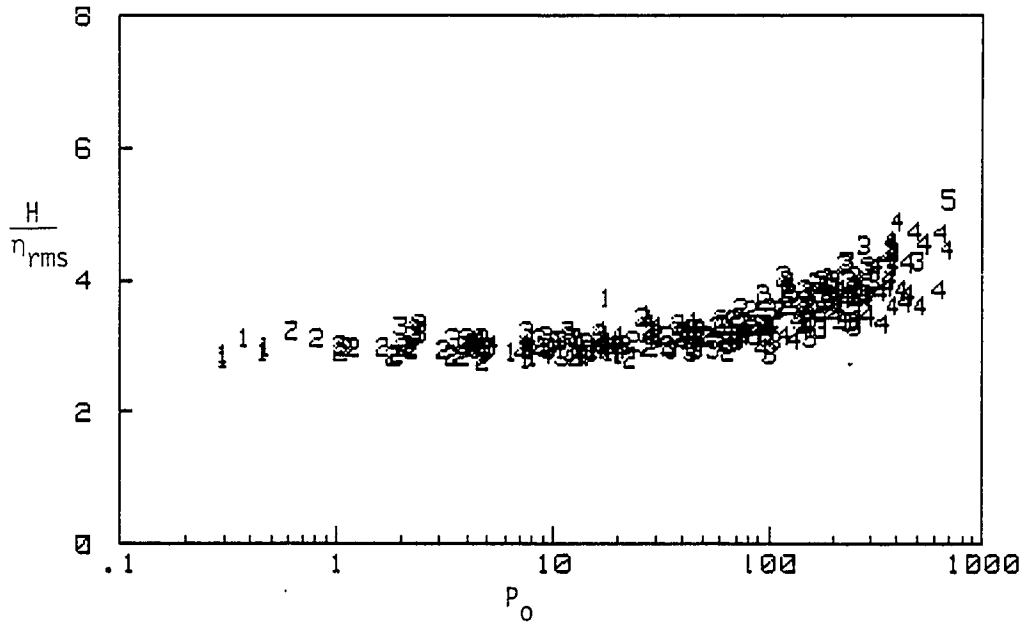

Figure 3.1 The ratio of non-broken wave height to root-mean-square surface elevation versus wave nonlinearity parameter, P_o. (Numbers plotted denote rounded wave periods.)

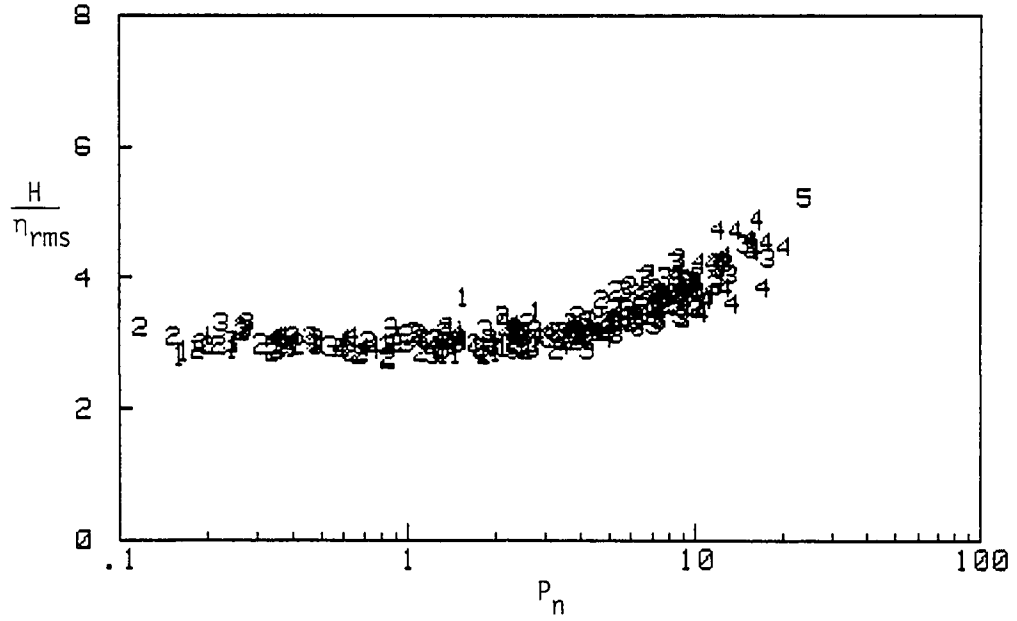

Figure 3.2 The ratio of non-broken wave height to root-mean-square surface elevation versus wave nonlinearity parameter, P_n. (Numbers plotted denote rounded wave periods.)

Examining Figure 3.1 we notice a dependency of H/η_{rms} on wave periods. The wave length, L_a, calculated using linear wave theory seems to be too large to represent the characteristic wave length in shallow water; i.e., in the area of large values of the nonlinearity parameter. It may be reasoned that wave energy is transfered mainly to higher frequency components as waves deform and also as secondary waves are produced in shallow water. In order to reduce the influence of the linear wave length in the nonlinearity parameter on H/η_{rms} , several smaller values for the power of the hyperbolic cotangent function were tried. The value of 2 was finally chosen as minimizing the influence of the linear wave length. In consequence Ursell's parameter was changed to HL_a/h^2 using the linear wave length. Using the above considerations a new nonlinearity parameter was defined as:

$$P_n = H/L_a \cdot \coth^2(D/L_a) \quad . \tag{3.2}$$

Using this new nonlinearity parameter, P_n , we can reduce the dependency of H/η_{rms} on wave periods. The result is shown in Figure 3.2. Figure 3.3 shows plots of data from Hansen and Svendsen (1979). The plots in Figure 3.3 are less scattered. This greater uniformity may be because Hansen and Svendsen controlled their experiments so as to be free of secondary waves. Hansen and Svendsen's data were fitted to a fifth order polynomial. An overlay of this curve on the plot of the data developed in the present study

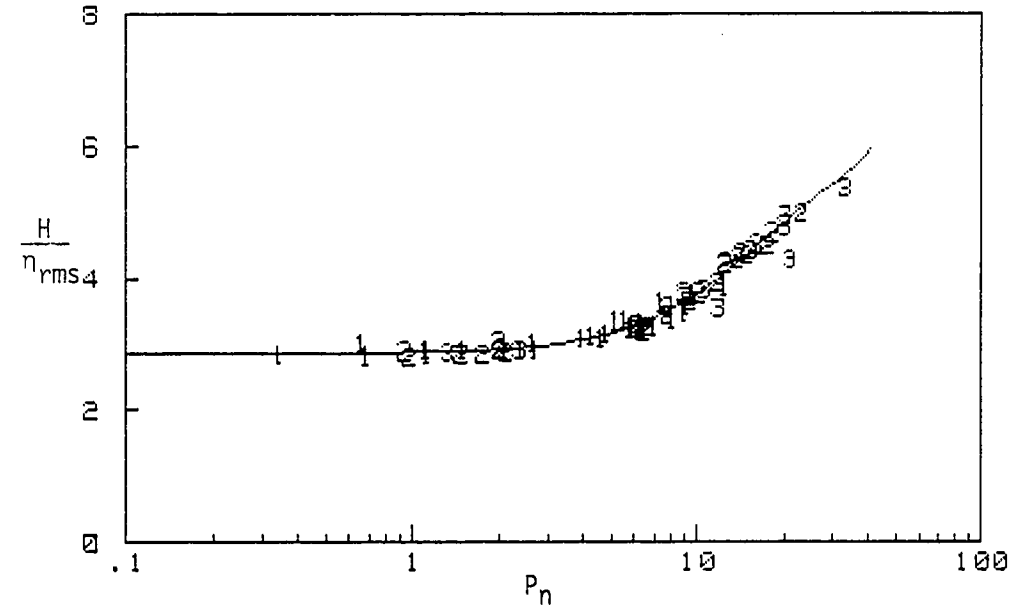

Figure 3.3 Hansen and Svendsen's data of the ratio of wave height to root-mean-square surface elevation versus nonlinearity parameter, P_n . (Numbers plotted denote rounded wave periods.)

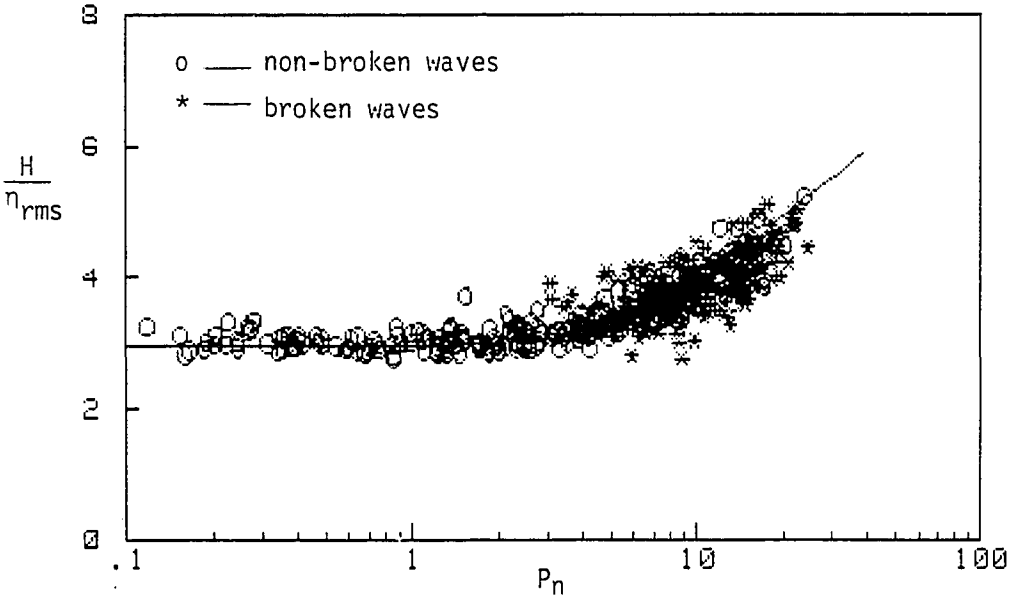

Figure 3.4 The ratio of non-broken and broken wave height to root-mean square surface elevation versus wave nonlinearity parameter, P_n .

shows that the curve also fits the data very well if the curve is shifted slightly upward. The need for this slight shift may be attributable to different definitions of wave height in the two sets of experiments. Our data were obtained in experiments over a compound slope of roughly 0, 1:80, 1:32, and 1:20. All data were measured over the slopes of 0 and 1:80. Hansen and Svendsen used a single plane slope of 1:34. Since both experimental data sets give similar curves we can conclude that there is little bed slope influence on the curve, at least for slopes in the range of 0 to 1:34.

The case of breaking waves is shown in Figure 3.4. It is evident that the curve for non-breaking waves also closely describes breaking waves. Similar results were also shown in Goda's data (1983). This feature is very useful in calculating wave heights in the breaking zone if the nonlinearity parameter is also expressed using η_{rms} instead of H. For this purpose a wave height was defined in function of η_{rms} as:

$$H_a = \sqrt{8}\ \eta_{rms} \ , \qquad (3.3)$$

which is based on wave energy from linear wave theory. Subsequently, the second nonlinearity parameter is:

$$P_a = H_a/L_a \cdot \coth^2(D/L_a) \ . \qquad (3.4)$$

The new and unique curve of H/η_{rms} versus P_a is applicable for calculating the wave height by knowing wave energy. In this case wave energy is defined as being propotional to the

variance of the water surface elevation. The calculation of wave energy from known data will be discussed in later chapters. The curve of H/η_{rms} on P_n is used to obtain wave energy by knowing wave height. These curves will be used in later chapters.

It should be mentioned that the curve of H/η_{rms} as a function of P_a was obtained based on the curve from P_n, not from curve fitting to the measured data, so that the error caused in the interchange of these nonlinearity parameters would be minimal.

Experimentally obtained H/η_{rms} are:

$$H/\eta_{rms} = f(P_n)$$
$$= a_0 + a_1 P_n + a_2 P_n^2 + a_3 P_n^3 + a_4 P_n^4 + a_5 P_n^5 \qquad (3.5)$$

and,

$$H/\eta_{rms} = f(P_a)$$
$$= b_0 + b_1 P_a + b_2 P_a^2 + b_3 P_a^3 + b_4 P_a^4 + b_5 P_a^5 \qquad (3.6)$$

where,

$a_0 = b_0 = 2.94$

$a_1 = -2.480 \times 10^{-4}$

$a_2 = 1.613 \times 10^{-2}$

$a_3 = -8.690 \times 10^{-4}$

$a_4 = 1.836 \times 10^{-5}$

$a_5 = -1.378 \times 10^{-7}$

TABLE 1

The Ratio of Wave Height to Root-Mean-Square Surface Elevation Versus Wave Nonlinearity Parameters, P_n and P_a.

Pn	Pa	H/η_{rms}	
		f(Pn)	f(Pa)
.1	.096	2.940	2.941
.2	.192	2.941	2.942
.3	.288	2.941	2.943
.4	.385	2.942	2.945
.5	.480	2.944	2.946
.6	.576	2.945	2.947
.7	.672	2.947	2.949
.8	.767	2.950	2.951
.9	.862	2.952	2.953
1.0	.957	2.955	2.955
2.0	1.887	2.997	2.989
3.0	2.771	3.062	3.051
4.0	3.596	3.146	3.138
5.0	4.359	3.244	3.245
6.0	5.060	3.354	3.366
7.0	5.702	3.472	3.493
8.0	6.293	3.596	3.622
9.0	6.838	3.723	3.750
10.0	7.345	3.851	3.875
12.0	8.271	4.104	4.113
14.0	9.116	4.344	4.334
16.0	9.917	4.563	4.540
18.0	10.699	4.759	4.731
20.0	11.476	4.929	4.908
22.0	12.259	5.076	5.068
24.0	13.050	5.202	5.210
26.0	13.845	5.311	5.332
28.0	14.640	5.410	5.434
30.0	15.423	5.502	5.522
32.0	16.185	5.592	5.600
34.0	16.916	5.685	5.677
36.0	17.608	5.783	5.763
38.0	18.260	5.886	5.865
40.0	18.878	5.993	5.993

and,

$$b_1 = 1.095 \times 10^{-2}$$

$$b_2 = 1.108 \times 10^{-3}$$

$$b_3 = 4.397 \times 10^{-3}$$

$$b_4 = -3.966 \times 10^{-4}$$

$$b_5 = 9.694 \times 10^{-6}$$

For $P_n > 40$ or $P_a > 18.88$, where there was no data available, H/η_{rms} was set equal to 5.99. In the case of Hansen and Svendsen's data a_0 and b_0 are 2.87 and the other coefficients are the same as our case.

3.3 Wave Celerity

The role of wave celerity is vital in calculation of wave energy from the conservation of energy flux. Eagleson (1956) studied the transformation of wave celerity. In his experimental study he found that the celerity calculated by linear wave theory was in close agreement with experimental results over the full range of transformations, including breaking waves. From linear wave theory the celerity is given by:

$$C_a^2 = gL_a/2\pi \cdot \tanh(2\pi h/L_a) , \qquad (3.7)$$

provided that the wave period is constant. Despite Eagleson's results, it is generally known that the celerity has some dependence on wave height in shallow water region. Walker (1974) concluded from his laboratory study that wave height and wave breaking have considerable influences on the

wave celerity. He gave expressions for the celerity of a shoaling wave as:

$$C = C_a (1 + 0.25 H/D) \tag{3.8}$$

for non-breaking waves and,

$$C_b = 1.25\sqrt{gD} \tag{3.9}$$

as the maximum wave celerity at breaking. Bretschneider (1960) found the maximum wave celerity during breaking to be:

$$C_b = \sqrt{2g\eta_c} \tag{3.10}$$

where η_c is the crest elevation above still water depth. Van Dorn (1978) also found the same result as (3.10) at the breaking points from his experiments on the assumption $u_b - C_b = 0$ on the crest, where C_b is the breaking wave velocity and u_b is the particle velocity in the breaking wave. These expressions show that the wave celerity is influenced to some degree by wave height.

For the examination of celerity deformation in this study, Hansen and Svendsen's data were used. Their experimental data gave similar results in wave height deformation, which were discussed in the previous section. The wave height deformation affects wave celerity. The ratio of the measured celerity to the celerity calculated using linear wave theory was plotted against the nonlinearity parameter, P_a, in Figure 3.5. In this figure, numbers denoting wave periods are rounded. From the figure, the deformation of celerity was approximated using the

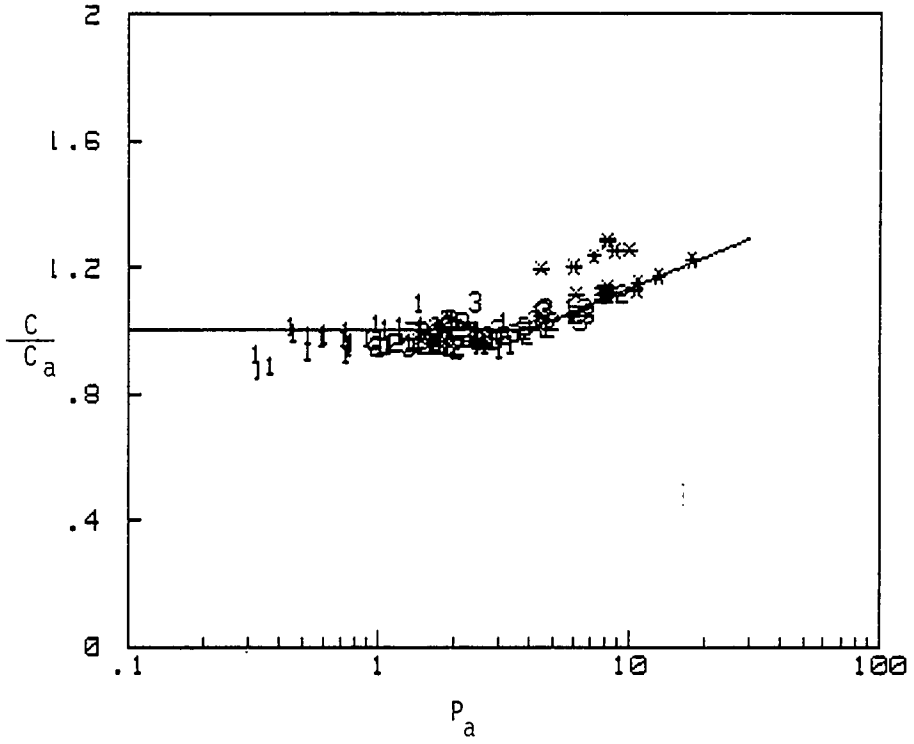

Figure 3.5 The ratio of measured wave celerity by Hansen and Svendsen to calculated wave celerity using linear wave theory versus wave nonlinearity parameter, P_a . (Numbers plotted denote rounded non-broken wave periods and cross marks refer to broken waves.)

following expressions:

$$C = C_a \qquad \text{for } P_a \leq 4 \ , \qquad (3.11)$$

$$C = C_a(1/3 \cdot \log P_a + 0.8) \qquad \text{for } 4 < P_a \leq 18.88 \qquad (3.12)$$

and,

$$C = 1.23\ C_a \qquad \text{for } P_a > 18.88 \ . \qquad (3.13)$$

The last expression was used since there were no measured data available for $P > 18.88$. The celerities predicted from these expressions were compared with the celerities by Walker's expressions and by linear wave theory. In Figure 3.6, the cross sign refers to the breaking wave. The celerity as a function of P_a appears to be the best predictor of overall deformation except in some cases of breaking waves. The celerities calculated by linear theory are good estimates as found by Eagleson, except for breaking waves. Although it overestimates the celerity for non-breaking waves, Walker's expression of (3.8) gives the best results for breaking waves.

From Figure 3.6, it was decided that the wave celerity would be predicted in this study by equations (3.11), (3.12) and (3.13) for non-breaking waves and by equation (3.8) for breaking waves.

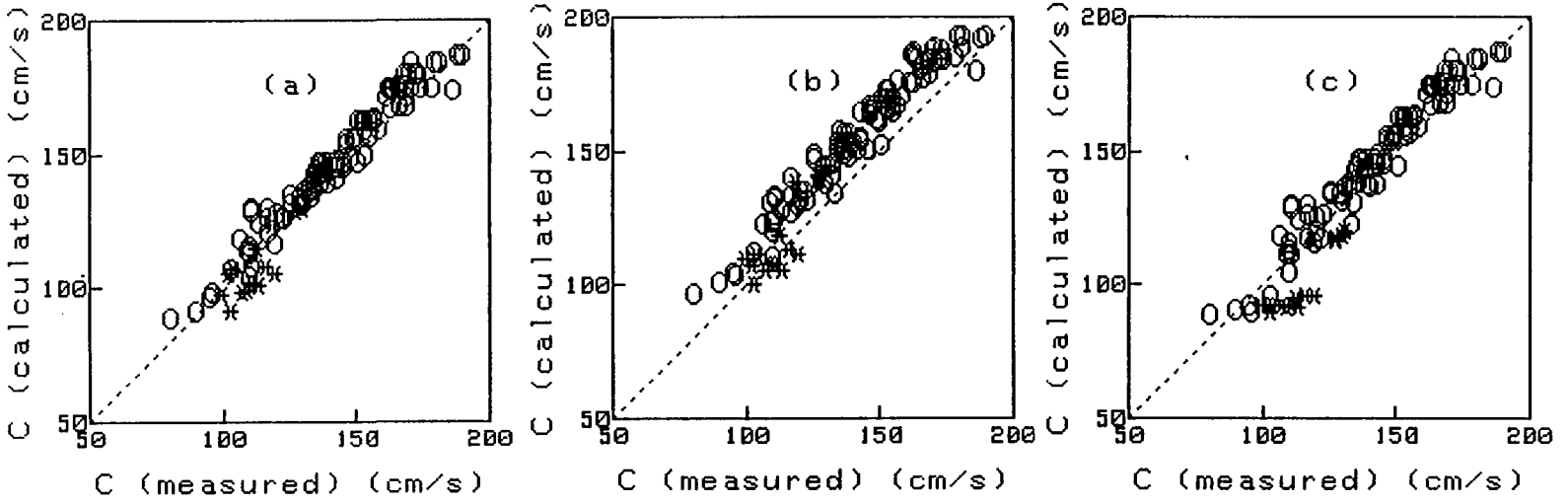

Figure 3.6 Comparisons between measured wave celerity and calculated wave celerities; (a) celerities from nonlinearity parameter, (b) celerities from Walker's formula and (c) celerities from linear theory. (o ___ non-broken waves, * ___ broken waves.)

CHAPTER 4

BED SHEAR STRESS AND ENERGY DISSIPATION

4.1 Introduction

The bed shear stress is an important consideration in coastal engineering. It is one of the dominant causes of energy dissipation in waves. The mean shear stress also influences the wave set-up, a subject which will be discussed in Chapter 6. This chapter begins with a review of the theory of an oscillatory boundary layer. This is followed by a discussion of pertinent existing formulas which were obtained based on sinusoidal oscillations. Finally, a comparison of experimental results, which were obtained under nonlinear wave conditions, is made with results from the existing formulas.

4.2 Oscillatory Boundary Layer

This section contains a discussion of the analytical expressions for the shear stress and the related energy dissipation for a two dimensional flow which combines wave oscillations and a steady weak current. The datum is taken at the bottom and z is measured upward from the bottom.

4.2.1 Basic Equations

By neglecting normal stresses, the governing equations for combined current wave motions are given by:

$$\partial V/\partial t + V\partial V/\partial x + w\partial V/\partial z + 1/\rho \cdot \partial P/\partial x = 1/\rho \cdot \partial \tau/\partial z \quad , \qquad (4.1)$$

for horizontal motions, and

$$\partial w/\partial t + V\partial w/\partial x + w\partial w/\partial z + 1/\rho \cdot \partial P/\partial z = 0 \quad . \qquad (4.2)$$

for vertical motions, where ρ is density, V and w are horizontal and vertical velocities, respectively. V is given by:

$$V = U + u \quad ,$$

where $U = U(x,z)$ is the steady current velocity and $u = u(x,z,t)$ is the wave particle velocity. The total pressure, P, consists of two components, a steady pressure, P_c, and an unsteady pressure, P_w, giving:

$$P = P_c + P_w \quad .$$

The shear stress, τ , is given using the eddy viscosity, ε :

$$\tau/\rho = \varepsilon \, \partial V/\partial z \quad .$$

The current motion is obtained by taking the time averaged values of (4.1) and (4.2). The bar, "—", refers to the time averaging. For the current motion:

$$U\partial U/\partial x + u\partial u/\partial x + w\partial u/\partial z + 1/\rho \cdot \partial P_c/\partial x = 1/\rho \cdot \partial \bar{\tau}/\partial z \quad , \qquad (4.3)$$

and,

$$u\partial w/\partial x + w\partial w/\partial z + 1/\rho \cdot \partial P_c/\partial z + g = 0 \quad . \qquad (4.4)$$

The wave motion is obtained by subtracting (4.3) and (4.4) from (4.1) and (4.2), respectively.

$$\partial u/\partial t + U\partial u/\partial x + u\partial U/\partial x + u\partial u/\partial x - \overline{u\partial u/\partial x} + w\partial u/\partial z - \overline{w\partial u/\partial z} + 1/\rho \cdot \partial P_w/\partial x = 1/\rho . \partial(\tau - \bar{\tau})/\partial z \quad , \tag{4.5}$$

and,

$$\partial w/\partial t + U\partial w/\partial x + u\partial w/\partial x + w\partial w/\partial z - \overline{u\partial w/\partial x} - \overline{w\partial w/\partial z} + 1/\rho \cdot \partial P_w/\partial z = 0 \quad . \tag{4.6}$$

Now, we simplify (4.3), (4.4) and (4.5) to the first order approximation. By neglecting second order terms in wave amplitude in (4.4), we obtain:

$$\partial P_c/\partial z + \rho g = 0 \quad . \tag{4.7}$$

Applying the boundary condition, $P_c = 0$ for $z=h$, to the integrated result of (4.7), yields:

$$P_c(z) = \rho g (h - z) \quad .$$

Differentiating the equation with respect to x, we have:

$$\partial P_c/\partial x = \rho g \, \partial h/\partial x \quad . \tag{4.8}$$

Using (4.8), and the first term in (4.3) we find:

$$\rho U \, \partial U/\partial x \; / \; \partial P_c/\partial x \sim U^2/gh \quad ,$$

which means that the first term of (4.3) can be neglected for small U. Neglecting second order terms in wave amplitude in (4.3), we find:

$$\partial P_c/\partial x = \partial \bar{\tau}/\partial z \quad . \tag{4.9}$$

Comparing the second term and the third in (4.5), we have:

$$u\partial U/\partial x \;/\; U\partial u/\partial x \sim 1/kU\cdot\partial U/\partial x$$

since,

$$\partial u/\partial x \sim ku \quad .$$

Because of small variation of current in x direction in a wave length, the third term can be neglected. Neglecting second order terms in the wave amplitude in (4.5), we find the simplified form of (4.5) is given by:

$$\partial u/\partial t + U\partial u/\partial x + 1/\rho\cdot\partial P_w/\partial x = \partial(\tau - \overline{\tau})/\partial z \quad . \tag{4.10}$$

4.2.2 Bed Shear Stress

It may be considered that the shear stress is negligible outside the wave boundary layer, where $z \geq \delta$. Using this assumption we find from (4.10):

$$\partial u/\partial t + U\partial u/\partial x + 1/\rho\cdot\partial P_w/\partial x = 0 \quad . \tag{4.11}$$

Inside the boundary layer, $z \leq \delta$, the second term in (4.10) can be neglected for the following reasons:

$$U\partial u/\partial x \;/\; \partial u/\partial t = U \;/\; \partial x/\partial t = U/C \quad .$$

and $U << C$ for $z \leq \delta$. C is the wave celerity. Considering at $z = \delta$, we find:

$$\partial u_\delta/\partial t = - 1/\rho\cdot\partial P_w/\partial x \tag{4.12}$$

where $u = u_\delta$ at $z = \delta$. Assuming that the pressure gradient is constant with repect to z within the wave boundary layer, we find the equation of motion given by:

$$\partial(u - u_\delta)/\partial t = 1/\rho\cdot\partial(\tau - \overline{\tau})/\partial z \quad .$$

Integrating the equation, the bed shear stress is obtained as:

$$1/\rho\cdot(\tau_b - \bar{\tau}_b) = -\int_0^{\delta}\partial(u - u_\delta)/\partial t\, dz \ . \qquad (4.13)$$

Integrating (4.9) and using the boundary condition, $P_c = 0$ at $z = h$, we find:

$$\bar{\tau} = (z - h)\ \partial P_c/\partial x \ .$$

The equation at $z = 0$ is:

$$\bar{\tau}_b = -h\ \partial P_c/\partial x \ . \qquad (4.14)$$

4.2.3 Energy Dissipation Due to Bed Shear Stress

The dissipation, E_d, is given by:

$$E_d = \overline{\int_0^{h+\eta}\tau\partial V/\partial z\, dz}$$

$$= \overline{|\tau\ (U + u)|_0^{h+\eta}} - \overline{\int_0^{h+\eta}(U + u)\partial\tau/\partial z\, dz}$$

where η is the water surface elevation above the mean water level. The first term is zero since $\tau = 0$ at $z = h+\eta$ and $u = U = 0$ at $z = 0$. The dissipation E_d can be separated into two terms:

$$E_d = -\overline{\int_0^{h+\eta} U\ \partial\tau/\partial z\, dz} - \overline{\int_0^{h+\eta} u\ \partial\tau/\partial z\, dz}$$

$$= E_{dc} + E_{dw}$$

where E_{dc} is the dissipation due to steady motion and E_{dw} is the dissipation due to waves. This equation is solved as

follows:

$$E_{dc} = - \overline{\int_0^{h+\eta} U \, \partial\tau/\partial z \, dz}$$

$$= - \int_0^h U \, \partial\overline{\tau}/\partial z \, dz - \overline{\int_h^{h+\eta} U \, \partial\tau/\partial z \, dz} \, .$$

The second term is zero since τ is zero at $z = h$. Using (4.9) and (4.14), we find:

$$\partial\overline{\tau}/\partial z = - \overline{\tau}_b/h$$

Using the above result, E_{dc} is given by:

$$E_{dc} = \overline{\tau}_b \, \overline{U} \, . \qquad (4.15)$$

where $\overline{U}$ is the current velocity averaged over the depth.

Now, solving for E_{dw}:

$$E_{dw} = - \overline{\int_0^{h+\eta} u \, \partial\tau/\partial z \, dz}$$

$$= - \overline{\int_0^{h+\eta} u_\delta \, \partial\tau/\partial z \, dz} + \overline{\int_0^{h+\eta} (u - u_\delta) \, \partial\tau/\partial z \, dz} \, .$$

Taking the second term as zero, as will be shown later, we find:

$$E_{dw} = - \overline{u_\delta \int_0^{h+\eta} \partial\tau/\partial z \, dz}$$

$$= - \overline{u_\delta \, \tau_b} \qquad (4.16)$$

The second term of E_{dw}, defined as I, can be shown to be zero using (4.9) and (4.10):

$$I = - \overline{\int_0^{h+\eta} (u - u_\delta) \, \partial\tau/\partial z \, dz}$$

$$= - \overline{\int_0^{h+\eta} (u - u_\delta) \cdot (\rho \partial u/\partial t + \rho U \partial u/\partial z + \partial(P_w + P_c)/\partial x \, dz}$$

$$= - \overline{\int_0^{h+\eta} (u - u_\delta) \cdot (\rho \partial u/\partial t + \rho U \partial u/\partial z + \partial P_w/\partial x) \, dz}$$

$$- \overline{\partial P_c/\partial x \int_0^{h+\eta} (u - u_\delta) \, dz} \, .$$

The second term is zero since there is no net mass transport by the wave motion. Dividing the first integral into two layers and applying (4.11) for $z > \delta$ and (4.12) for $z \leq \delta$, we find:

$$I = -\overline{\int_0^{\delta}(u - u_{\delta})\,\rho\partial(u - u_{\delta})/\partial t\,dz}$$

$$= -\overline{\int_0^{\delta}\rho/2\cdot\partial(u - u_{\delta})^2/\partial t\,dz}$$

$$= 0$$

since there is no net mass transport by the wave motion.

4.3 Existing Theories

The important factor in the study of oscillatory boundary layer is the type of flow, such as a laminar flow, smooth turbulence flow or a rough turbulence flow. Also of importance are the friction factor and the boundary layer thickness.

4.3.1 Transition to Rough Turbulence

In the prototype, flow under the wave motion is always rough turbulent near the sea bed in the coastal zone. In the scale model, however, this is not always true. It is important to be able to produce a given type of flow, because each type of flow has different boundary layer characteristics. Flows are categorized into three types, laminar, smooth turbulent and rough turbulent.

Several investigators have given criteria for the rough turbulent condition. That criterion is generally expressed by the amplitude Reynolds number, RE, which is defined as:

$$RE = u_{\delta m} a_\delta / \nu \quad .$$

$u_{\delta m}$ is the maximum fluid velocity at the height of the boundary layer thickness, δ, a_δ is the maximum travelling distance in a half cycle and ν is the kinematic viscosity. For the case of very rough walls, Jonsson (1980) gave the lower limit of RE as:

$$RE = 5500 \, (a_\delta / K_s)^{0.33} \quad . \tag{4.17}$$

Sleath (1974) gave a criterion for the rough turbulent condition and Jonsson (1980) re-expressed the limit in terms of RE as given by:

$$RE = 4130 \, (a_\delta / K_s)^{0.45} \quad . \tag{4.18}$$

For the less rough wall condition Jonsson proposed the limit as:

$$RE = 223 \, (a_\delta / K_s)^{1.17} \quad . \tag{4.19}$$

Kajiura (1968) found the following limit based on Kalkanis' data:

$$RE = 2000 \, a_\delta / K_s \quad . \tag{4.20}$$

Kamphuis (1975) defined the limit where the friction factor starts being dependent on RE. He gave the limit as:

$$u_{fm} K_s / \nu = 200 \, , \tag{4.21}$$

for $a_\delta / K_s < 100$. In this expression, u_{fm} is the wall friction velocity defined as:

$$u_{fm} = (\tau_{bm} / \rho)^{1/2} \quad .$$

4.3.2 Friction Factor for Rough Turbulence

For the rough turbulent flow condition, Jonsson gave the friction factor, f_w, as:

$$1/4\sqrt{f_w} + \log(1/4\sqrt{f_w}) = -0.08 + \log(a_\delta/K_s) \qquad (4.22)$$

by applying the logarithmic velocity profile to (4.13) where $\overline{\tau}_b = 0$. He defined f_w in the form:

$$\tau_{bm} = 1/2 \cdot f_w \rho\, u_{\delta m}|u_{\delta m}| \ .$$

Kajiura found the friction factor, C_{fm}, from an eddy viscosity model. His expression is:

$$0.4/\sqrt{C_{fm}} + \ln(1/\sqrt{C_{fm}}) = -2.25 + \ln(u_{\delta m}/\omega z_o) \ .$$

Replacing C_{fm}, $u_{\delta m}/\omega$ and Z_o by $f_w/2$, a_δ and $K_s/30$, his formulation becomes:

$$1/4.05\sqrt{f_w} + \log(1/4\sqrt{f_w}) = -0.254 + \log(a_\delta/K_s) \ . \qquad (4.23)$$

He defined C_{fm} in the form of the instantaneous shear stress as:

$$\tau_b = (C_{fm} \cos\theta)\cdot(u_{\delta m}\, u_{\delta m} \cos\theta) \ .$$

From direct measurement of bed shear stress Riedel et.al. (1972) obtained the friction factor expresses as:

$$f_w = 0.25\ (K_s/a_\delta)^{0.77} \qquad \text{for } 0.1 < a_\delta/K_s < 25 \ ,$$

and,

$$1/4.95\sqrt{f_w} + \log(1/4\sqrt{f_w}) = 0.122 + \log(a_\delta/K_s) \qquad \text{for } a_\delta/K_s > 25 \ .$$

Reanalyzing Riedel's data, Kamphuis (1975) obtained an empirical formula for f_w as:

$$1/4\sqrt{f_w} + \log(1/4\sqrt{f_w}) = -0.35 + 4/3\cdot\log(a_\delta/K_s) \ . \qquad (4.24)$$

For small values of a_δ/K_s, Jonsson suggested $f_w = 0.3$ for $a_\delta/K_s < 1.57$, and Kajiura proposed $f_w = 0.25$ for $a_\delta/K_s < 1.67$.

4.3.3 Boundary Layer Thickness

Using a logarithmic velocity profile, Jonsson obtained the boundary layer thickness, δ , in terms of a_δ/K_s . He defined δ as the height from the bottom where the fluid velocity equals that of the free stream. He experimentally found that $\tau_{\delta m}$ was $0.35\,\tau_{bm}$ at the level of δ and τ_m practically disappears at the level of 2δ . From Jonsson, δ is given in the following forms:

$$u_{\delta m}/u_{fm} = 2.5\ \ln(30\delta/K_s) \quad , \tag{4.25}$$

and,

$$30\delta/K_s \cdot \log(30\delta/K_s) = 1.2\ a_\delta/K_s \quad . \tag{4.26}$$

4.4 Experimental Results

4.4.1 Introduction

First, the friction factors for the nonlinear wave case were determined over a concrete surface bed and a bed covered by gravel. The calculations were based on the measurement of wave forces on the shear plate and on the fluid velocity at a single level. Second, the energy friction loss calculated from the fluid velocity data was compared with the result calculated by linear wave theory.

4.4.2 Nikuradse Roughness, Boundary Layer Thickness and Wave Particle Amplitude

Nikuradse roughness, K_s, was defined only from a roughness size. Kamphuis (1974) obtained K_s values applying

TABLE 2

Nikuradse roughness and roughness size from Kamphuis (1974).

D_{90} (mm)	K_s (mm)
0.54	0.84
0.98	2.37
2.2	5.76
4.2	9.75
9.1	14.0
46.0	35.7

a logarithmic velocity profile to experimental results. The results are given in Table 2. The range of roughness diameters used was from 0.54 mm to 46 mm for D_{90}. This range covers the roughness sizes used in our experiments. Kamphuis' data were fit to the linear relationship as:

$$K_s = a\, D_{90} \quad . \tag{4.27}$$

In order to accommodate a wide distribution of data in the regression analysis, a log-log regression line was used as:

$$\log K_s = \log a + \log D_{90} \quad .$$

Solving for "a" yields,

$$a = 1.735 \quad , \tag{4.28}$$

which is different from the value that Kamphuis suggested. He recommended a=2.

In our experiments, two types of bed surfaces were used, a concrete surface and a surface covered by gravel. It was estimated that the roughness of the concrete surface was equivalent to sieved sand between 0.71 mm and 0.83 mm in

size. Assuming a uniform distribution of grain sizes, D_{90} for the sand was determined as:

$$D_{90} = 0.82 \quad (mm) .$$

Gravel was initially sieved to between 1.3 cm and 2.5 cm. In order to determine D_{90} for the gravel, some amount of sieved gravel was randomly taken and placed in a flat bottom container. Individual stone heights were measured by adding water in the container and counting stones completely covered by water at each water level. The total number of sampled stones was 222 and the cumulative distribution of the stone height is shown in Figure 4.1. From that figure D_{90} for the gravel was determined as:

$$D_{90} = 18 \quad (mm) .$$

For the case of the gravel covered bed, the datum height from the concrete bed was approximated as the average gravel height which was obtained by dividing the volume of gravel in a container by the area where the volume of gravel was placed. The average height was 13 mm, which is nearly equal to D_{90}.

The current meter should be placed at the height where the fluid velocity represents the free stream. For this purpose, the boundary thickness was estimated using (4.26) for all experimental waves. A single level from the bed was chosen for each roughness. These levels were 1.5 cm for the concrete bed and 3 cm for the gravel bed.

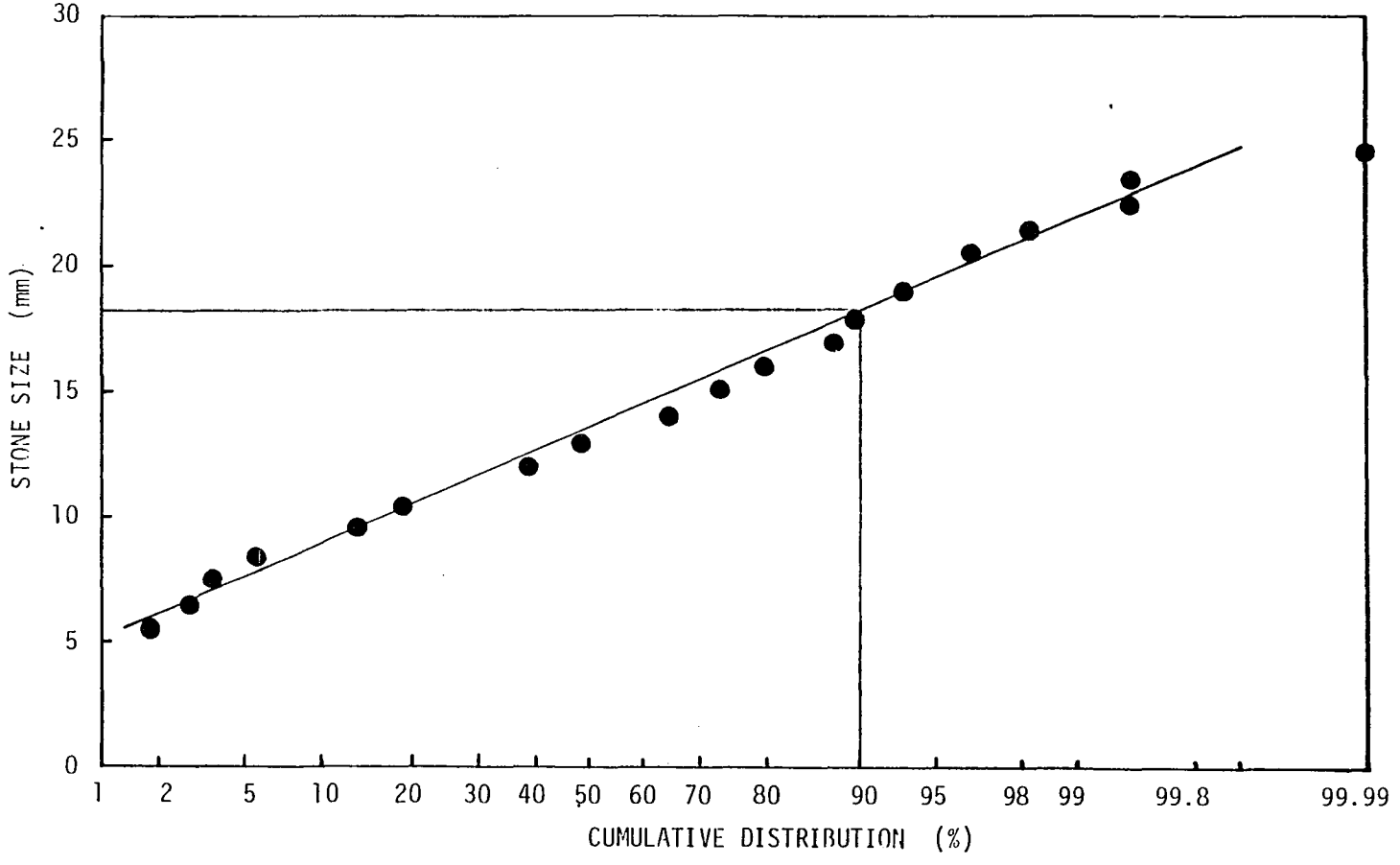

Figure 4.1 Cumulative distribution of sampled gravel heights.

For a sinusoidal wave, the wave particle amplitude is defined as:

$$a_{\delta 1} = T\, u_{\delta m}/2\pi$$

where "1" stands for a linear wave. For nonlinear waves, however, the definition of a_δ is not clear. In this study a_δ was defined as one half of the mean value of the largest one-third of the particle traveling ranges, which was obtained through the zero-up crossing method. For this purpose, the time series of the particle position was produced in such a way that the velocity time series was integrated with respect to time through Fourier transformation, and the result was inversely transformed. In the process of integration, frequency components lower than the first harmonic frequency were discarded. The results of the ratio of a_δ to $a_{\delta 1}$ are shown in Figure 4.2 against the nonlinearity parameter, P_n. According to Figure 4.2, the wave particle amplitude by linear wave theory overestimate the a_δ for highly nonlinear waves. From the figure, we estimate a_δ values as:

$$a_\delta = a_{\delta 1} \qquad \text{for } P_n \leq 3.6\ , \qquad (4.29)$$

and

$$a_\delta = a_{\delta 1}\,(-0.805 \log P_n + 1.45) \qquad \text{for } P_n > 3.6\ . \qquad (4.30)$$

4.4.3 Friction Factor

The arrangement for the measurement of the friction factor is indicated in Figure 4.3. The measured total

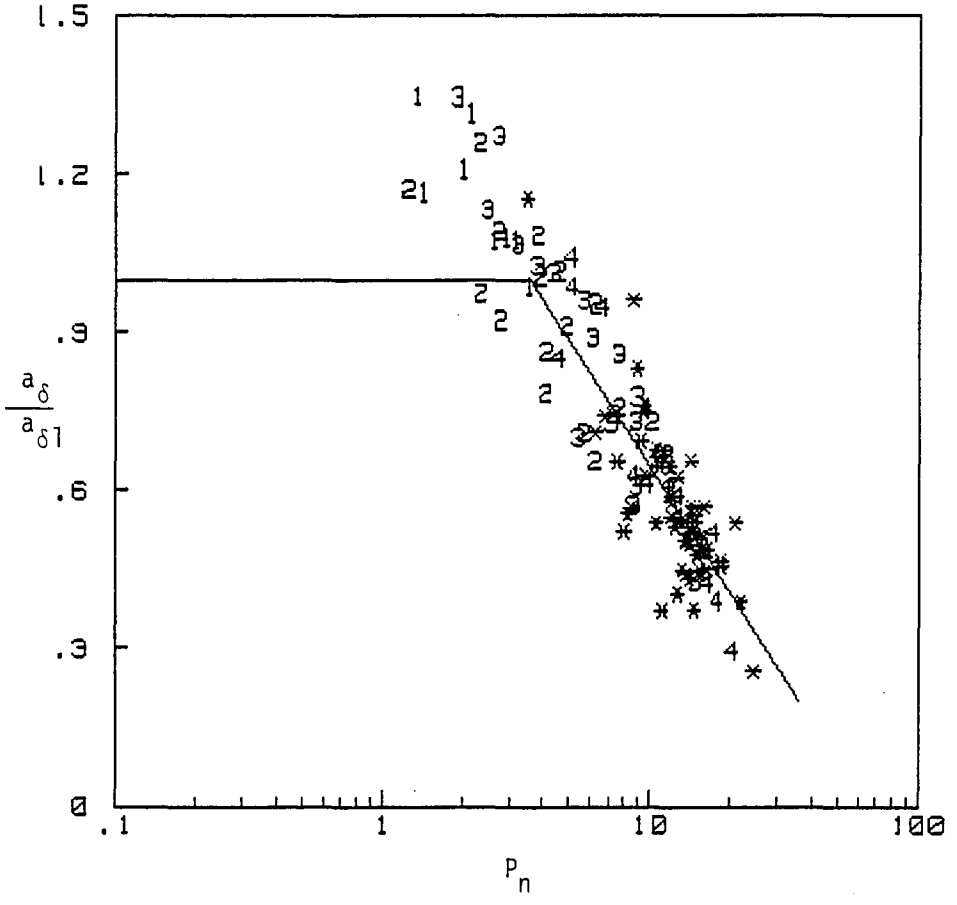

Figure 4.2 The ratio of nonlinear wave particle amplitude to linear wave particle amplitude at the bed versus wave nonlinearity parameter, P_n. (Numbers plotted denote rounded non-broken wave periods and cross marks refer to broken waves.)

force, F_T , on the shear plate is expressed as a combination of the inertial force, F_I , and the drag force. The drag force consists of two types of forces, the shear stress, F_S , acting on the plate surface and the pressure gradient force, F_P , acting on the front and back plate edges.

The inertial force per unit length of the shear plate is:

$$F_i = \alpha \dot{V}(x,t) \quad .$$

where,

$$\alpha = 1/\ell \cdot (m + \rho \forall) \quad .$$

ℓ is the plate length, m is the added mass, ρ is the fluid density, $\forall$ is the plate volume and $\dot{V}_\delta$ is the derivative of the particle velocity at the bed with respect to time. The total inertial force is obtained by integrating F_i over

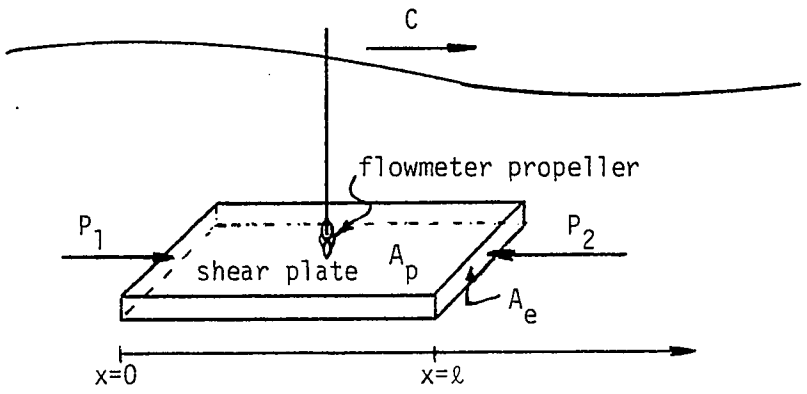

Figure 4.3 Diagram of measurements.

the plate. In order to estimate the space integration from a time series, two assumptions are made; i.e. the fluid velocities at the front and back plate edges have the same time history with a time lag, t_1, and the wave celerity, C, is constant over the shear plate. Using these assumptions, F_I is expressed in terms of an instantaneous velocity.

$$\begin{aligned} F_I &= \int_0^{\ell} \alpha \, \partial V_\delta(x,t)/\partial t \, dx \\ &= \int_{V_\delta(0,t)}^{V_\delta(\ell,t)} \alpha \, (-C) \, dV \\ &= -C\alpha \{V_\delta(\ell,t) - V_\delta(0,t)\} \\ &= -C\alpha \{V_\delta(t-t_1) - V_\delta(t)\} \quad , \end{aligned} \tag{4.31}$$

where,

$$t_1 = \ell/C \quad .$$

The pressure gradient force is approximated from linear theory. The pressure by a wave is:

$$P_w = \rho g \cosh kz/\cosh kh \cdot \eta \quad .$$

The particle velocity is:

$$V = \omega \cosh kz/\sinh kh \cdot \eta \quad .$$

In these equations z is taken zero at the bottom and is measured upward from the bottom. Dividing P_w by V, we have a relationship between P_w and V.

$$P_w = \rho g \frac{\cosh kz}{\cosh kh} \frac{\omega}{\sinh kh} \eta \quad .$$

$$= \rho \frac{g}{\omega} \frac{\cosh kz}{\tanh kh} V \quad . \tag{4.32}$$

Using this relationship, the pressure gradient force can be expressed in terms of velocity.

$$\begin{aligned} F_P &= A_e \, \Delta P \\ &= A_e \, (P_1 - P_2) \\ &= A_e \{ \rho C \, V_\delta(o,t) - \rho C \, V_\delta(\ell,t) \} \\ &= A_e \rho C \, \{V_\delta(t) - V_\delta(t-t_1)\} \end{aligned} \tag{4.33}$$

where A_e is the cross section area of a plate edge.
The inertial force and the pressure gradient force are combined and expressed by:

$$\begin{aligned} F_{IP} &= F_I + F_P \\ &= C \, (\alpha + A_e \rho)\{V_\delta(t) - V_\delta(t-t_1)\} \\ &= A \, \{V_\delta(t) - V_\delta(t-t_1)\} \end{aligned} \tag{4.34}$$

where,

$$A = C \, (\alpha + A_e \rho)$$
$$= 1/t_1 \cdot (m + 2\rho \forall)$$

The shear force per unit length of the plate is:

$$F_s = 1/2 \cdot \rho C_f \, A_p/\ell \cdot V_\delta(x,t) |V_\delta(x,t)|$$
$$= \beta \, V_\delta(x,t) |V_\delta(x,t)|$$

where,

$$\beta = 1/2 \cdot \rho C_f \, A_p/\ell \quad ,$$

and the friction factor, C_f, is defined in the form of the instantaneous bed shear stress, τ_b, giving:

$$\tau_b = 1/2 \cdot \rho C_f \, V_\delta |V_\delta| \, . \tag{4.35}$$

A_p is the area of the shear plate. Introducing a new

variable, $X_V(x,t) = V(x,t)|V(x,t)|$, the shear force per unit length is;

$$F_s = \beta X_V(x,t) \quad .$$

The total shear force on the plate is:

$$\begin{aligned} F_S &= \int_0^{\ell} F_s \, dx \\ &= \int_0^{\ell} \beta \, X_V(x,t) \, dx \\ &= \int_0^{\ell} \beta \, \partial Y_V(x,t)/\partial t \, dx \\ &= \int_{Y_V(0,t)}^{Y_V(\ell,t)} - \beta C \, dY_V \\ &= - \beta C \{Y_V(\ell,t) - Y_V(0,t)\} \\ &= - \beta C \{Y_V(t-t_1) - Y_V(t)\} \\ &= B \{Y_V(t) - Y_V(t-t_1)\} \quad , \end{aligned} \tag{4.36}$$

where,

$$Y_V(x,t) = \int X_V(x,t) \, dt$$

and,

$$\begin{aligned} B &= \beta C \\ &= 1/t_1 \cdot (\rho C_f A_p/2) \quad . \end{aligned} \tag{4.37}$$

Finally, the measured total force, F_T , is;

$$\begin{aligned} F_T(t-t_2) &= F_{IP}(t) + F_S(t) \\ &= A \{V_\delta(t) - V_\delta(t-t_1)\} + B \{Y_V(t) - Y_V(t-t_1)\} \, . \end{aligned} \tag{4.38}$$

The time lag, t_2, between the wave force measurement on the shear plate and the fluid velocity measurement is due to three reasons: the physical phase shift between the bed

shear stress and the fluid velocity, the position of the current meter relative to the shear plate position and the small time lag in recording, which is 1/90 of a second at Station 5 and 1/45 of a second at Station 5A.

Applying a Fourier transform to each term of (4.38) yields:

$$\int_{-\infty}^{\infty} F_T(t-t_2)\, e^{-i2\pi ft}\, dt = F_T(f)\, e^{-i2\pi ft_2}$$

$$\int_{-\infty}^{\infty} A\,\{V_\delta(t) - V_\delta(t-t_1)\}\, e^{-i2\pi ft}\, dt = A\, V_\delta(f)\{1 - e^{-i2\pi ft_1}\}$$

$$\int_{-\infty}^{\infty} B\,\{Y_v(t) - Y_v(t-t_1)\}\, e^{-i2\pi ft}\, dt = B\, Y_v(f)\{1 - e^{-i2\pi ft_1}\}$$

$$= B/i2\pi f \cdot X_v(f)\{1 - e^{-i2\pi ft_1}\}$$

where, $X_v(f = 0) = 0$. Separating each force into the real part and the imaginary part, we find the expression for each force as:

$$F_T(f)\, e^{-i2\pi ft_2}$$

$$= \sqrt{R_t + iI_t}\, \cos(\theta_1 - \theta_2) + i \sin(\theta_1 - \theta_2) \qquad (4.39)$$

$$A\, V_\delta(f)\,\{1 - e^{-i2\pi ft_1}\}$$

$$= A\,\{(R_v \cdot S - I_v \cdot T) + i(R_v \cdot T + I_v \cdot S)\} \qquad (4.40)$$

$$B/i2\pi f \cdot X_v(f)\,\{1 - e^{-i2\pi ft_1}\}$$

$$= B/2\pi f \cdot \{(R_x \cdot T + I_x \cdot S) - i(R_x \cdot S - I_x \cdot T)\} \qquad (4.41)$$

In the above equations, the following definitions apply:

$$\cos\theta_1 = R_t/(R_t^2 + I_t^2)^{1/2}$$

$$\sin\theta_1 = I_t/(R_t^2 + I_t^2)^{1/2}$$

$$\theta_2 = 2\pi ft_2$$

$$S = 1 - \cos 2\pi f t_1$$

$$T = \sin 2\pi f t_1$$

also R and I denote the magnitude of the real part and the imaginary part, respectively. Collecting the real parts and the imaginary parts separately from (4.39), (4.40) and (4.41), we have:

$$(R_t^2 + I_t^2)^{1/2} \cos(\theta_1 - \theta_2) = A(R_v \cdot S - I_v \cdot T) + B/2\pi f \cdot (R_x \cdot T + I_x \cdot S) \quad (4.42)$$

$$(R_t^2 + I_t^2)^{1/2} \sin(\theta_1 - \theta_2) = A(R_v \cdot T + I_v \cdot S) - B/2\pi f \cdot (R_x \cdot S - I_x \cdot T) \quad . \quad (4.43)$$

Squaring and summing (4.42) and (4.43), the term of t_2 is eliminated:

$$R_t^2 + I_t^2 = 2(1 - \cos 2\pi f t_1)\{A^2(R_v^2 + I_v^2) + (B/2\pi f)^2(R_x^2 + I_x^2) + 2AB/2\pi f \cdot (R_v \cdot I_x - I_v \cdot R_x)\} \quad . \quad (4.44)$$

We can re-express (4.44) in a simple form as:

$$A^2 X + B^2 Y + AB Z = W \quad (4.45)$$

where,

$$X = 2(1 - \cos 2\pi f t_1)(R_v^2 + I_v^2) \quad ,$$

$$Y = 2(1 - \cos 2\pi f t_1)(R_x^2 + I_x^2)/(2\pi f)^2 \quad ,$$

$$Z = 4(1 - \cos 2\pi f t_1)(R_v I_x - I_v R_x)/(2\pi f) \quad ,$$

and,

$$W = R_t^2 + I_t^2 \quad .$$

From the expression $(1-\cos 2\pi f t_1)$ we can see the limitation of the frequency range with respect to the size of the shear plate. When $f t_1 \geq 1$, the shear plate is longer than the wave

length of the frequency components and the shear plate no longer distinguishes these components.

Equation (4.45) is solved for A and B using a least square method. The details of this procedure are shown in Appendix A. It should be noted that an increase in the amount of data results in an increase in the reliabilty of the least square method. There are two ways to increase the data. One is to increase the wave nonlinearity; i.e. to increase frequency components. The other is to shorten the shear plate length. Conversely, the accuracy of the results decreases for waves with less frequency components and for short period waves. As shown in Appendix A, the final equation from the least square method in this case is a fourth order polynomial. The polynomial was numerically solved using the Siljak function. Only the positive real roots were taken. If there were more than one positive real root, the root with a better fit to the time series of wave forces was chosen. Figure 4.4 and 4.5 show a comparison of the calculated shear force with the measured total force as well as a comparison of the calculated total force with the measured total force. Figure 4.4 is an example for the concrete bed and Figure 4.5 is one for the gravel bed. For the concrete bed, the results were not very successful. Many cases for the smooth roughness did not have a positive real root, and even if having a positive real root, in some cases the calculated answer did not fit to the measured time

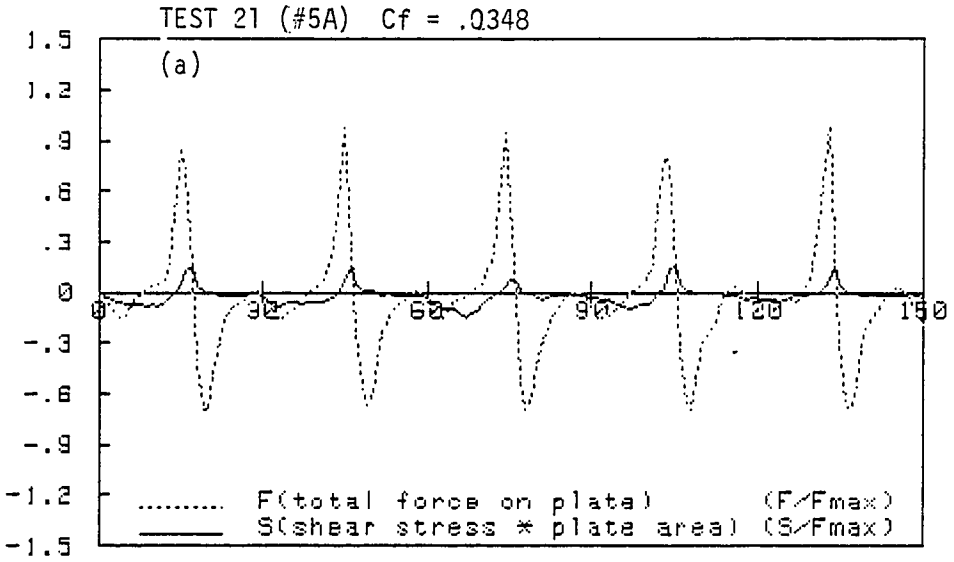

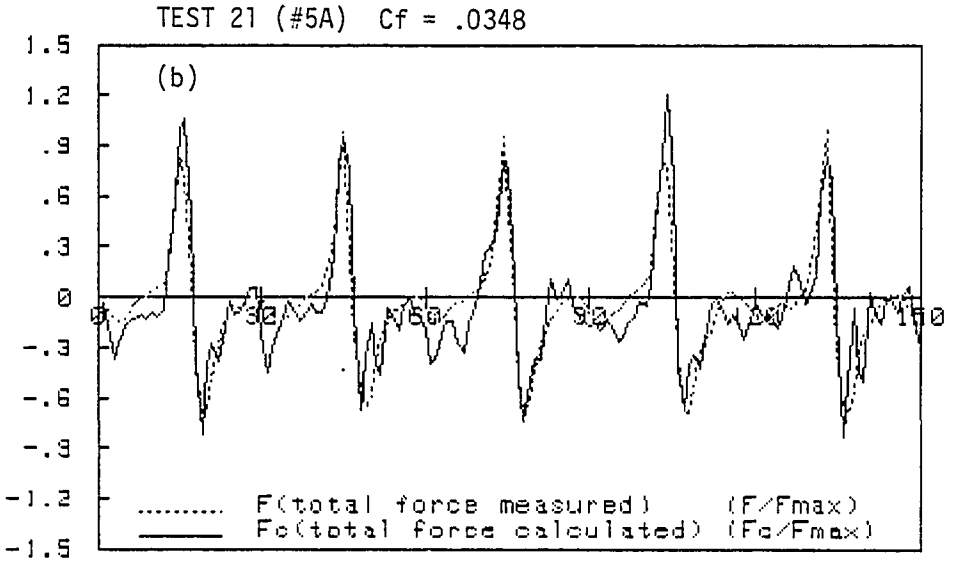

Figure 4.4 Comparison of the measured total wave force on the shear plate with (a) the calculated shear force and with (b) the calculated total wave force: for the concrete bed.

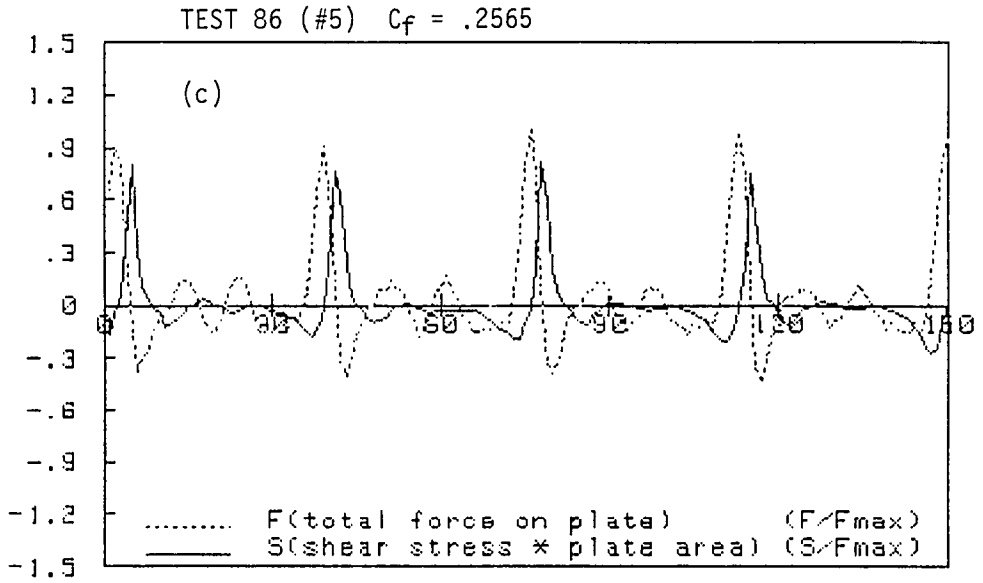

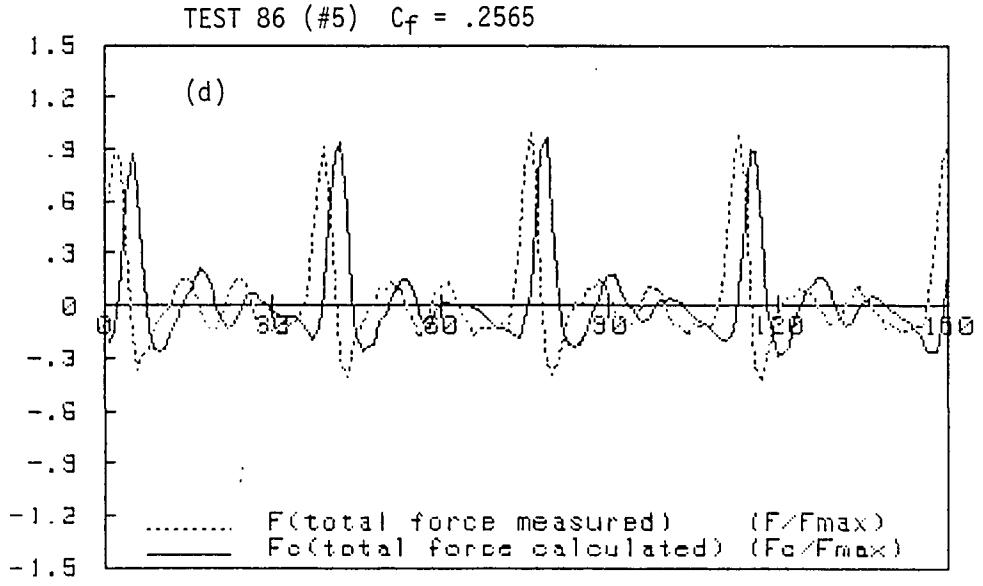

Figure 4.5 Comparison of the measured total wave force on the shear plate with (c) the calculated shear force and with (d) the calculated total wave force: for the gravel bed.

series well. One of the reasons is that the magnitude of the shear force for such a smooth surface is very small relative to the total force, as shown in Figure 4.4. A small error in the total force strongly affects the determination of the shear force. The possible sources of error are the static calibration of shear plate and two assumptions made, i.e., the same time history of velocity at the front and back plate edges and the constant wave celerity over the plate. For the gravel bed, the results were very good in that the predicted total force was very similar to the measured force, with the exception of a few cases in which the wave periods are short (one second) and waves are very small. The results of the friction factor determination are shown in Figure 4.6. It is interesting to note that the friction factors for the gravel bed fit Jonsson's curve, (4.22). For the concrete bed the friction factors are rather large relative to those predicted from existing theories. Figure 4.7 examines the types of turbulence which were used in the experiments. This figure shows that the experiments for the gravel bed belong to the rough turbulent zone and the ones for the concrete bed are in the transition from the smooth turbulent zone to the rough turbulent zone. Consequently, it is reasonable for the concrete surface to exhibit rather large friction factors.

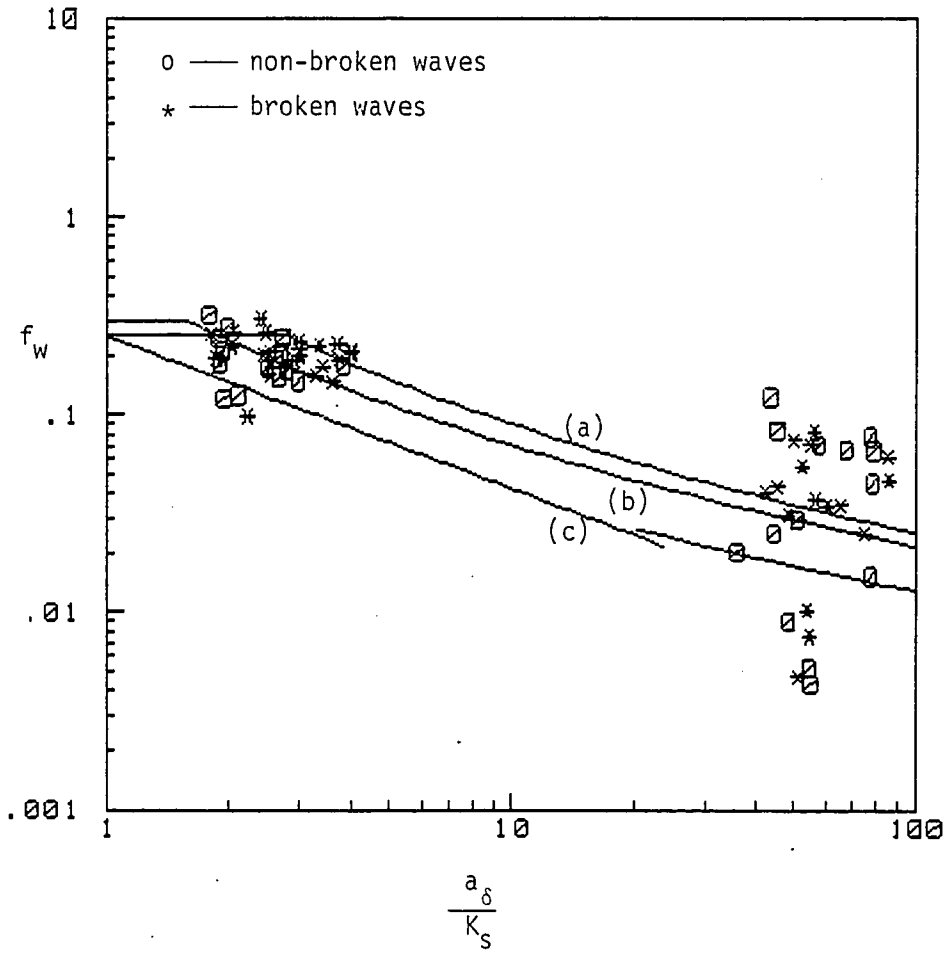

Figure 4.6 Comparisons of experimental friction factors under nonlinear wave conditions with existing curves of friction factors, (a) Kajiura, (b) Jonsson, and (c) Riedel.

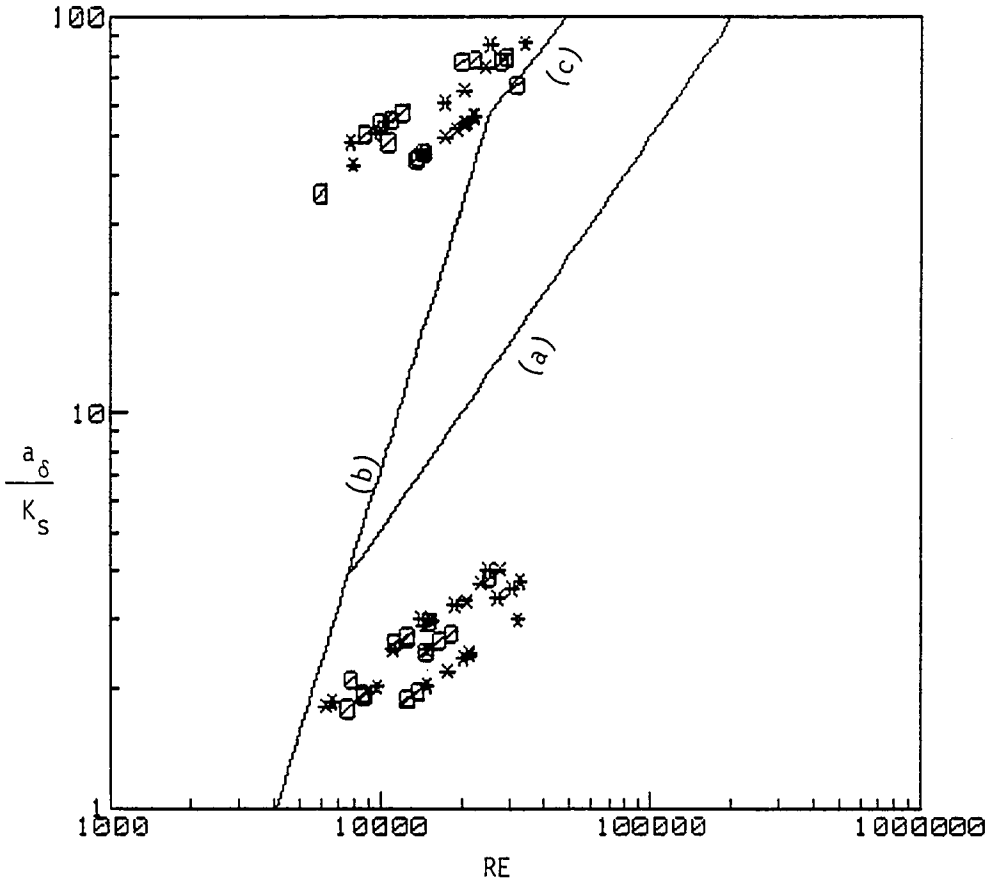

Figure 4.7 Examination of very rough turbulent conditions in the experiments, (a) Kajiura, (b) Sleath and (c) Jonsson. (o —— non-broken waves, * —— broken waves.)

4.4.4 Empirical Energy Dissipation

The energy dissipation pertinent to this experiment is defined by (4.16) since there is no net mass transport, i.e. $\bar{U} = 0$ in (4.15). (It is, however, possible that there is shoreward mass transport in the surface water layer and offshoreward mass transport in the bottom water layer.) From (4.16) and (4.35), energy dissipation is:

$$E_{dw} = -\overline{u_\delta \tau_b} = -1/2 \cdot \rho C_f |u_\delta| V_\delta^2 \qquad (4.46)$$

where $V_\delta = U_\delta + u_\delta$ and U_δ is the steady velocity. From linear wave theory, the maximum fluid velocity, $u_{\delta lm}$, at the bed is:

$$u_{\delta lm} = \pi H/(T \sinh kh) \quad . \qquad (4.47)$$

Inserting (4.47) into (4.46), energy dissipation, E_{dl}, for the linear wave is:

$$E_{dl} = -2/3\pi \cdot \rho C_f \{\pi H/(T \sinh kh)\}^3 \qquad (4.48)$$

where $U_\delta = 0$ for the linear waves.

Now, we can compare the empirical energy dissipation to the theoretical results by dividing (4.46) by (4.48) giving:

$$E_{dw}/E_{dl} = 3\pi/4 \cdot |u_\delta| V_\delta^2 \quad . \qquad (4.49)$$

This ratio was plotted against the nonlinearity parameter P_n and is shown in Figure 4.8. In the calculation of $u_{\delta lm}$, the measured significant wave height was used. The figure shows that the energy dissipation predicted by linear wave theory overestimates that for highly nonlinear waves. The trend of the plot, however, is not conclusive because the data do not

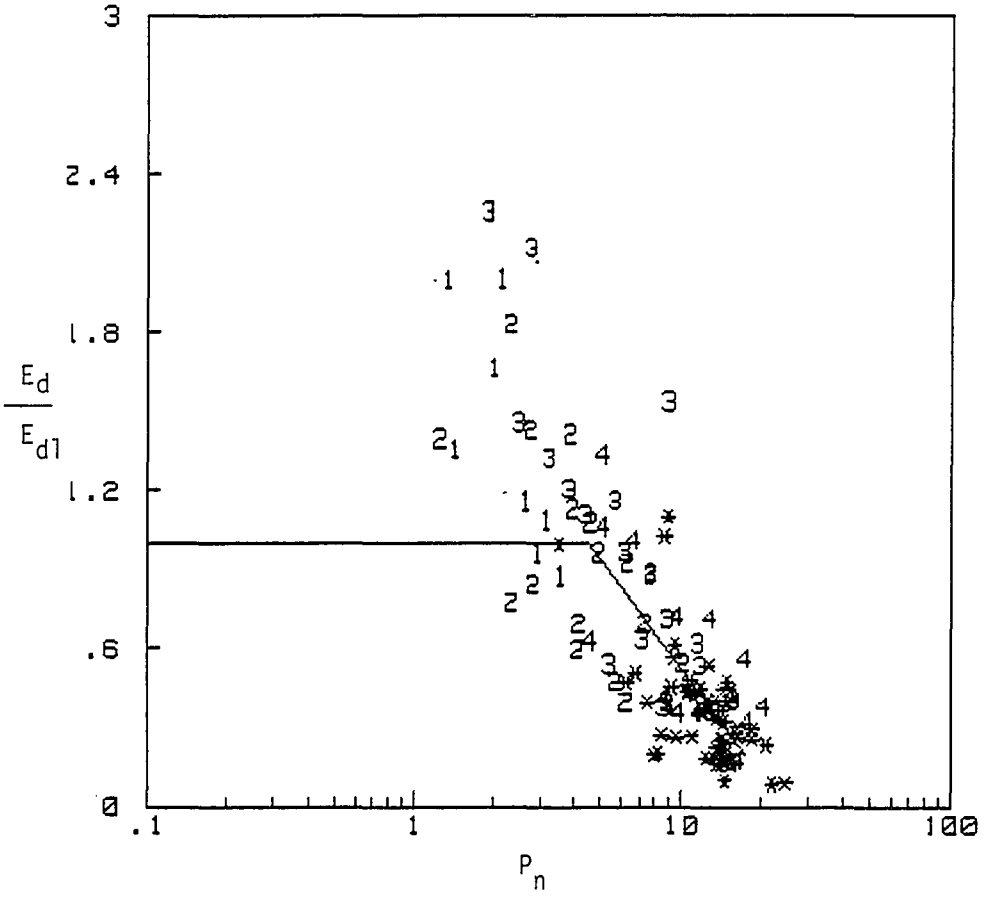

Figure 4.8 The ratio of experimental energy dissipation due to bed shear stress to energy dissipation calculated using linear wave theory versus wave nonlinearity parameter, P_n. (Numbers plotted denote rounded non-broken wave periods and cross marks refer to broken waves.)

cover the whole range of P_n. For small values of P_n, the ratio should approach the value of unity, but such a trend is not seen from the available data. In Figure 4.8, the cross sign indicates breaking or broken waves. An approximated empirical rule is:

$$E_d = E_{dl} \qquad \text{for } P_n \leq 4.5, \qquad (4.50)$$

$$E_d = E_{dl} \, (-1.365 \log P_n + 1.891) \qquad \text{for } P_n > 4.5, \qquad (4.51)$$

and minimum energy dissipation, E_{dmn} is :

$$E_{dmn} = 0.1 \, E_{dl} \; . \qquad (4.52)$$

The value of E_{dmn} is arbitrarily chosen.

CHAPTER 5

WAVE BREAKING AND ENERGY DISSIPATION

5.1 Wave Breaking

The breaking wave phenomenon is an important area of study in coastal engineering. It is the dominant factor in wave energy dissipation. Since there are no generally acceptable theories available regarding the breaking phenomenon, analysis in this area must depend on empirical rules.

Michell (1893) found that the limiting steepness for deep water waves is:

$$H_b/L_b = 0.142 \simeq 1/7 \quad . \tag{5.1}$$

McCowan (1894) obtained the familiar wave breaking condition from solitary wave theory as:

$$H_b/D_b = 0.78 \quad .$$

Iversen (1952) and Galvin (1969) found from their laboratory experiments that the ratio of the breaking wave height, H_b, to the depth, D_b, depends on the beach slope, s. Bowen (1968) demonstrated that H_b/D_b is a function of a parameter which consists of the beach slope and the deep water wave steepness. Replacing the deep water wave height in this combined parameter by the local wave height, Battjes (1974) called it a similarity parameter and discussed the usefulness of the parameter. The similarity parameter was

defined as:

$$\varepsilon = s/(H/L_o)^{1/2} \quad . \tag{5.2}$$

Le Méhauté and Koh (1967) also showed that the breaking wave condition is a function of the beach slope and the deep water wave steepness. They obtained the following empirical formula:

$$H_b/L_b = 0.76\, s^{1/7}(H_o/L_o)^{-1/4} \quad . \tag{5.3}$$

Weggel (1972) analyzed the dependence of H_b/D_b on the wave steepness and on the beach slope and proposed this relationship:

$$H_b/D_b = b[s] - a[s]\, H_b/T^2 \tag{5.4}$$

where,

$$a[s] = 1.36\,(1 - e^{-19s}) \qquad (sec^2/ft)$$

and,

$$b[s] = 1/\{0.64\,(1.0 + e^{-19.5s})\} \quad .$$

In (5.4), a[s] has dimensions of (sec^2/ft).

Meanwhile, Svendsen and Hansen (1976) found that the ratio, H_b/D_b, is primarily a function of a slope parameter. The slope parameter is a combination of the beach slope and the relative water depth:

$$S_p = s/(D_b/L_b) \quad . \tag{5.5}$$

In this study, an attempt was made to obtain the wave breaking condition in terms of the beach slope and the nonlinearity parameter, P_n, which consists of the wave steepness and the relative depth. Data used were from other investigations; Iversen (1952), Bowen et.al. (1968), Galvin

(1969), Van Dorn (1976), Hansen and Svendsen (1979) and Nadaoka et.al. (1982). The range of beach slopes used was from 1/5 to 1/50. Using (5.1), the empirical form of H_b/D_b was modeled by a power regression curve as:

$$H_b/D_b = B\,(P_b - 1/7)^A$$

where P_b is the nonlinearity parameter, P_n, for the breaking waves. Coefficients A and B were determined for each beach slope. Using another power regression curve, A and B can be expressed as:

$$A = a_1\, s^{a2}$$

$$B = b_1\, s^{b2}$$

where a_1, a_2, b_1, and b_2 are constant coefficients. They were determined to have the following values:

$$a_1 = 1/2$$

$$a_2 = 1/4$$

$$b_1 = 1/2$$

$$b_2 = 0 \quad .$$

Consequently, the final form for H_b/D_b is:

$$H_b/D_b = 1/2 \cdot (P_b - 1/7)^{1/2 \cdot s^{1/4}} \quad . \qquad (5.6)$$

The estimates of H_b from (5.3), (5.4) and (5.6) are shown in Figures 5.1. Correlation coefficients of these estimates to measured values of H_b are 0.96 for (5.4) and 0.98 for (5.3) and (5.6). From this it may be concluded that the empirical relationship expressed by (5.6) gives a better estimate of H_b than does (5.4), and as good as (5.3). In (5.6), H_b is

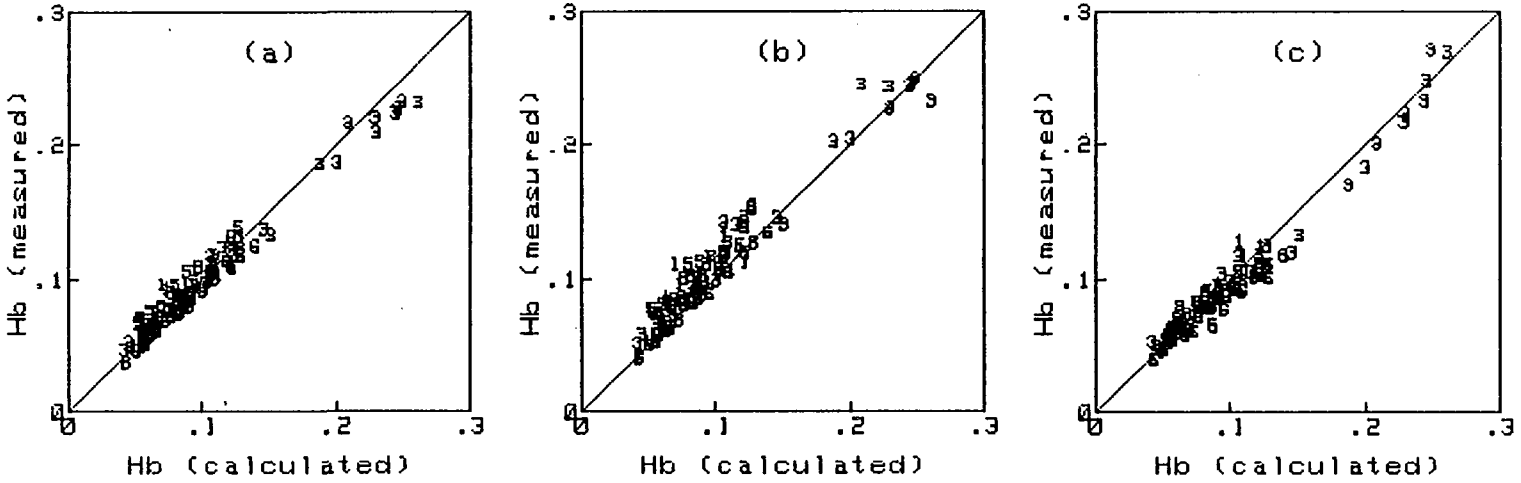

Figure 5.1 Comparisons between measured initial wave breaking height and calculated wave breaking heights; (a) wave breaking height from the present formula, (b) wave breaking from Weggel formula and (c) Le Mehaute and Kou's formula.

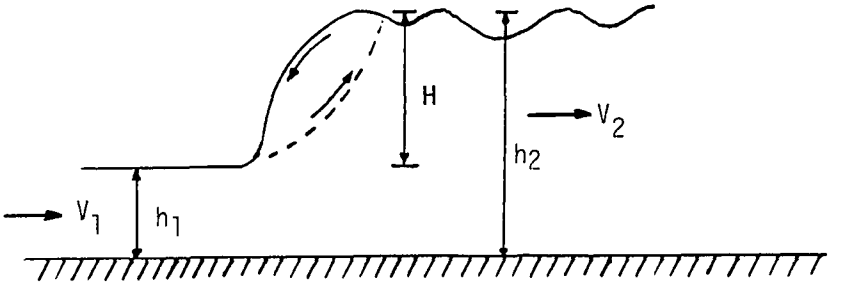

Figure 5.2 Diagram of hydraulic jump.

determined only from local properties, whereas (5.3) requires the deep water wave height.

5.2 Energy Dissipation Due to Wave Breaking

The energy dissipation in a breaking wave is the main cause of wave attenuation. Investigators of this process have estimated the dissipation by adopting the related phenomenon of a hydraulic jump as a model for breaking wave. Those are Hwang and Divoky (1970), Svendsen et.al. (1978), Battjes (1978), Gerritsen (1981) and Stive (1984).

The change in energy level, ΔH, through a hydraulic jump is given by:

$$\Delta H = (h_2 - h_1)^3/(4\, h_1 h_2) \qquad (5.7)$$

where h_1 is water depth before the jump and h_2 is the one after the jump. See Figure 5.2 for an illustration of this process. The rate of energy change, dE_T/dt per unit width

in a bore, which is referred to a moving hydraulic jump, is given by:

$$dE_1/dt = - \rho g q \Delta H \qquad (5.8)$$

where the discharge of water per unit width is defined by:

$$q = (C - V_1)\, h_1 \quad . \qquad (5.9)$$

C is the velocity of the bore and V_1 is the flow velocity before the jump. Relating the rate of dissipation of the total energy in a bore to the rate of energy dissipation per unit of distance, we find:

$$dE_1/dt = C\, dE_1/dx \quad . \qquad (5.10)$$

The mean energy per unit area, E, equals:

$$E = E_1/L \qquad (5.11)$$

where L is considered as a distance between consecutive bores.

The energy flux, F, is given by:

$$F = C_{gr}\, E \quad . \qquad (5.12)$$

The rate of change of the energy flux is:

$$dF/dx = d(C_{gr}\, E)/dx$$

$$= C_{gr}\, dE/dx + E\, dC_{gr}/dx \quad . \qquad (5.13)$$

From (5.10) and (5.11) the gradient of the mean energy per unit area is:

$$dE/dx = (1/C \cdot dE_1/dt - E\, dL/dx)/L \quad . \qquad (5.14)$$

Inserting (5.14) into (5.13), we obtain:

$$dF/dx = n/L \cdot dE_1/dt + E\, (-C_{gr}/L \cdot dL/dx + dC_{gr}/dx) \qquad (5.15)$$

The second term of the right hand side of (5.15) implicitly

shows the bed slope and the change of wave height influence on the energy flux in addition to the dissipation from hydraulic jump. Including the second term of (5.15) in the first term, we define the energy dissipation, E_b, in a breaking wave as:

$$E_b = - dF/dx = - A_\varepsilon/L \cdot dE_1/dt \qquad (5.16)$$

where A_ε is an empirical coefficient. From (5.7), (5.8) and (5.9), dE_1/dt can be expressed in terms of the wave height, H, and the mean water depth, D:

$$dE_1/dt = - \rho g C \alpha^2/4 \cdot (H/D)/(\alpha H/D + 1)\ H^2 \qquad (5.17)$$

where,

$$H = h_2 - h_1$$

$$V_1 h_1 = \eta_t\ C$$

and,

$$D = h_1 - \eta_t = \alpha\ h_1 \ .$$

α is an empirical constant determined to be 1.22, see Figure 5.3. Inserting (5.17) into (5.16) we obtain:

$$E_b = A_\varepsilon \alpha^2/4 \cdot \rho g/T \cdot (H/D)/(\alpha H/D + 1)\ H^2 \qquad (5.18)$$

or

$$E_b = A_\varepsilon \alpha^2/8\pi \cdot \rho g \cdot (H/D)/(\alpha H/D + 1)\ \omega H^2 \ . \qquad (5.19)$$

Introducing a coefficient ζ, which is defined as:

$$\zeta = \sqrt{2}\ A_\varepsilon \alpha^2\ (H/D)/(\alpha H/D + 1) \ ,$$

E_b is expressed in the same form as Gerritsen (1981) used:

$$E_b = \zeta/(8\pi\sqrt{2}\ ) \cdot \rho g \omega H^2 \ . \qquad (5.20)$$

Using (3.6) we can express (5.20) in terms of the total mean

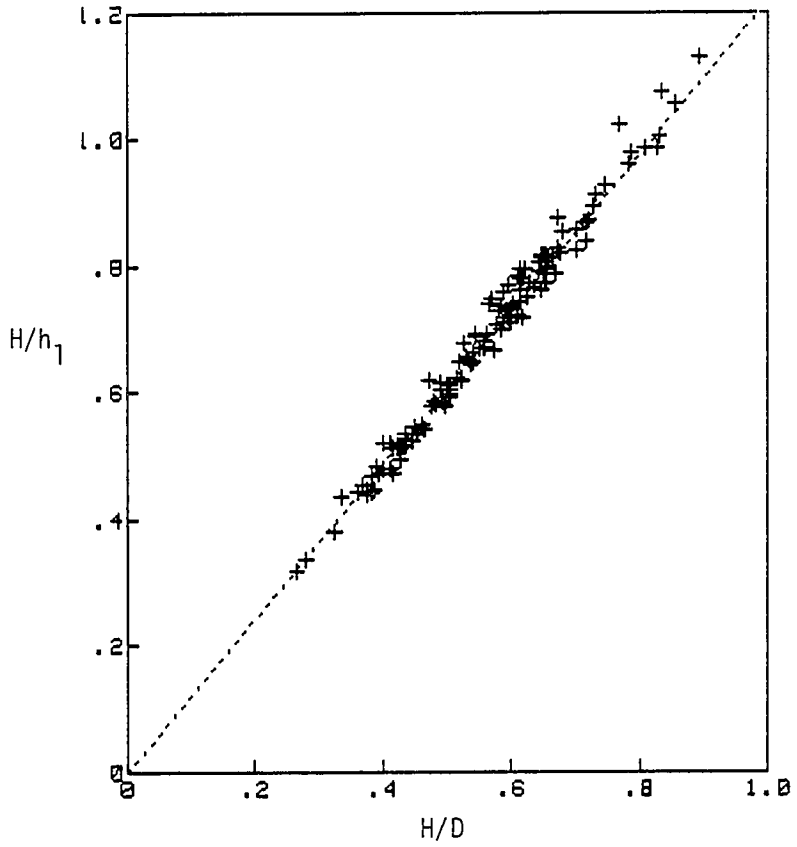

Figure 5.3 The ratio of broken wave height to water depth at the trough versus the ratio of broken wave height to mean water depth.

energy density, E, and the nonlinearity parameter, P_a:

$$E_b = \zeta/(8\pi\sqrt{2}) \cdot \omega E f^2(P_a) \quad . \tag{5.21}$$

It should be noted that in this formulation E is defined as two times the potential energy, and the wave height is the mean value of the largest one-third of wave heights. The potential energy is defined in terms of the variance of water surface fluctuations.

Hwang and Divoky used an A_ε value of 0.8 in an analytical prediction of wave set-up and wave height in the breaking zone.

Svendsen et.al. found A_ε to range from 1.4 to 1.6 . Battjes used an A_ε of 1.0 in an irregular wave analysis and found good agreement between predictions and experimental data. Gerritsen used ζ values in his laboratory study. ζ values used by Gerritsen ranged from 0.3 to 0.5. Using H/D=0.6 A_ε values corresponding to these ζ values are estimated from 0.4 to 0.7. Stive experimentally obtained A_ε values and used A_ε values of 1.3 and 1.6 in his prediction model. He generalized A_ε as a function of the similarity parameter, ε_0 , expressed as (5.2) in terms of H_0.

In order to determine A_ε values in this study, the energy equation, (5.16) was numerically solved for E including the dissipation by bottom friction. The calculated values of E were fitted to the data by adjusting A_ε values. The A_ε values obtained in this way are 0.15 for one-second waves, 0.27 for two-second waves, 0.40 for

three-second waves and 0.50 for four-second waves. Wave heights and mean wave energies calculated using these values of A_ε are compared with data in Figure 5.4 to 5.7. There appears to be little dependence on the deep water wave steepness. In this regard, the results do not agree with Stive's results. Using Stive's experimental wave heights in the present semi-emprical model, values of A_ε were found to be 0.9 for both tests. The quantitative difference of A_ε between Stive's model and the present model result mainly from the discrepancies in the energy density values. Stive showed that the experimentally obtained mean energy flux, F, was closely predicted from the following approximation in the inner region of breaking zone:

$$F = 1/8 \cdot \rho g H^2 (gh)^{1/2} \quad . \tag{5.22}$$

In performing calculations using the present model, P_a values were found to be about 6 for test 1 and about 10 for test 2 of Stive's experiments; i.e., H/η_{rms} are 3.5 and 4.6, respectively. This means that the mean energy densities used by Stive are 1.5 and 2.6 times greater than the energy density used in the present model for test 1 and test 2, respectively. Nonetheless, the predicted wave height decay rates agree well with Stive's data, see Figure 5.8. A_ε values were also obtained using Horikawa and Kuo's data (1966),see Figure 5.9. These A_ε values are plotted in Figure 5.10 against the modified slope parameter, $S_*=s/(D/L)^{1/2}$ The trend is quite clear. However, the values

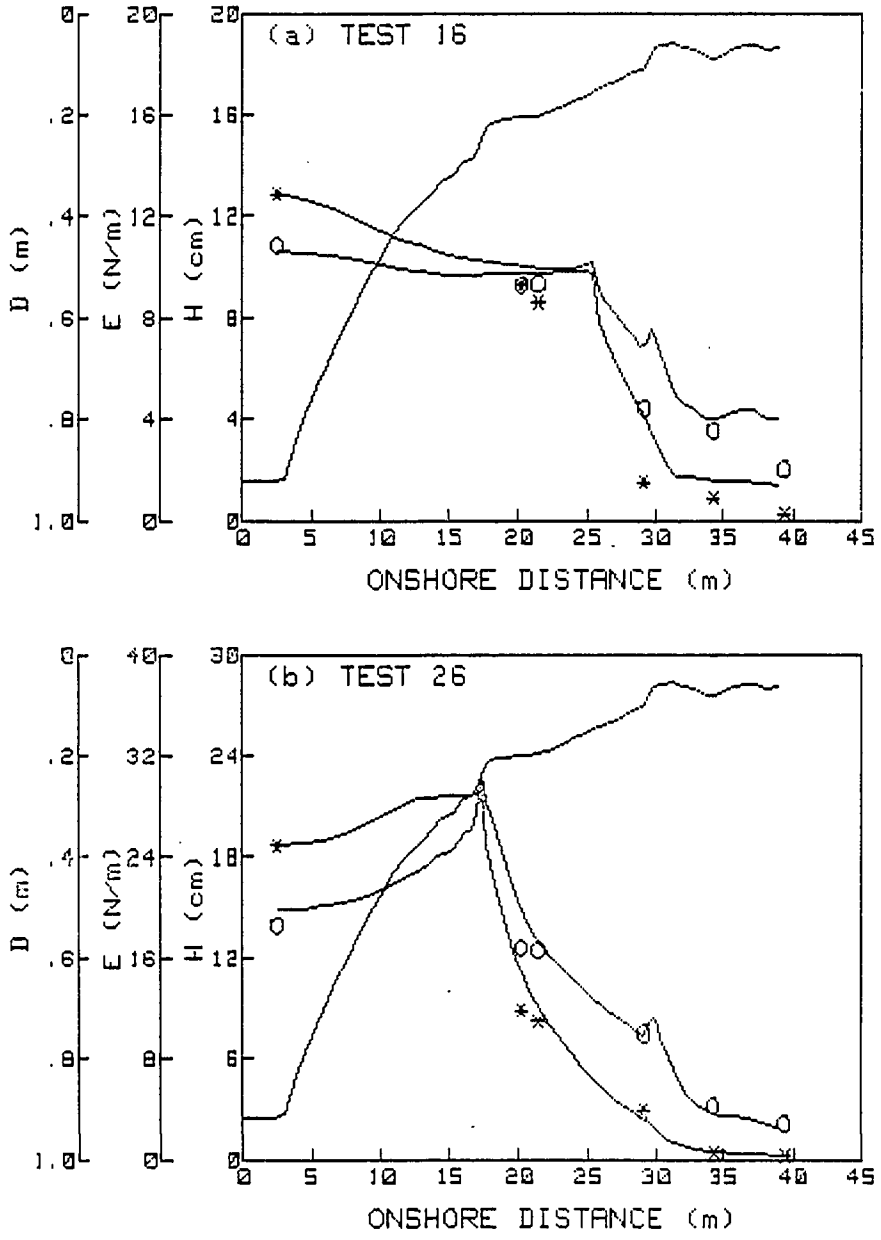

Figure 5.4 Changes in wave Heights and in mean wave energy for the wave periods, (a) one second and (b) two seconds over the concrete bed. (* —— mean wave energy per unit area, o —— wave heights)

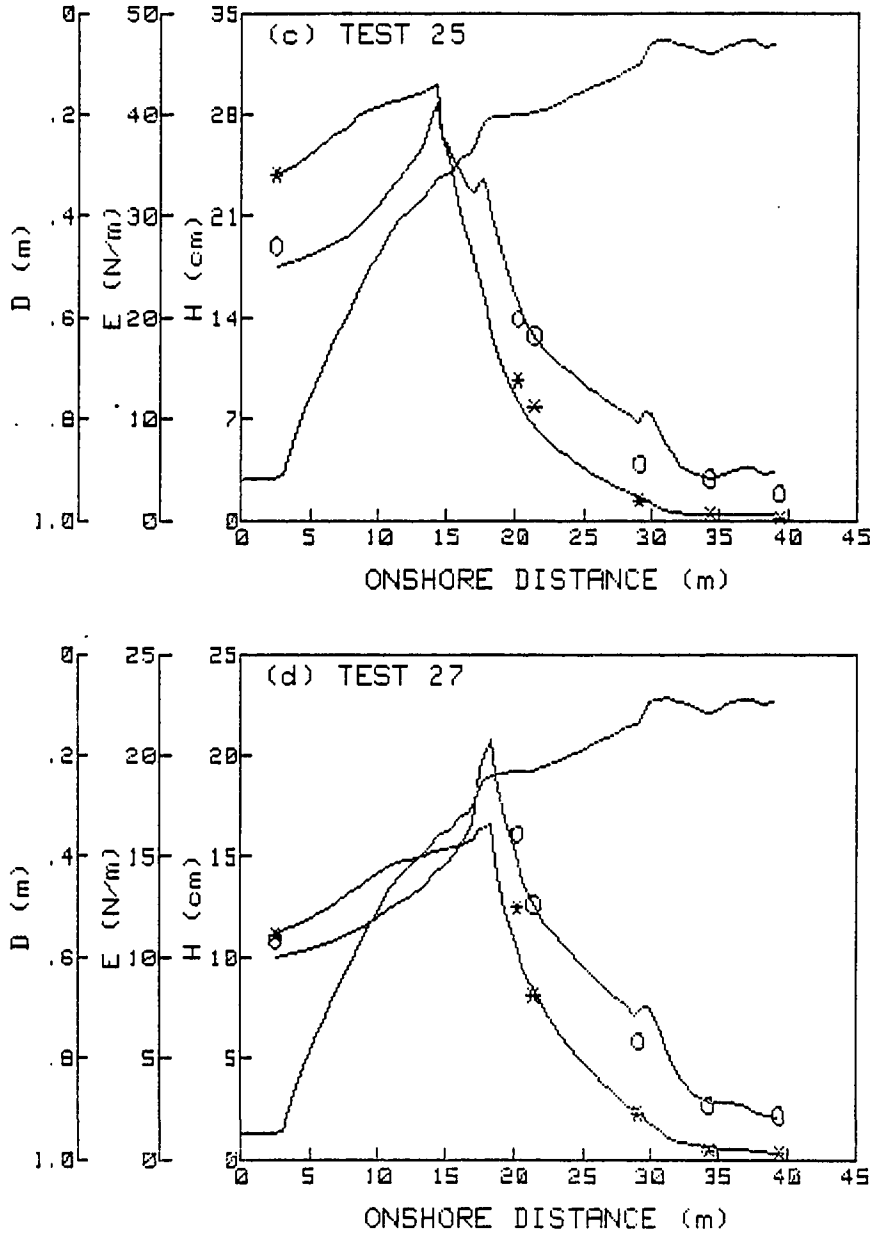

Figure 5.5 Changes in wave heights and in mean wave energy for the wave periods, (c) three seconds and (d) four seconds over the concrete bed. (* —— mean wave energy per unit area, o ___ wave heights)

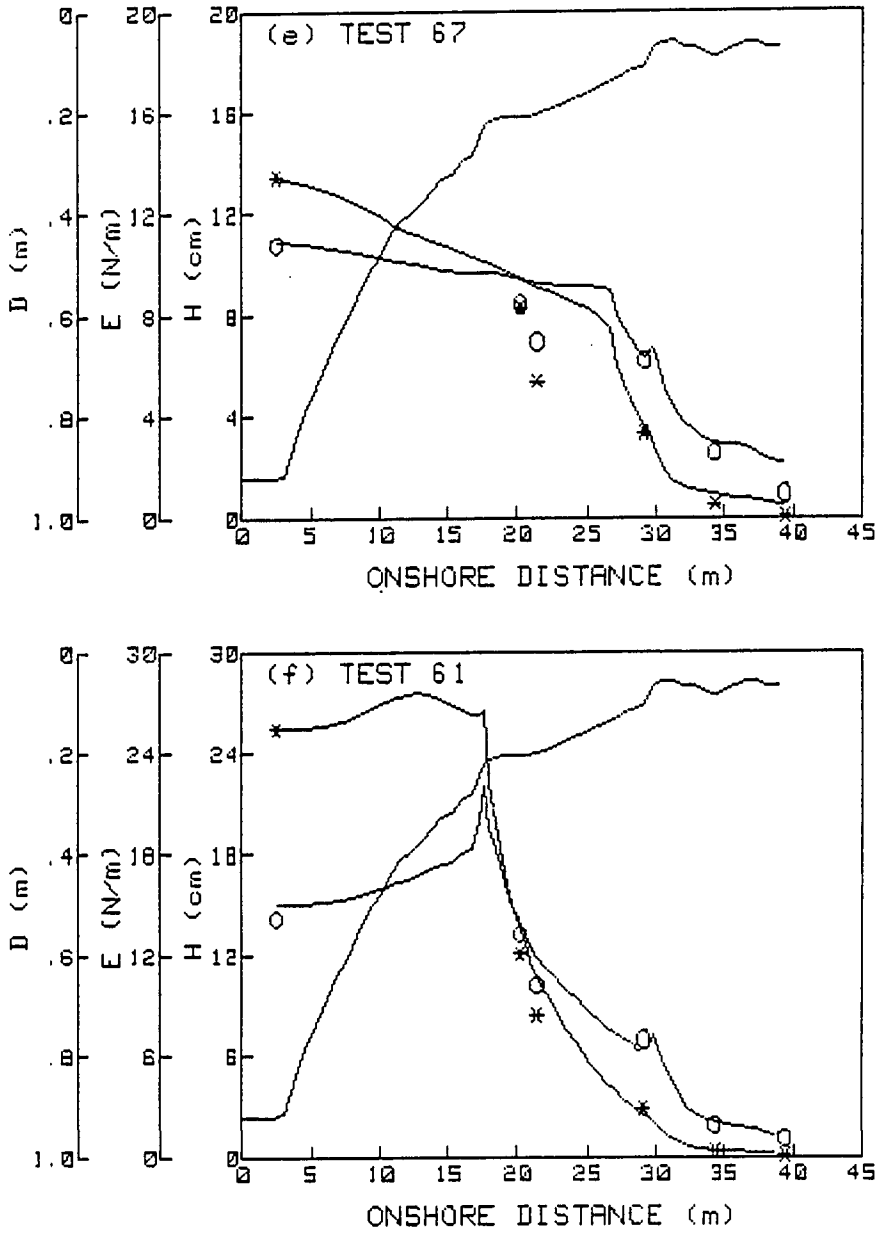

Figure 5.6 Changes in wave heights and in mean wave energy for the wave periods; (e) one second and (f) two seconds over the gravel bed. (* ___ mean wave energy per unit area, o ___ wave heights)

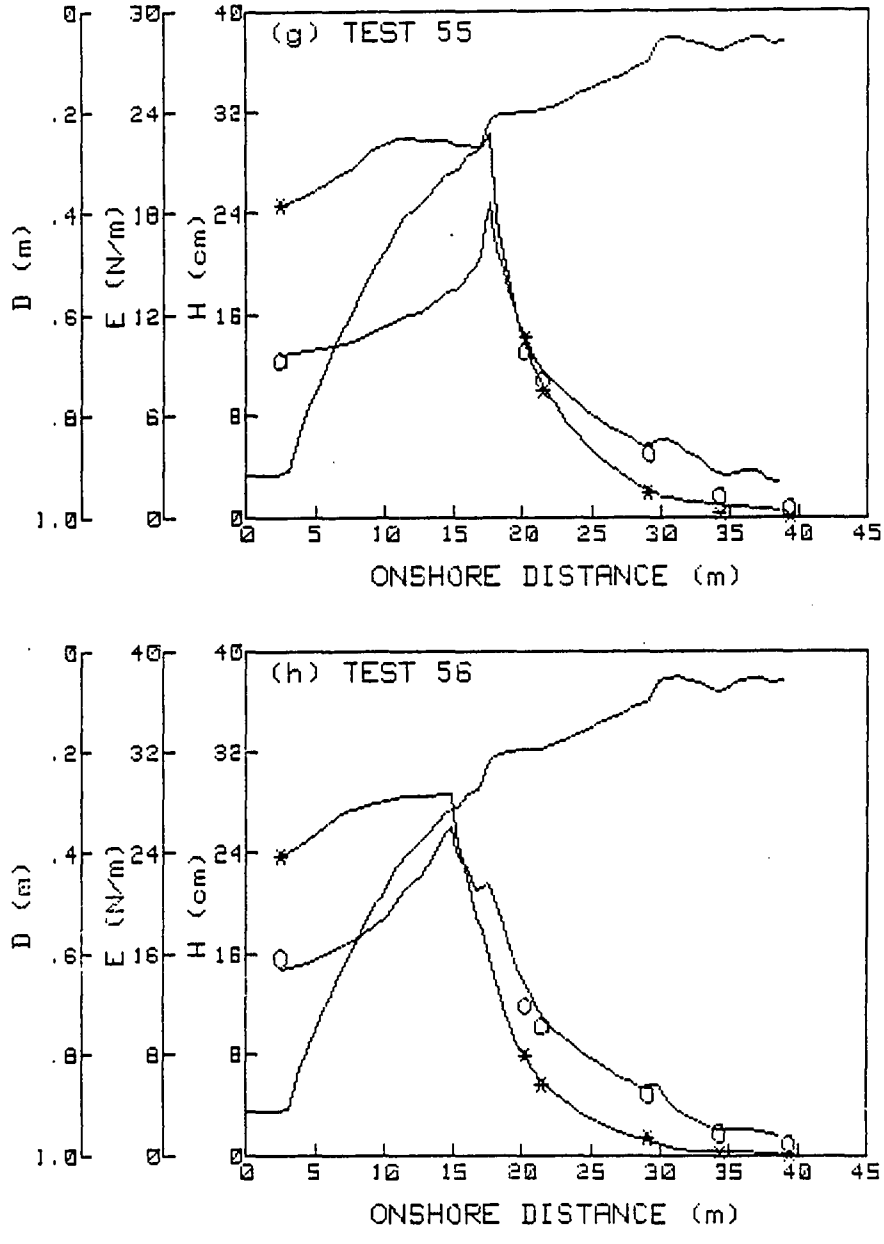

Figure 5.7 Changes in wave heights and in mean wave energy for the wave periods; (g) three seconds and (h) four seconds over the gravel bed. (* —— mean wave energy per unit area, o —— wave heights)

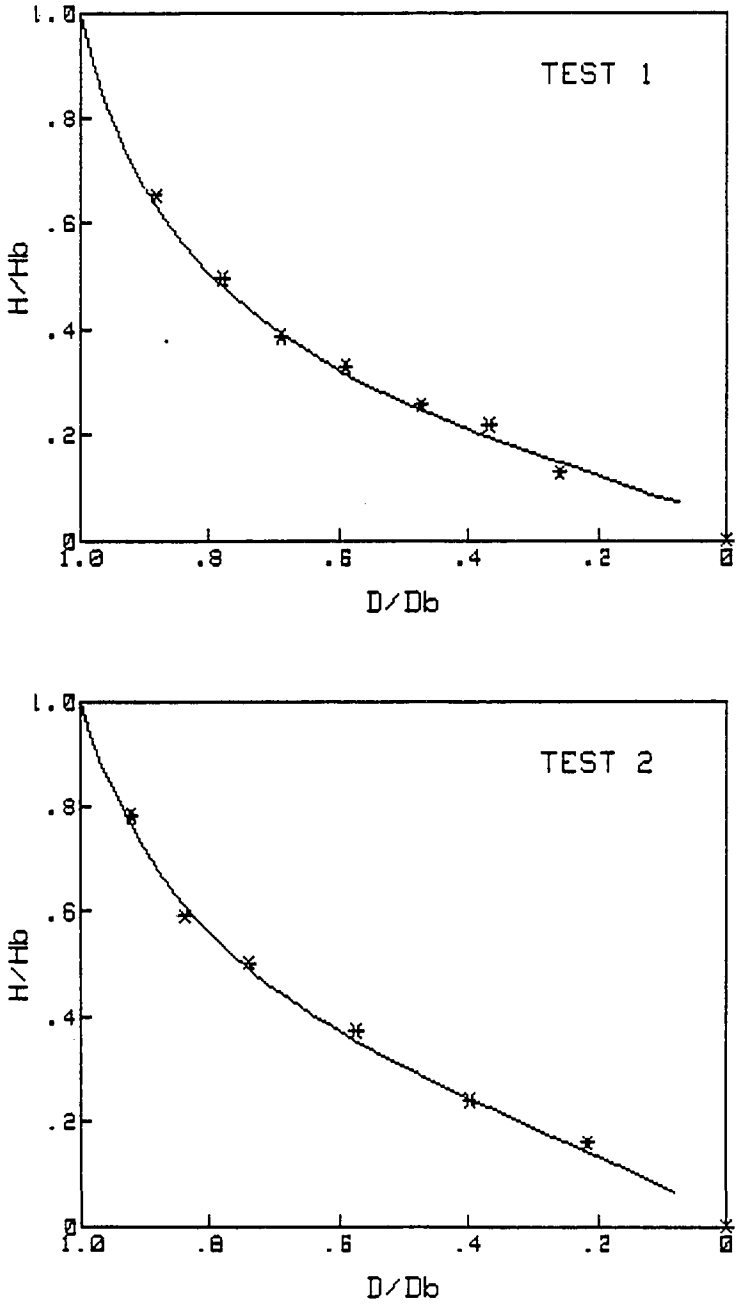

Figure 5.8 Comparisons of calculated wave decays in the breaking zone with Stive's data for Test 1 and Test 2 (1984).

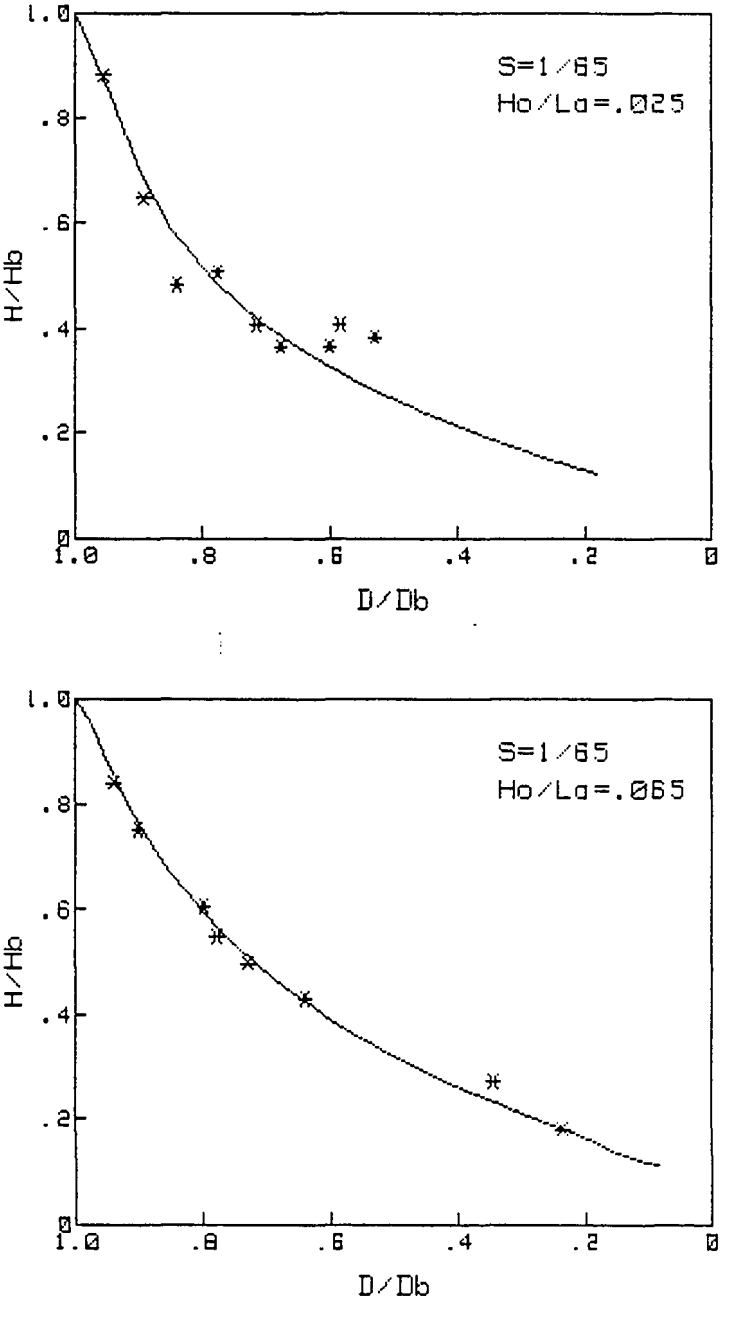

Figure 5.9 Comparisons of calculated wave decays in the breaking zone with data from Horikawa and Kuo (1966).

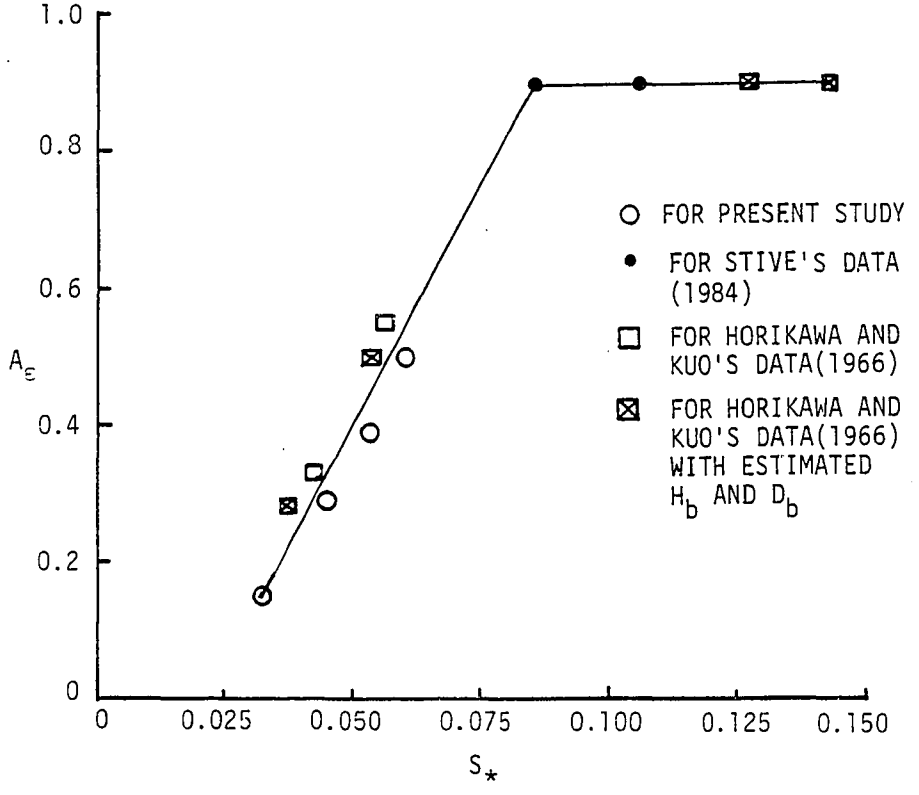

Figure 5.10 Non-dimensional dissipation coefficient, A_ε, versus modified slope parameter, S_*.

of A_ε for small values of S_* are uncertain, especially for the case of a horizontal slope. In Figure 5.10, "x" marks were calculated using estimated wave height and water depth at the breaking points for Horikawa and Kuo's data. The value for a slope of 1/80 was used to obtain the modified slope parameter for this experiment. From Figure 5.10, approximate A_ε values are:

$$A_\varepsilon = 14\, S_* - 0.3 \qquad \text{for } 0.03 < S_* < 0.085 , \qquad (5.23)$$

and,

$$A_\varepsilon = 0.9 \qquad \text{for } S_* > 0.085 . \qquad (5.24)$$

CHAPTER 6

WAVE SET-UP

6.1 Introduction

Wave set-up refers to the mean change in water level due to wave deformations in the process of shoaling and breaking. The mean water level is lowered in the shoaling process and rises after the wave breaks. The wave set-up is an important design parameter in coastal engineering. The increase of mean water level allows higher waves to exist in the shallow water region. The higher water levels also creates a current structure in this water region. Laboratory measurements of wave set-up by Bowen et.al. (1968) indicate that the maximum elevation of the water level can be as much as 50 % of the breaking wave height. Hansen (1978) also found from field measurements that the maximum wave set-up is 50 % of the significant wave height at the breaking point.

Longuet-Higgins and Stewart (1964) successfully explained the phenomena of wave set-up by introducing the concept of radiation stress. Under steady state conditions, the horizontal momentum equation is generally given by:

$$d(UM)/dx + dS_{xx}/dx + \rho g(h + \overline{\eta})\cdot d\overline{\eta}/dx + \overline{\tau} = 0 \quad . \qquad (6.1)$$

The first term in this equation is the gradient of the mass transport and the last term is the average bed shear stress. Neglecting the mass transport for flume experiments, this

mometum equation becomes:

$$dS_{xx}/dx + \rho g\,(h + \bar{\eta})\,d\bar{\eta}/dx + \bar{\tau} = 0 \quad . \tag{6.2}$$

By neglecting the mean shear stress term in (6.2), Longuet-Higgins and Stewart obtained the following formula for wave set-up in the area before the breaking point:

$$\bar{\eta} = -\,k\,H^2/(8 \sinh 2kh) \quad . \tag{6.3}$$

Bowen et.al. found good agreement between the wave set-up calculated from (6.3) and measured data in the region well outside the breaking point. However, measured values near the breaking point were always less than the calculated values. In contrast, Van Dorn (1976) showed that calculated set-up values from (6.3) fit his data quite well. Van Dorn obtained values for k in (6.3) using observed wave speeds. Van Dorn also found that the mean surface slope of the wave set-up after waves breaking on a plane slope is independent of wave periods and depends only on the beach slope. The relationship was given by:

$$d\bar{\eta}/dx = 3.4\,s^2 \quad . \tag{6.4}$$

6.2 Radiation Stress

Longuet-Higgins and Stewart (1964) developed the concept of radiation stress by beginning with linear wave theory. According to them, the radiation stress component, S_{xx}, in the direction perpendicular to the coastline is given by:

$$S_{xx} = E\,(2n - 0.5) \quad , \tag{6.5}$$

where E is the mean wave energy per unit area and n is the ratio of the wave group velocity to the wave velocity. These parameters are defined from linear wave theory as:

$$E = 1/8 \cdot \rho g H^2 \quad , \tag{6.6}$$

and,

$$n = (1 + 2kh/\sinh 2kh)/2 \quad ,$$

where $k = 2\pi/L$ and h is the still water depth. In shallow water, n is unity and S_{xx} is given by:

$$S_{xx} = 3/2 \cdot E \quad . \tag{6.7}$$

Gerritsen (1981) developed expressions for radiation stress for nonlinear waves. According to Gerritsen, radiation stress for long waves and cnoidal waves is given by:

$$S_{xx} = E\,(F_{rl}^2 + 0.5) \quad , \tag{6.8}$$

where F_{rl} is defined as:

$$F_{rl} = C/\sqrt{gh} \quad .$$

Radiation stress for long waves and cnoidal waves is larger than radiation stress for linear waves since F_{rl} is always greater than unity for these nonlinear waves. Stive (1982) obtained the radiation stress for two laboratory tests based on the measurement of the fluid velocity and the water surface elevation. He compared the resulting radiation stresses with radiation stresses calculated from linear wave theory and from nonlinear wave theories. These nonlinear wave theories were the Cokelet's wave theory and the hyperbolic wave theory. His two test results showed that calculated radiation stresses from linear wave theory and

from these nonlinear wave theories overestimated the experimental radiation stresses before wave breaking. After wave breaking the calculated radiation stresses from these nonlinear wave theories underestimated the data while the radiation stresses from linear wave theory overestimated the data.

According to Longuet-Higgins (1974), the potential energy for solitary waves is 45 % of the total energy. Consequently, two times of the potential energy is a reasonable approximation of the mean wave energy. If we define the mean wave energy as two times the potential energy, as expressed as equation (3.1), the energy calculated from (6.6) is much greater than this wave energy estimate. It is worthwhile to see how the radiation stress from (6.5) changes if we use the mean energy defined from the potential energy instead of the energy from (6.6). The comparisons are made in Figure 6.1 using Stive's experimental results and radiation strsses for Cokelet's waves calculated by Stive. The radiation estimate from (6.5) with the wave energy obtained from potential energy is in very good agreement with data at and just after the breaking point. Inside the breaking region however, the radiation stress from (6.5) underestimates the data values. This disagreement between the radiation stress calculated from (6.5) and the data results primarily from the difference of the wave energies from the data and the

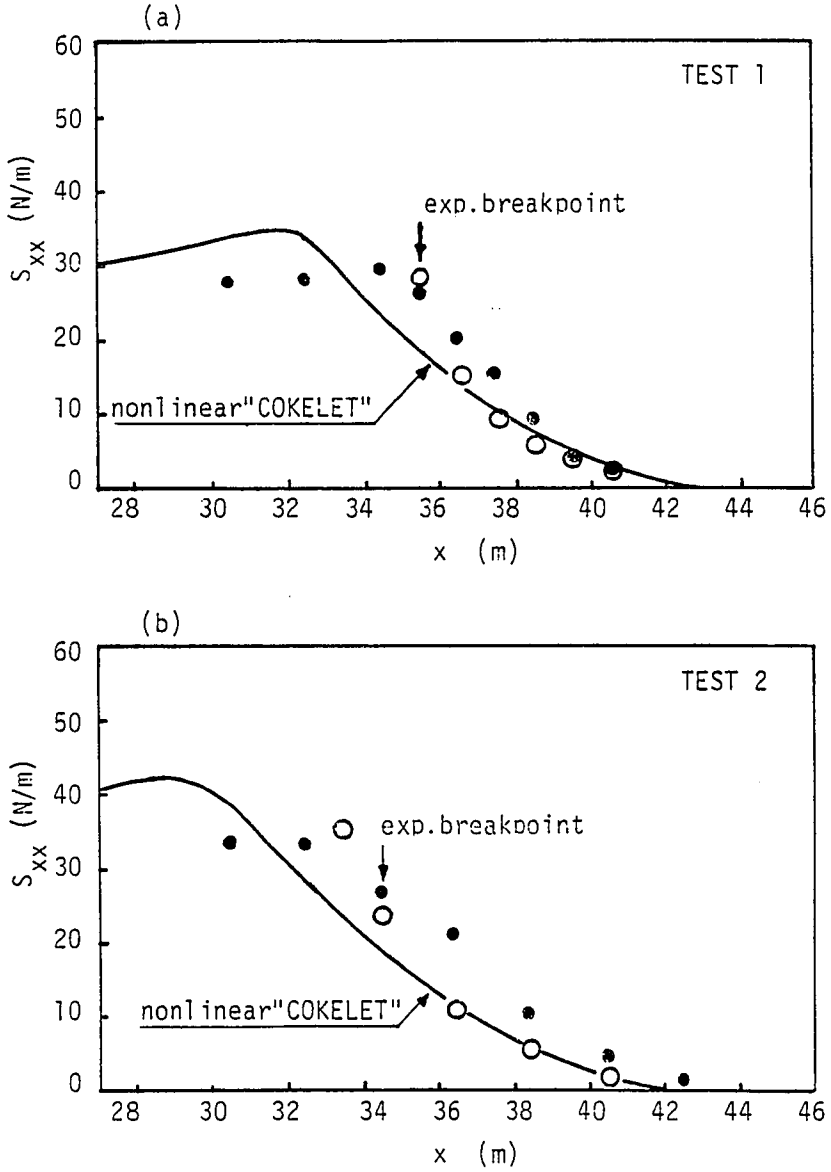

Figure 6.1 Comparison of calculated radiation stresses with data from Stive (1982).
(O —— present study, • —— Stive's data)

estimate inside the breaking region. Although the radiation stress from (6.5) along with the wave energy defined from potential energy underestimates the data from Stive's test inside the breaking region, it is as good as the calculated values from the nonlinear wave theories.

6.3 Experimental Results of Mean Shear Stress and Its Effect on Wave Set-Up

The mean shear stress in the momentum equation (6.2) is usually considered to be negligible. The mean water levels calculated using (6.2) without the mean shear stress have shown good agreement with laboratory data; for example, Van Dorn (1976) and Stive (1982). On the other hand, Gerritsen (1981) reported that the results of both field observations on Ala Moana reef and model studies indicated a shoreward mean shear stress.

In the past, experiments were commonly carried out over a smooth bed with the exception of those by Gerritsen (1981). In the present study, experiments were done both over a smooth bed and a rough bed in order to evaluate the effects of bed roughness on the mean shear stress.

Time averaged shear stresses were obtained using measured bottom particle velocities and experimentally obtained friction factors. The pertinent relationship is given by:

$$\bar{\tau} = \overline{1/2 \cdot \rho C_f V_\delta(t) |V_\delta(t)|} \quad .$$

The measured mean shear stresses were separated into four cases; i.e., for non-broken waves and for broken waves over two types of bottom surfaces. Non-dimensional mean shear stresses, $\bar{\tau}/\rho gD$, are plotted against the ratio of the wave height to the water depth in Figures 6.2 and 6.3. For both types of bottom, it appears that the mean shear stress in the non-broken wave increases with H/D. Although there is some difficulty in determining accurate trends from the small amount of data which also is susceptible to lack of precision, linear regression lines for both types of beds are drawn in the figures. Comparing these regression lines, the mean shear stresses for the rough bed are approximately twice those for the smooth bed. According to friction factors obtained in Chapter 4, however, the friction factors for the rough bed are approximately four times those for the smooth bed.

For broken wave cases, the mean shear stresses are plotted in Figure 6.4. These data are scattered around zero with no readily apparent trend. For this reason, the mean shear stress for broken waves is considered to be zero.

The mean water levels were calculated both with and without these empirical mean shear stresses. The smooth bed cases are shown in Figures 6.5 to 6.7. Comparisons are made in Figures 6.8 and 6.10 for the rough bed. All cases show some improvement in the mean water levels when calculated values include the mean shear stress. In these calculations

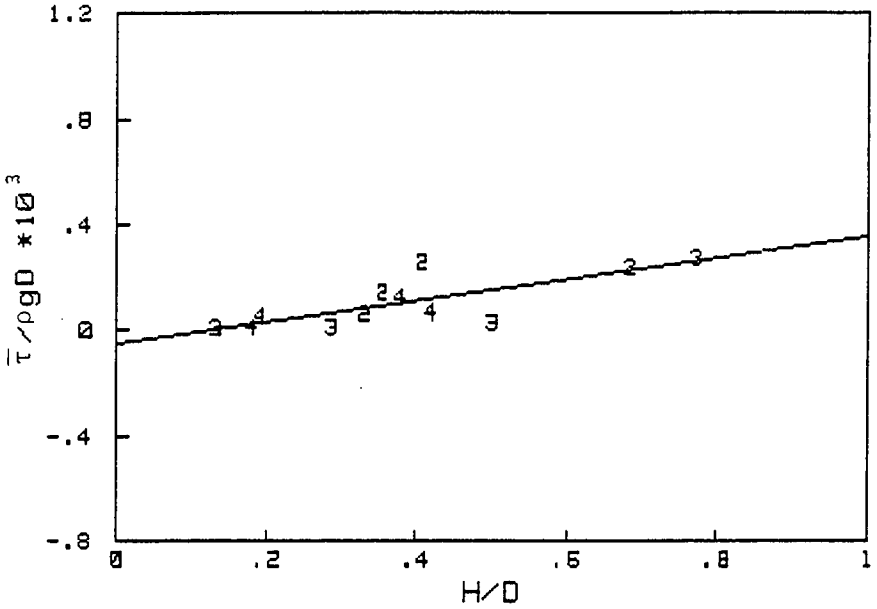

Figure 6.2 Non-dimensional mean shear stress versus the ratio of non-broken wave height to water depth; for the concrete bed. (Numbers plotted denote rounded wave periods.)

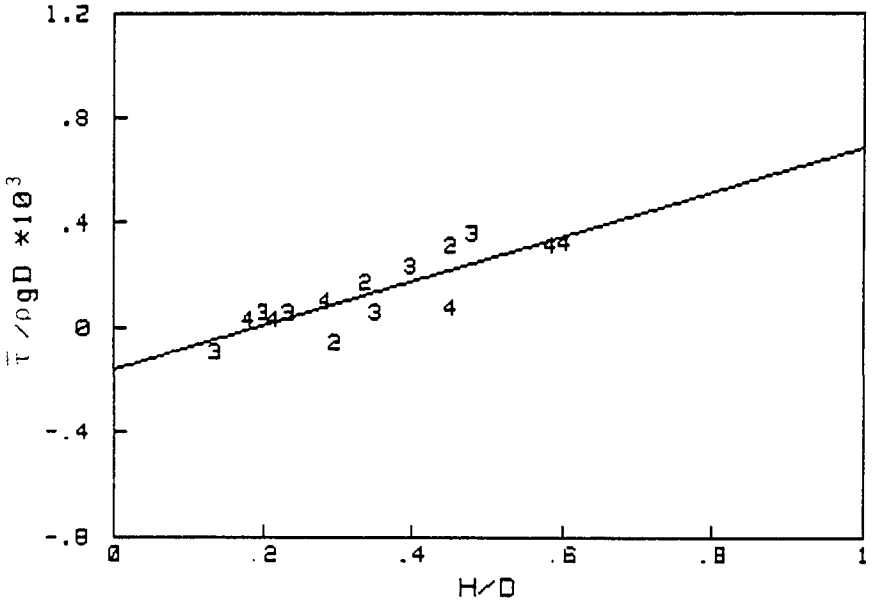

Figure 6.3 Non-dimensional mean shear stress versus the ratio of non-broken wave height to water depth; for the gravel bed. (Numbers plotted denote rounded wave periods.)

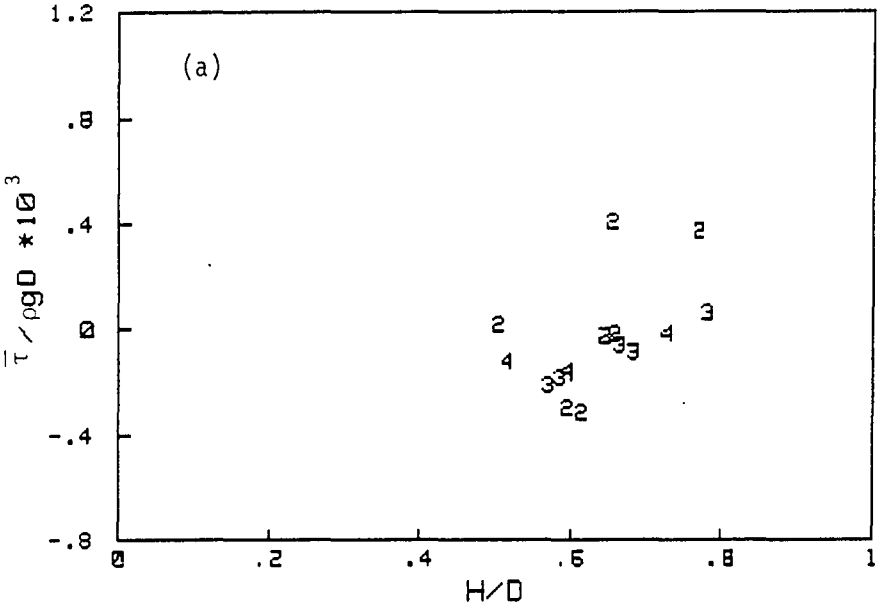

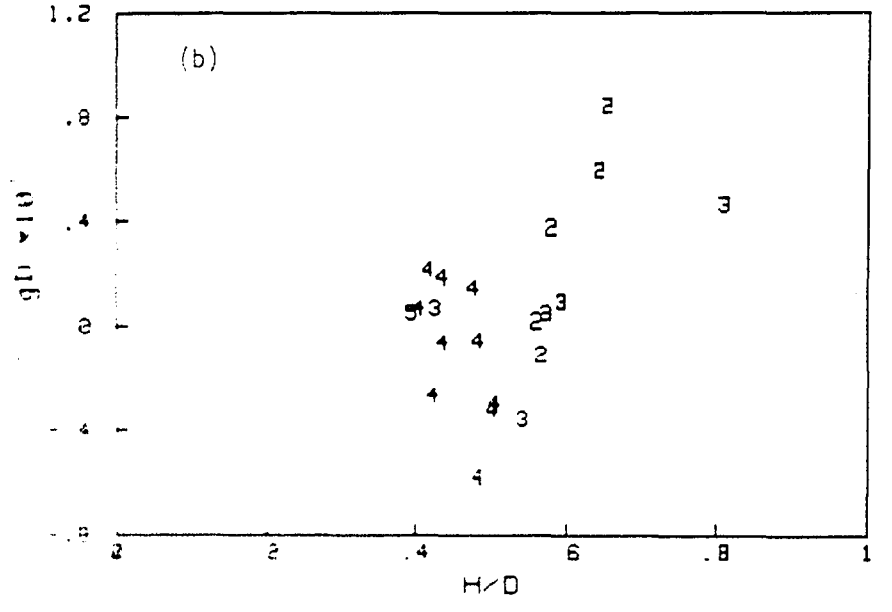

Figure 4.1 Non-dimensional mean shear stress versus the ratio of wave height to water depth; (a) for the concrete bed and (b) for the gravel bed. (Numbers plotted denote wave periods).

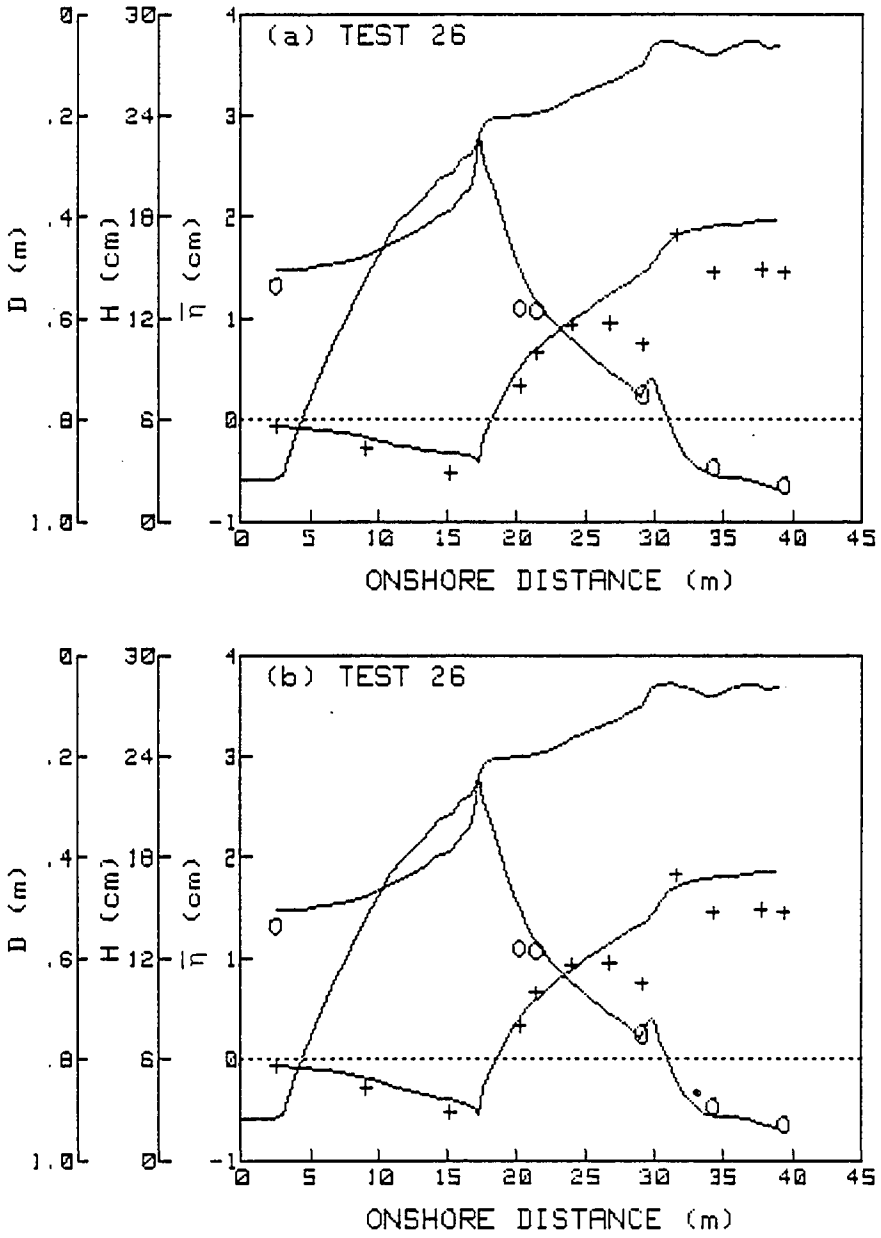

Figure 6.5 Comparisons between calculated mean water levels and measured mean water levels for a two-second wave over the concrete bed; (a) without mean shear stress and (b) with mean shear stress only outside the wave breaking zone. (+ —— mean water levels, o —— wave heights)

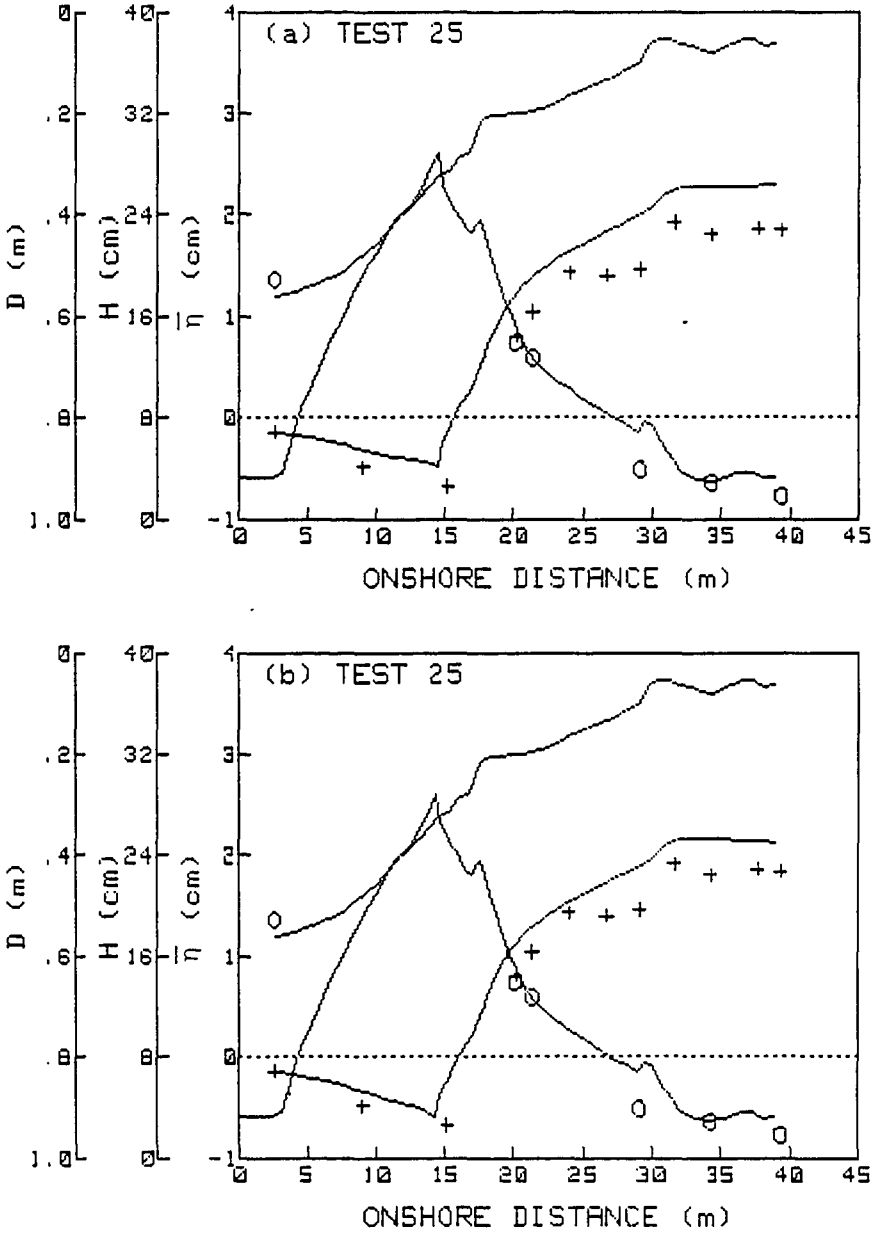

Figure 6.6 Comparisons between calculated mean water levels and measured mean water levels for a three-second wave over the concrete bed; (a) without mean shear stress and (b) with mean shear stress only outside the wave breaking zone. (+ —— mean water levels, o —— wave heights)

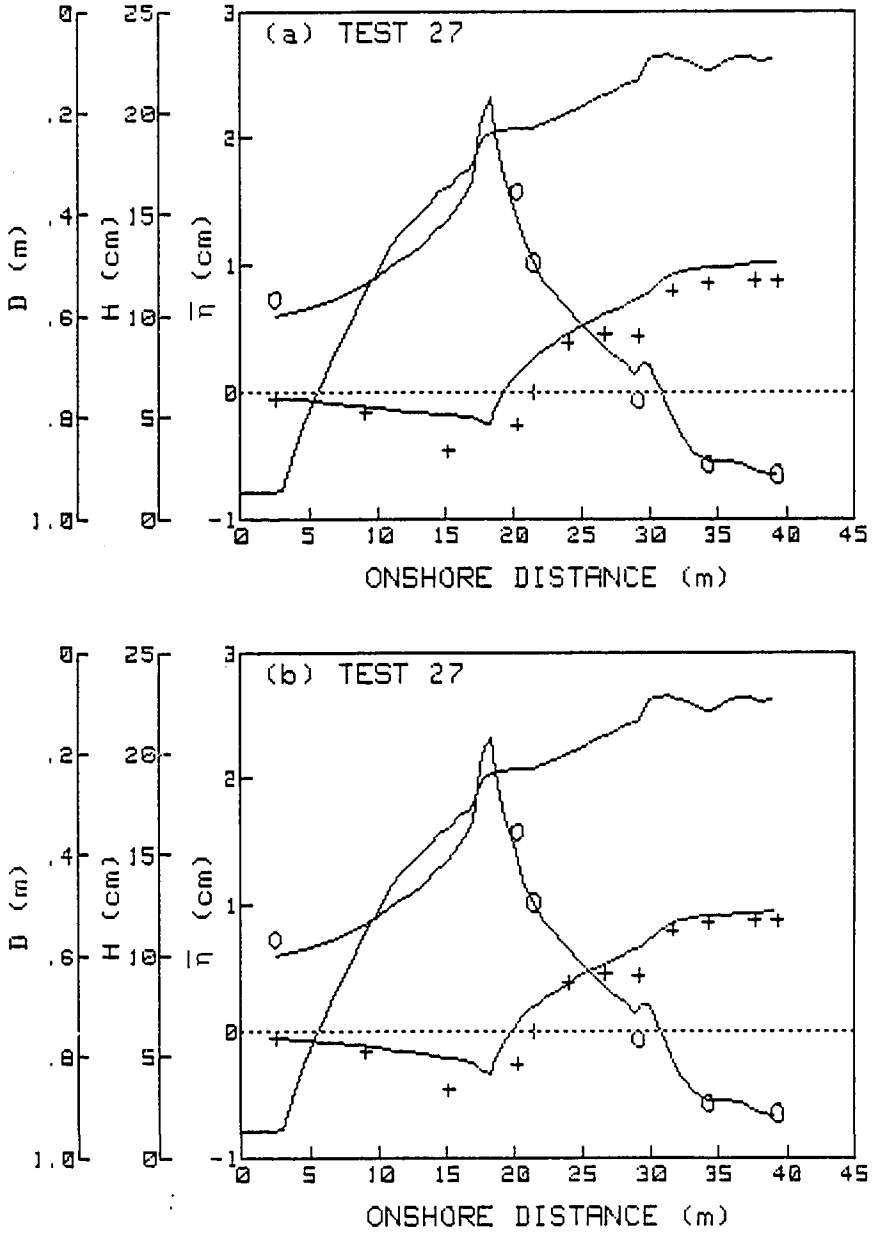

Figure 6.7 Comparisons between calculated mean water levels and measured mean water levels for a four-second wave over the concrete bed; (a) without mean shear stress and (b) with mean shear stress only outside the wave breaking zone. (+ ___ mean water levels, o ___ wave heights)

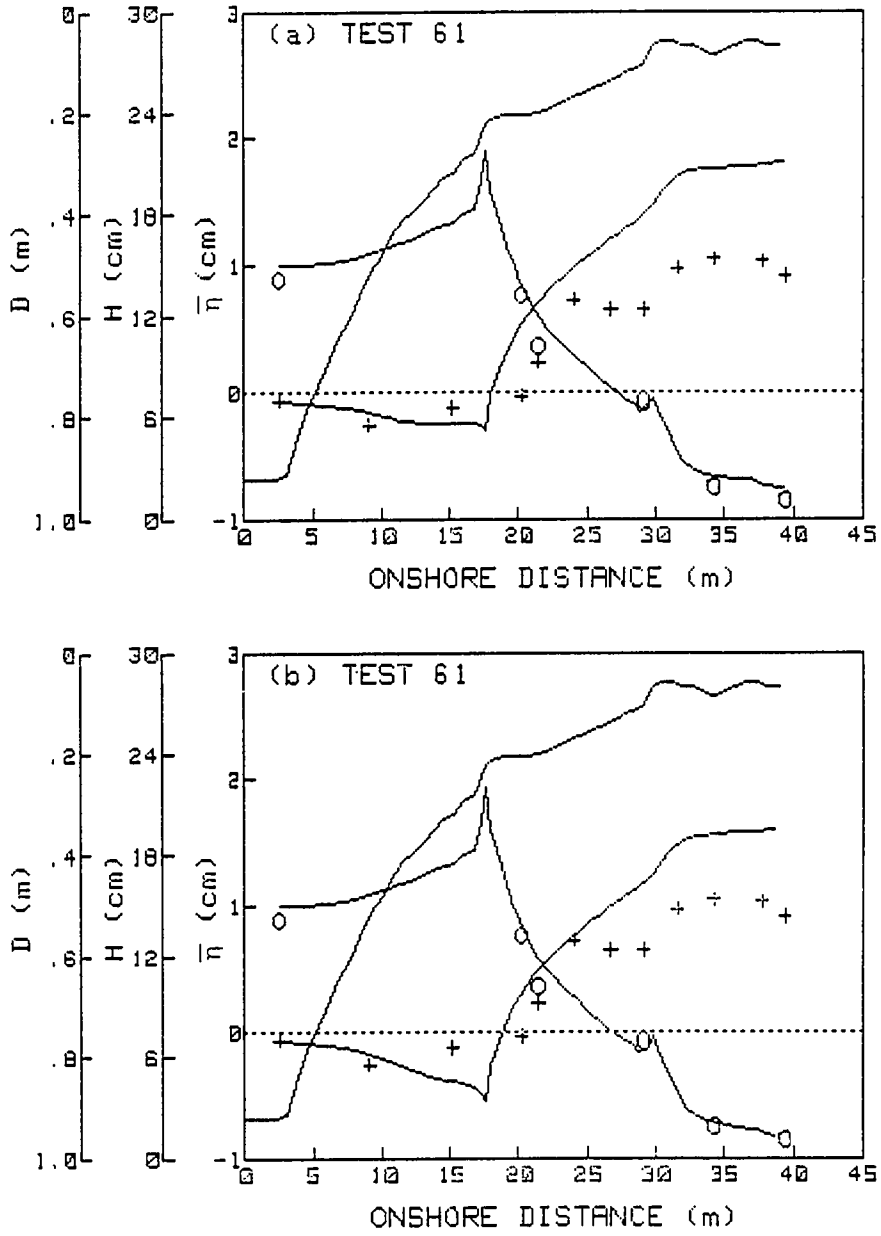

Figure 6.8 Comparisons between calculated mean water levels and measured mean water levels for a two-second wave over the gravel bed; (a) without mean shear stress and (b) with mean shear stress only outside the wave breaking zone. (+ ___ mean water levels, o ___ wave heights)

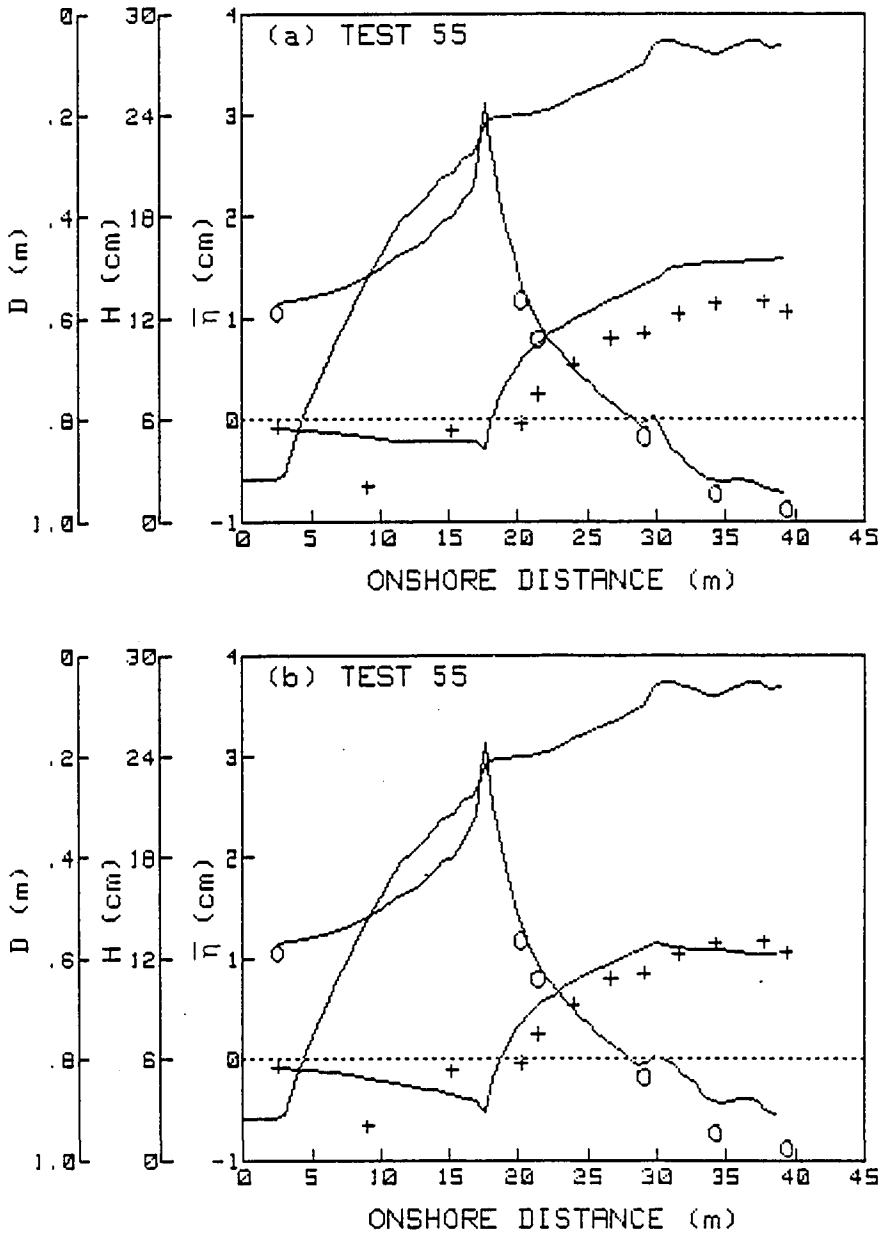

Figure 6.9 Comparisons between calculated mean water leves and measured mean water levels for a three-second wave over the gravel bed; (a) without mean shear stress and (b) with mean shear stress only outside the wave breaking zone. (+ —— mean water levels, o —— wave heights)

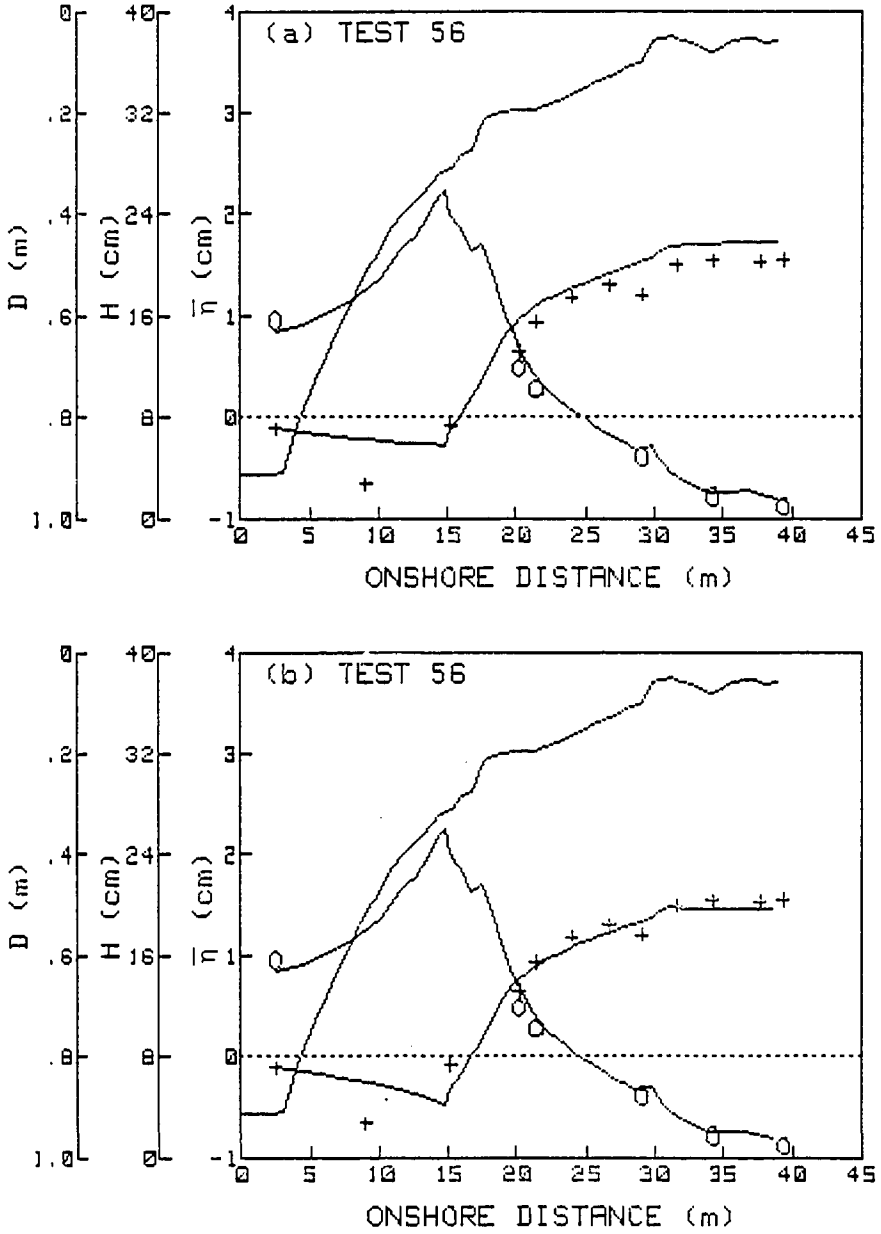

Figure 6.10 Comparisons between calculated mean water levels and measured mean water levels for a four-second wave over the gravel bed; (a) without mean shear stress and (b) with mean shear stress only outside the wave breaking zone. (+ ___ mean water levels, o ___ wave heights)

of the mean water level, positive shear stresses were applied to the non-broken waves and the shear stresses for the broken waves were taken as zero. Stive's experimental results also indicate positive mean shear stresses just before and at the breaking points. For four-second waves in Figures 6.7 and 6.10, the calculated mean water levels are in very good agreement with measured values. For cases of three-second waves the predicted mean water levels are less satisfactory but still reasonable. For cases of two-second waves the deviations of calculated mean water levels in the wave breaking zone from measured data are most apparent. The deviations of calculated values from measured values are seen in both two-second waves over the concrete bed and over the gravel bed. This evidence suggest positive mean shear stresses in broken waves for the case of two-second waves. This suggestion also agrees with the results in Figure 6.4. From Figure 6.4 there are evident positive mean shear stresses for two-second waves in the area where H/D is greater than 0.6. From this figure the values of the mean shear stresses in the broken two-second waves were found to be approximated by $\overline{\tau}/\rho g D \cdot 10^3 = 0.25$ for the case of concrete bed and 0.8 for the gravel bed only in the area where H/D is greater than 0.6. These values were tried for tests 26 and 61 and the results are shown in Figure 6.11. The predicted mean water levels are in very good agreement with measured

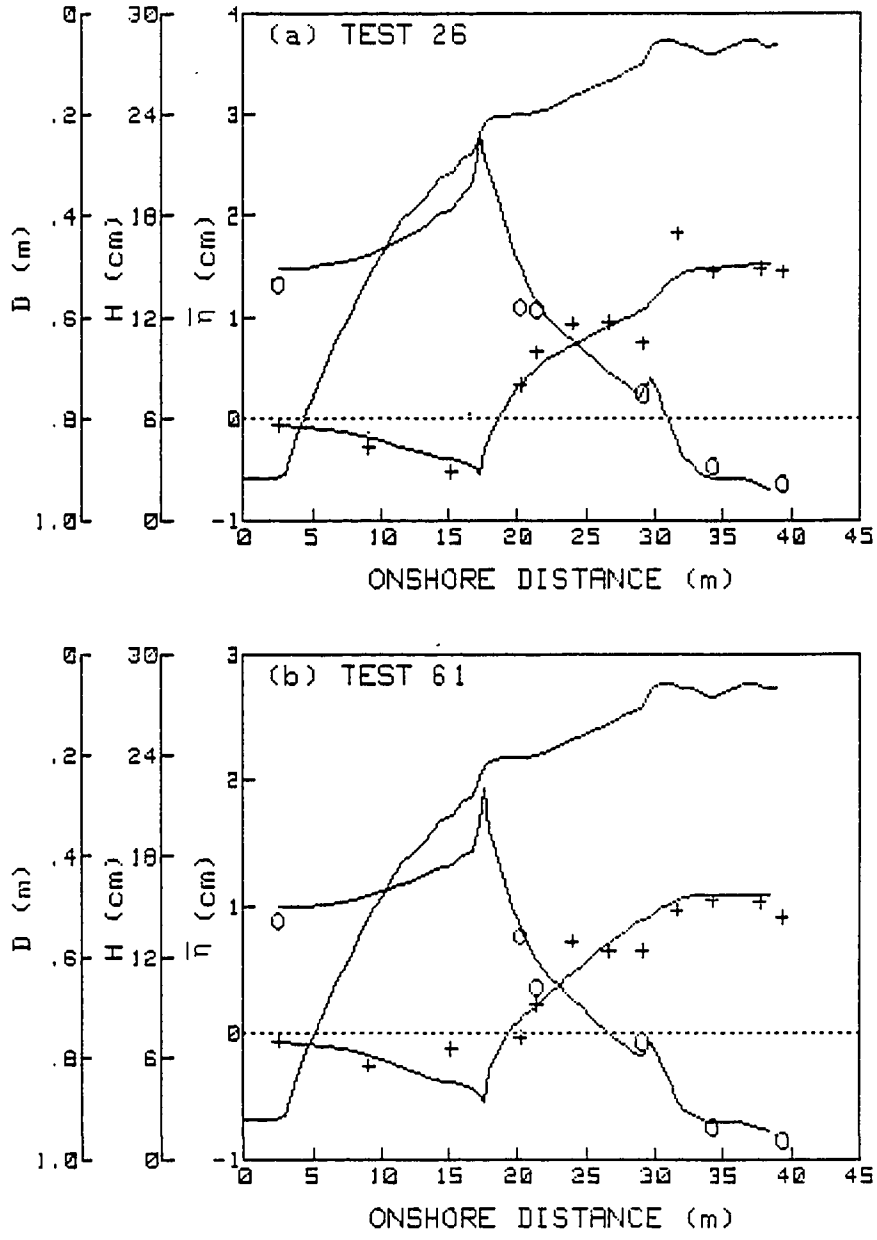

Figure 6.11 Comparisons between measured mean water levels and calculated mean water levels with mean shear stress inside and outside the wave breaking zone for two-second waves; (a) over the concrete bed and (b) over the gravel bed. (+ ___ mean water levels, o ___ wave heights)

values. These results suggest that the mean shear stress in broken waves is dependent on H/D and the wave period.

In summary, it may be said that non-broken nonlinear waves produce positive mean shear stress. The magnitude of the mean shear stress depends on the ratio of the wave height to the water depth. The mean shear stress is most significant at the breaking point where H/D is maximum. The magnitude and the direction of the mean shear stress for broken waves are not conclusive and were found to not be very significant except for two-second waves. The mean shear stess for broken waves are a function of the wave period and the ratio of the wave height to the water depth. The relative significance of the mean shear stress in the calculation of the mean water level primarily depends on the bed roughness. For the gravel-covered bed used in the present experiments, the estimate of the meam shear stress in non-breaking waves is given by:

$$\bar{\tau} = 0 \qquad \text{for } H/D \leq 0.190 \qquad (6.9)$$

and,

$$\bar{\tau} = \rho g D \{0.844(H/D) - 0.160\} \cdot 10^{-3} \qquad \text{for } H/D > 0.190 \ . \qquad (6.10)$$

For the concrete bed the mean shear stress is approximated by:

$$\bar{\tau} = 0 \qquad \text{for } H/D \leq 0.113 \qquad (6.11)$$

and,

$$\bar{\tau} = \rho g D \{0.398(H/D) - 0.045\} \cdot 10^{-3} \qquad \text{for } H/D > 0.113 \ . \qquad (6.12)$$

For broken waves the mean shear stress is tentatively considered to be zero in this study.

CHAPTER 7

COMPUTATIONAL PROCEDURE

7.1 Introduction

The computational procedure developed herein is appropriate for calculating the mean wave energy, the wave height and the mean water level in the near shore zone. The formulations used in the calculations are primarily based on linear wave theory with experimental results applied as nonlinear wave corrections. These nonlinear wave effects were discussed in previous chapters; i.e., wave height in Chapter 3, energy dissipation due to bed shear stress in Chapter 4, energy dissipation due to wave breaking in Chapter 5 and effects of mean shear sress on wave set-up in Chapter 6. All these nonlinear wave effects are included in the computational procedure. The mean wave energy is calculated using the stationary two dimensional energy equation with experimental energy dissipation relationships. The mean wave energy links this energy equation and the stationary momentum equation. Subsequently, the mean water level is calculated using this momentum equation. The mean wave energy also links to the wave height calculation through the nonlinearity parameter.

Comparisons between results calculated using this procedure and measured data were made in previous chapters;

i.e., concerning wave height and mean wave energy in Chapter 5 and concerning wave set-up in Chapter 6.

7.2 Equations Used in the Computational procedure

In the computational procedure the governing equations are:

$$dF/dx = - E_t \qquad (7.1)$$

and,

$$dS_{xx}/dx + \rho g\,(h + \bar{\eta})\, d\bar{\eta}/dx + \bar{\tau} = 0 \quad . \qquad (7.2)$$

In (7.1) F is the energy flux given by the mean wave energy times the group velocity. The dominant dissipations are considered to be due to bottom friction, E_d, and wave breaking, E_b. In flume experiments, the viscous dissipation, E_v, on the side walls is also included. Subsequently, the total dissipation of energy is given by:

$$E_t = -E_d + E_b + E_v \quad . \qquad (7.3)$$

E_d, E_b and E_v were discussed in Chapter 4, Chapter 5 and Chapter 2, respectively.

Re-organizing (7.2) the momentum equation becomes:

$$dY/dx = \rho g\bar{\eta}\, dh/dx - \bar{\tau} \quad , \qquad (7.4)$$

where;

$$Y = 1/2 \cdot \rho g\bar{\eta}^2 + \rho gh\bar{\eta} + S_{xx} \qquad (7.5)$$

and S_{xx} is defined as:

$$S_{xx} = (2n - 0.5)\, E \quad . \qquad (7.6)$$

In equation (7.4) dh/dx is obtained from the given bottom profile. The mean shear stress, $\bar{\tau}$, was discussed in Chapter

6. E and $\bar{\eta}$ are expressed in terms of F and Y:

$$E = F/C_{gr} \tag{7.7}$$

and,

$$\bar{\eta} = -h + [h^2 - \{(4n - 1)\, F/C_{gr} - 2Y\}/\rho g]^{1/2} \quad . \tag{7.8}$$

In this study the two simultaneous first-order ordinary differential equations, (7.1) and (7.4), are solved for F and Y using the fourth-order Runge-Kutta method. The initial value for F is obtained from the wave energy, E, a given value and from the group velocity, C_{gr}, which is calculated using linear wave theory. The initial value for Y is obtained from values for wave set-up and radiation stress, S_{xx}, which are also calculated using linear wave theory. Equation (6.3) is used in calculating the initial value of wave set-up as expressed as:

$$\bar{\eta} = - k\, H^2/(8 \sinh 2kh) \quad .$$

E and $\bar{\eta}$ are then calculated using (7.7) and (7.8). After calculating E, the wave height is determined using the empirical relationship (3.6).

As a example this computational procedure is applied to Hansen and Svendsen's (1979) experimental test number 051071. Comparisons between measured values of wave heights and mean water levels and results calculated using this procedure are shown Figure 7.1. The figure shows that the calculated values of wave heights and mean water levels are almost exactly the same as the measured values before the wave breaking point. After the wave breaking point the

calculated wave heights exibit very satisfactory agreement with the measured values. The calculated values of wave set-up are less satisfactory but still reasonable. The predicted wave breaking point is also in very good agreement with the experimetal wave breaking point.

The empirical relationships used in the computational procedure are summarized in Table 3.

7.3 Notes Regarding Calculation Procedures

The mean wave energy is defined from the variance of the water surface fluctuations; i.e., two times the potential energy. The wave height is defined as the mean value of the largest one-third of the wave heights. The initial point of the calculations should be a point far away from the breaking point, where linear wave theory is applicable in calculating wave set-up values. For the mean wave energy and wave height calculations the unique curves of (3.5) and (3.6) are applicable at least for bottom slopes ranging from 0 to 1:34. The first approximations of C and n are made taking D=h at each calculation step. If necessary, the resulting D value is used to again calculate C and n in an iterative process. It was, however, noticed that the first approximations of C and n do not significantly change the calculated results. The increment of Δx is changed at each calculation step according to the ratio, H/D. Additionally, the limitations of Δx are used; for example,

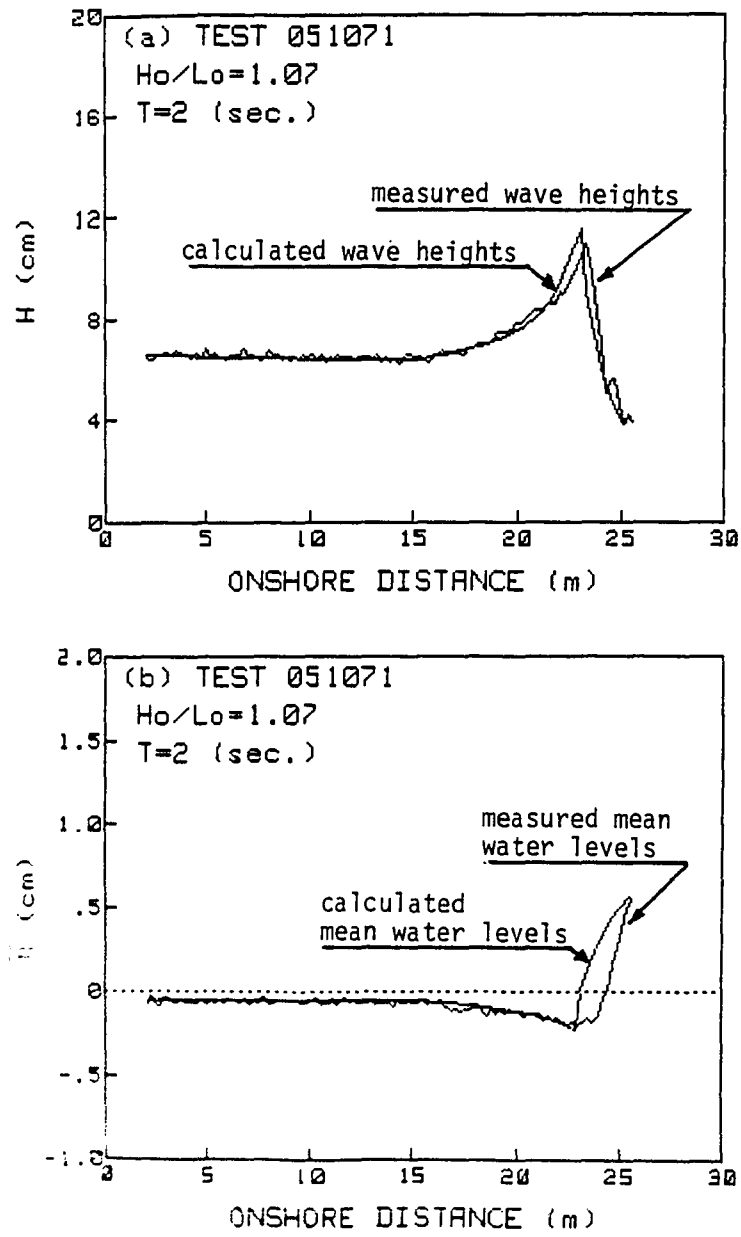

Figure 7.1 Comparisons between measured values of wave heights and mean water levels by Hansen and Svendsen (1979) and values calculated using the computation procedure in this study; (a) wave heights and (b) mean water levels.

the maximum value of Δx is 2 m and minimum is 10 cm for this flume experiment.

Required initial values are the wave period and either the wave height or the mean wave energy. Data describing the bottom profile and the bottom roughness are also required.

TABLE 3

Empirical Relationships Used in the Computational Procedure.

(a) Wave nonlinearity parameter

H = the mean value of the largest one-third of wave heights

$H_a = \sqrt{8}\,\eta_{rms}$

$P_n = \frac{H}{L_a}\coth^2(\frac{D}{L_a})$

$P_a = \frac{H_a}{L_a}\coth^2(\frac{D}{L_a})$

(b) Wave height from mean wave energy density and vice versa

$\frac{H}{\eta_{rms}} = f(P_n)$

$= a_0 + a_1P_n + a_2P_n^2 + a_3P_n^3 + a_4P_n^4 + a_5P_n^5$

$\frac{H}{\eta_{rms}} = f(P_a)$

$= b_0 + b_1P_a + b_2P_a^2 + b_3P_a^3 + b_4P_a^4 + b_5P_a^5$

$a_0 = b_0 = 2.94$

$a_1 = -2.480 \times 10^{-4}$ $\quad b_1 = 1.095 \times 10^{-2}$

$a_2 = 1.613 \times 10^{-2}$ $\quad b_2 = 1.108 \times 10^{-3}$

$a_3 = -8.690 \times 10^{-4}$ $\quad b_3 = 4.397 \times 10^{-3}$

$a_4 = 1.836 \times 10^{-5}$ $\quad b_4 = -3.966 \times 10^{-4}$

$a_5 = -1.378 \times 10^{-7}$ $\quad b_5 = 9.694 \times 10^{-6}$

(c) Wave celerity

$C_a^2 = \frac{gL_a}{2\pi}\tanh(\frac{2\pi h}{L_a})$

i) Non-breaking waves

$C = C_a$ for $P_a \leq 4$

$C = \{\frac{1}{3}\log(P_a) + 0.8\}\,C_a$ for $4 < P_a \leq 18.88$

$C = 1.23\,C_a$ for $P_a > 18.88$

TABLE 3 (continued)

Empirical Relationships Used in the Computational Procedure.

ii) Breaking waves

$C = (1 + 0.25\ H/D)\ C_a$

(d) Nonlinear wave particle amplitude at the bed

$a_{\delta 1} = Tu_{\delta m}/2\pi$

$a_\delta = a_{\delta 1}$ for $P_n \leq 3.6$

$a_\delta = (-0.805 \log(P_n) + 1.45)\ a_{\delta 1}$ for $P_n > 3.6$

(e) Nikuradse roughness

$k_s = 1.735\ D_{90}$ for $0.54 \leq D_{90} \leq 46$ (mm)

(f) Friction factors

$1/(4\sqrt{f_w}) + \log\{1/(4\sqrt{f_w})\} = -0.08 + \log(a_\delta/K_s)$ by Jonsson

(g) Energy dissipation due to bed friction

$E_{d1} = -(2/3\pi)\ \rho f_w\ \{\pi H/(T \sinh kh)\}^3$

$E_d = E_{d1}$ for $P_n \leq 4.5$

$E_d = (-1.365 \log(P_n) + 1.891)\ E_{d1}$ for $P_n > 4.5$

$E_{dmin} = 0.1\ E_{d1}$

(h) Wave breaking criterion

$H_b/D_b = 1/2 \cdot (P_n - 1/7)^{1/2 \cdot s^{1/4}}$

(i) Energy dissipation due to wave breaking

$E_b = (A_\varepsilon \alpha^2/T) \cdot (H/D)/(\alpha H/D + 1) \cdot E\ f(P_a)^2$

$\alpha = 1.22$

$A_\varepsilon = 0.15$ for one-second waves

$= 0.27$ for two-second waves

$= 0.40$ for three-second waves

$= 0.50$ for four-second waves

TABLE 3 (continued)

Empirical Relationships Used in the Computational Procedure.

(j) Radiation stress

$S_{xx} = E\,(2n - 0.5)$

$E = \rho g \eta_{rms}^2$

$n = (1 + 2kD/\sinh 2kD)/2$

(k) Mean shear stress

i) Non-breaking waves

For the gravel bed (D_{90} = 18 mm)

$\overline{\tau} = 0$ for $H/D \leq 0.190$

$\overline{\tau} = \rho g D\,(0.844\ H/D - 0.160)\cdot 10^{-3}$ for $H/D > 0.190$

For the concrete bed

$\overline{\tau} = 0$ for $H/D \leq 0.113$

$\overline{\tau} = \rho g D\,(0.398\ H/D - 0.0450)\cdot 10^{-3}$ for $H/D > 0.113$

ii) Breaking waves

$\overline{\tau} = 0$

CHAPTER 8
CONCLUSIONS

Based on this study, it is concluded that:

(a) The new and unique curve obtained in this study for wave height prediction, Figure 3.4, is applicable in the entire nearshore region, even in the breaking zone, at least for slopes ranging from 0 to 1:34.

(b) For rough turbulent conditions, friction factors determined under highly nonlinear wave and breaking wave conditions fit well to the Jonsson's friction factor curve, which was developed from sinusoidal waves.

(c) The phase shift between the shear stress and the particle velocity at the bed has little effects on the friction factor. This conclusion is based on the fact that the friction factors in this study were determined with the phase shift whereas, the friction factors by Jonsson were without the phase shift. This conclusion comfirms Jonsson's results.

(d) The energy dissipation calculated using linear wave theory overestimates the energy dissipation due to bottom friction in the shallow water region.

(e) The energy dissipation due to wave breaking is accurately predicted by assuming similarity to a

bore. The energy dissipation coefficient is a function of the modified slope parameter, $S_* = s/(D_b / L_b)^{1/2}$.

(f) The mean shear stress is a function of the bottom roughness and the ratio of the wave height to the water depth for non-breaking waves. For breaking waves the mean shear stress depends on the wave period in addition to the bottom roughness and the ratio of the wave height to the water depth.

(g) The effect of the mean shear stress on the wave set-up depends on the bottom roughness and the wave period. The mean shear stress is important in calculations of wave set-up for the rough bed and for short period waves.

(h) By using the method developed in this study it is possible to accurately calculate the wave set-up and energy dissipation of waves approaching the shoreline given the incident wave height, wave period and water depth, the bottom profile and the bottom roughness on a gentle slope.

APPENDIX A

Solution of Equation (4.45)

The equation (4.45) is solved for A and B using the least square method. The difference, d_i, between the left side and the right side of (4.45) is defined as:

$$d_i = W_i - (A^2X_i + B^2Y_i + ABZ_i)$$

where i denotes an individual data. The summation of square of differences is:

$$D = \sum_{i=1}^{N} d_i^2$$

$$= \sum_{i=1}^{N} (W_i - A^2X_i - B^2Y_i - ABZ_i)^2 \quad .$$

Taking derivatives of D;

$$\partial D/\partial A = 2\Sigma\ (W - A^2X - B^2Y - ABZ)(-2AX - BZ) = 0 \qquad (1)$$

$$\partial D/\partial B = 2\Sigma\ (W - A^2X - B^2Y - ABZ)(-2BY - AZ) = 0 \qquad (2)$$

where the subscript, i , is omitted hereafter. Re-arranging (1) and (2);

$$2A^3\ \Sigma X^2 + 3A^2B\ \Sigma XZ + AB^2(2\ \Sigma XY + \Sigma Z^2) + B^3\ \Sigma YZ - 2A\ \Sigma WX - B\ \Sigma WZ = 0 \qquad (3)$$

$$A^3\ \Sigma XZ + A^2B\ (2\ \Sigma XY + \Sigma Z^2) + 3AB^2\ \Sigma YZ + 2B^3\ \Sigma Y^2 - A\ \Sigma WZ - 2B\ \Sigma WY = 0 \qquad (4)$$

Dividing (3) and (4) by A^3;

$$2\,\Sigma X^2 + 3(B/A)\,\Sigma XZ + (B/A)^2(2\,\Sigma XY + \Sigma Z^2) + (B/A)^3\Sigma YZ - 2(1/A)^2\Sigma WX - (B/A)\cdot(1/A)^2\Sigma WZ = 0 \quad , \quad (5)$$

$$\Sigma XZ + (B/A)\cdot(2\,\Sigma XY + \Sigma Z^2) + 3(B/A)^2\Sigma YZ + 2(B/A)^3\Sigma Y^2 - (1/A)^2\Sigma WZ - 2(B/A)\cdot(1/A)^2\Sigma WY = 0 \quad . \quad (6)$$

Introducing new variables, P and Q;

$$P = (1/A)^2 \quad (7)$$

$$Q = B/A \quad , \quad (8)$$

where P and Q are always positive since A and B are positive values.

Inserting P and Q into (5) and (6);

$$2\,\Sigma X^2 + 3Q\,\Sigma XZ + Q^2(2\,\Sigma XY + \Sigma Z^2) + Q^3\,\Sigma YZ - 2P\,\Sigma WX - PQ\,\Sigma WZ = 0 \quad , \quad (9)$$

$$\Sigma XZ + Q(2\,\Sigma XY + \Sigma Z^2) + 3Q^2\,\Sigma YZ + 2Q^3\,\Sigma Y^2 - P\,\Sigma WZ - 2PQ\,\Sigma WY = 0 \quad . \quad (10)$$

From (9) and (10) the final equation is obtained in terms of Q.

$$A_0 + A_1Q + A_2Q^2 + A_3Q^3 + A_4Q^4 = 0 \quad , \quad (11)$$

where,

$$A_0 = \Sigma WX\cdot\Sigma XZ - \Sigma WZ\cdot\Sigma X^2$$

$$A_1 = 2(\Sigma WX\cdot\Sigma XY - \Sigma X^2\cdot\Sigma WY) + (\Sigma WX\cdot\Sigma Z^2 - \Sigma WZ\cdot\Sigma XZ)$$

$$A_2 = 3(\Sigma WX\cdot\Sigma YZ - \Sigma WY\cdot\Sigma XZ)$$

$$A_3 = 2(\Sigma WX\cdot\Sigma Y^2 - \Sigma WY\cdot\Sigma XY) + (\Sigma WZ\cdot\Sigma YZ - \Sigma WY\cdot\Sigma Z^2)$$

$$A_4 = \Sigma WZ\cdot\Sigma Y^2 - \Sigma WY\cdot\Sigma YZ$$

$$W = R_t^2 + I_t^2$$

$$X = 2(1 - \cos 2\pi f t_1)\cdot(R_v^2 + I_v^2)$$

$$Y = 2(1 - \cos 2\pi f t_1)\cdot(R_x^2 + I_x^2)/(2\pi f)^2$$

$$Z = 4(1 - \cos 2\pi f t_1)\cdot(R_v\cdot I_x - I_v\cdot R_x)/2\pi f$$

$$Q = B/A$$

and,

$$P = (1/A)^2$$

$$= \{2\ \Sigma X^2 + 3Q\ \Sigma XZ + Q^2(2\ \Sigma XY + \Sigma Z^2) + Q^3\ \Sigma YZ\}\ /(2\ \Sigma WX + Q\ \Sigma WZ)$$

The equation (11) is numerically solved for Q using Siljak function and only positive real roots of Q are taken.

APPENDIX B

Tables 4 to 15

TABLE 4

Bottom Profile for the Two-Dimensional Hydraulic Model.

X(m)	D(cm)	X(m)	D(cm)	X(m)	D(cm)	X(m)	D(cm)
0.00	88.90	12.23	36.51	23.66	14.29	35.09	4.45
1.57	88.90	13.00	34.29	24.43	13.34	35.86	3.49
2.33	88.90	13.76	31.75	25.19	12.38	36.62	2.86
3.09	88.27	14.52	29.53	25.95	11.43	37.38	2.86
3.85	80.65	15.28	28.58	26.71	10.48	38.14	3.81
4.61	75.57	16.04	26.04	27.47	9.53	38.90	3.49
5.38	70.49	16.81	24.77	28.24	8.26	39.67	3.18
6.14	65.41	17.57	19.05	29.00	7.62	40.43	2.70
6.90	60.96	18.33	17.78	29.76	3.49	41.19	2.70
7.66	57.15	19.09	17.46	30.52	2.86	41.95	4.13
8.42	53.02	19.85	17.15	31.28	2.54	42.71	3.49
9.19	48.26	20.62	17.15	32.05	3.49	43.48	2.54
9.95	45.09	21.38	16.83	32.81	3.81	44.24	2.54
10.71	41.28	22.14	16.19	33.57	5.08	45.00	2.54
11.47	38.10	22.90	15.24	34.33	5.40		

TABLE 5

Locations of Equipment.

DISTANCE (m)	DEPTH(MLLW) (cm)	MANOMETER	WAVE GAUGE	SHEAR PLATE
41.30	2.91	#1		
39.38	3.29	#2	#3	
37.70	3.26	#3		
34.25	5.36	#4	#4	
31.60	2.94	#5		
29.62	3.61			#5
29.12	6.96	#6	#5	
26.70	10.49	#7		
24.00	13.87	#8		
21.70	16.74			#5A
21.38	16.83	#9	#5A	
20.18	17.15	#10	#6	
15.20	28.68	#11		
9.10	48.80	#12		
2.50	88.76	#13	#7	

TABLE 6

Wave Breaking Points, End Points of Broken Waves and Types of Breaking Waves. (Distance Is in (m). SP and PL Stand for Spilling and Plunging Breakers, Respectively.)

TEST #	B.P.1		B.P.2		B.P.3		TYPE1	TYPE2	TYPE3
12	26.5	33.0	-	-	-	-	SP	-	-
13	25.5	32.5	-	-	-	-	SP	-	-
14	27.5	32.0	-	-	-	-	SP	-	-
15	30.5	33.0	-	-	-	-	SP	-	-
16	23.5	31.6	-	-	-	-	SP	-	-
17	30.2	33.0	-	-	-	-	PL	-	-
18	30.2	32.0	-	-	-	-	SP	-	-
19	19.5	31.5	-	-	-	-	PL	-	-
20	18.8	31.6	-	-	-	-	PL	-	-
21	19.3	31.7	-	-	-	-	PL	-	-
22	-	-	-	-	-	-	-	-	-
23	-	-	-	-	-	-	-	-	-
24	17.2	32.0	-	-	-	-	PL	-	-
25	11.8	13.0	15.7	32.0	-	-	SP	PL	-
26	18.0	27.0	29.5	34.0	-	-	PL	SP	-
27	19.5	34.2	-	-	-	-	PL	-	-
28	21.4	32.5	-	-	-	-	SP	-	-
29	19.6	30.0	30.0	33.6	-	-	SP	PL	-
30	-	-	-	-	-	-	-	-	-
31	-	-	-	-	-	-	-	-	-
32	27.3	34.5	-	-	-	-	SP	-	-
33	-	-	-	-	-	-	-	-	-
34	31.0	34.0	39.7	40.9	-	-	SP	SP	-
35	41.5	45.0	-	-	-	-	SP	-	-
36	31.0	33.8	-	-	-	-	SP	-	-
37	28.4	36.5	33.7	38.0	-	-	SP	SP	-
38	29.8	35.4	37.5	39.0	-	-	SP	SP	-
39	18.5	28.2	29.0	34.2	-	-	PL	PL	-
40	19.5	32.8	-	-	-	-	PL	-	-
41	19.0	29.0	29.0	33.0	39.7	40.0	PL	PL	SP
42	30.0	34.5	38.0	39.5	-	-	SP	SP	-
43	-	-	-	-	-	-	-	-	-
44	32.3	36.2	-	-	-	-	SP	-	-
45	-	-	-	-	-	-	-	-	-
46	31.2	35.3	36.5	39.0	-	-	PL	SP	-
47	29.0	30.5	30.5	34.5	-	-	SP	PL	-
48	31.4	34.5	41.0	42.0	-	-	PL	SP	-
49	26.0	33.5	-	-	-	-	PL	-	-
50	22.5	33.8	-	-	-	-	SP	-	-
51	25.5	34.7	-	-	-	-	SP	-	-
52	19.4	33.7	-	-	-	-	PL	-	-
53	19.2	34.2	-	-	-	-	SP	-	-
54	-	-	-	-	-	-	-	-	-

TABLE 6 (continued)

Wave Breaking Points, End Points of Broken Waves and Types of Breaking Waves. (Distance Is in (m). SP and PL Stand for Spilling and Plunging Breakers, Respectively.)

TEST #	B.P.1		B.P.2		B.P.3		TYPE1	TYPE2	TYPE3
55	17.7	30.0	-	-	-	-	PL	-	-
56	17.6	30.0	-	-	-	-	PL	-	-
57	19.0	31.0	-	-	-	-	PL	-	-
58	19.1	31.1	-	-	-	-	PL	-	-
59	19.5	31.7	-	-	-	-	PL	-	-
60	19.0	31.5	-	-	-	-	PL	-	-
61	19.0	32.4	-	-	-	-	PL	-	-
62	20.2	32.0	-	-	-	-	SP	-	-
63	30.0	32.7	-	-	-	-	SP	-	-
64	26.6	32.4	-	-	-	-	SP	-	-
65	29.6	32.4	-	-	-	-	SP	-	-
66	31.2	32.2	-	-	-	-	SP	-	-
67	29.3	31.5	-	-	-	-	SP	-	-
68	30.2	32.5	-	-	-	-	SP	-	-
69	-	-	-	-	-	-	-	-	-
70	-	-	-	-	-	-	-	-	-
71	-	-	-	-	-	-	-	-	-
72	-	-	-	-	-	-	-	-	-
73	-	-	-	-	-	-	-	-	-
74	30.7	33.5	-	-	-	-	SP	-	-
75	29.4	33.7	-	-	-	-	PL	-	-
76	30.9	33.4	-	-	-	-	PL	-	-
77	19.5	22.7	25.0	32.2	-	-	SP	SP	-
78	20.0	33.9	-	-	-	-	PL	-	-
79	20.2	32.8	-	-	-	-	SP	-	-
80	19.5	33.0	-	-	-	-	PL	-	-
81	19.4	32.7	-	-	-	-	PL	-	-
82	18.4	32.5	-	-	-	-	PL	-	-
83	17.5	32.5	-	-	-	-	PL	-	-
84	18.5	32.5	-	-	-	-	PL	-	-
85	20.0	34.4	-	-	-	-	SP	-	-
86	18.6	33.2	-	-	-	-	PL	-	-
87	18.4	33.3	-	-	-	-	PL	-	-
88	28.6	35.0	-	-	-	-	SP	-	-
89	22.0	33.2	-	-	-	-	SP	-	-
90	19.8	32.8	-	-	-	-	SP	-	-
91	27.5	34.3	-	-	-	-	SP	-	-
92	-	-	-	-	-	-	-	-	-
93	30.6	34.3	-	-	-	-	PL	-	-
94	-	-	-	-	-	-	-	-	-
95	-	-	-	-	-	-	-	-	-
96	-	-	-	-	-	-	-	-	-
97	-	-	-	-	-	-	-	-	-
98	-	-	-	-	-	-	-	-	-

TABLE 7

Significant Wave Height in (cm).

TEST No.	STATION NUMBER #7	#6	#5A	#5	#4	#3
12	4.90	7.64	8.45	7.82	2.11	3.39
13	4.28	7.78	8.40	5.33	1.77	1.99
14	6.08	7.83	8.20	5.41	1.68	2.34
15	2.55	3.56	3.31	3.61	2.00	1.67
16	10.87	9.30	9.34	4.45	3.57	2.02
17	2.59	3.84	3.91	5.14	2.72	2.12
18	3.09	3.94	4.21	4.46	2.61	2.21
19	11.18	12.11	12.01	8.48	2.90	1.60
20	10.01	12.57	11.43	4.69	1.81	1.58
21	10.81	14.59	13.33	6.12	2.32	1.72
24	16.49	11.31	10.61	6.91	1.62	2.26
25	18.90	13.91	12.74	3.92	2.89	1.83
26	13.93	12.59	12.44	7.50	3.19	2.14
27	10.83	16.13	12.63	5.84	2.66	2.17
28	10.61	15.93	17.52	7.74	3.83	3.18
29	11.18	15.61	11.48	9.03	3.25	3.93
32	5.85	7.23	7.66	8.95	4.64	2.91
33	2.46	3.02	3.09	4.43	3.91	4.26
34	2.71	3.57	4.17	5.31	3.28	2.75
35	3.32	4.10	4.37	5.36	4.56	4.30
36	6.76	6.27	5.77	6.49	3.05	0.00
37	4.73	8.37	8.86	10.16	5.20	3.62
38	5.02	7.45	6.71	8.89	3.90	4.13
39	14.15	15.17	12.46	7.82	3.76	0.00
40	10.51	19.54	13.67	6.98	2.78	3.15
41	14.16	18.05	15.77	8.32	3.91	3.51
42	9.39	8.21	7.14	7.55	6.90	3.51
43	3.85	4.43	3.16	5.27	5.04	5.73
44	3.19	3.98	4.58	5.10	5.70	6.58
45	3.05	3.59	2.88	4.79	4.48	4.93
46	7.67	9.42	9.34	11.44	5.87	5.28
47	5.22	8.90	9.53	12.51	6.75	6.47
48	4.60	6.77	5.77	8.86	9.01	6.92
49	10.92	15.02	14.05	11.36	5.64	4.08
50	8.91	17.39	17.48	10.65	4.79	5.30
51	9.98	15.10	13.09	12.07	7.12	4.30
52	12.27	23.39	17.06	7.83	5.04	4.28
53	15.36	21.67	20.32	11.03	6.44	5.15
54	2.16	2.44	2.84	3.13	3.99	3.11

TABLE 7 (continued)

Significant Wave Height in (cm).

TEST No.	STATION NUMBER #7	#6	#5A	#5	#4	#3
55	12.32	13.04	10.77	4.96	1.62	.67
56	15.63	11.82	10.20	4.89	1.70	.90
57	9.90	13.28	11.24	4.97	2.09	.88
58	9.54	12.00	9.93	5.49	1.35	.74
59	10.03	13.18	8.48	5.06	1.12	.74
60	10.03	10.53	9.67	6.08	2.16	.99
61	14.18	13.24	10.18	6.96	1.92	1.11
62	11.66	14.08	11.15	6.39	2.01	1.14
63	5.49	7.34	7.09	6.84	2.17	1.41
64	5.43	7.69	9.07	5.48	1.57	1.24
65	6.17	7.19	6.00	5.99	2.09	1.24
66	2.82	3.22	2.78	2.54	2.25	1.42
67	10.79	8.44	6.92	6.18	2.55	.94
68	2.89	3.98	3.65	3.84	1.82	.99
70	7.43	6.29	5.56	4.81	3.04	1.93
71	3.53	3.70	3.45	3.34	2.63	1.66
72	2.67	3.43	3.10	3.97	3.28	2.25
73	2.86	3.17	2.88	3.28	2.57	1.78
74	6.13	6.67	6.37	6.27	3.54	3.24
75	5.43	8.13	8.06	8.34	4.05	2.68
76	5.19	6.19	5.60	6.66	3.79	2.44
77	12.78	14.33	14.02	7.97	3.33	2.21
78	11.25	19.98	11.51	6.14	2.49	1.90
79	9.88	18.96	14.30	5.56	3.01	2.38
80	15.87	15.75	10.43	9.25	4.53	3.01
81	11.71	16.37	14.08	8.34	3.03	2.45
82	17.23	14.36	8.61	6.97	3.46	2.59
83	14.96	12.43	8.40	6.01	2.54	2.85
84	13.75	16.75	13.38	6.06	3.26	2.30
85	13.98	22.07	18.52	9.09	4.06	3.66
86	14.93	16.37	10.23	7.06	4.98	3.78
87	16.83	17.17	14.67	7.59	3.89	3.75
88	9.41	13.80	12.19	13.58	5.68	4.98
89	9.74	17.52	17.48	8.13	4.67	3.46
90	15.99	17.38	13.70	9.95	4.40	4.58
91	10.95	12.27	11.43	10.92	6.48	4.04
92	5.25	6.51	5.83	6.74	7.45	3.82
93	6.17	9.38	9.52	9.89	6.23	4.01
94	3.14	3.50	2.95	3.42	2.63	2.08
95	5.76	5.74	5.29	5.72	4.88	3.88
96	2.93	3.39	3.02	3.65	3.33	2.80
97	8.10	7.35	6.27	4.99	3.62	2.69
98	2.32	2.95	2.49	2.68	2.38	1.93

TABLE 8

Root-Mean-Square Wave Height in (cm).

	STATION NUMBER					
TEST No.	#7	#6	#5A	#5	#4	#3
12	4.80	7.49	8.31	7.50	1.73	2.30
13	4.17	7.65	6.17	3.76	1.30	1.46
14	5.96	7.69	8.07	5.07	1.47	1.60
15	2.47	3.43	3.26	2.32	1.33	1.30
16	10.66	9.02	8.88	3.29	2.78	1.49
17	2.50	3.28	3.85	3.28	1.94	1.61
18	2.97	3.77	4.15	4.39	1.94	2.08
19	11.05	10.73	11.23	7.28	2.30	1.12
20	9.86	9.75	8.34	3.45	1.37	1.11
21	10.62	10.81	12.57	4.58	1.58	1.26
24	16.26	8.24	7.87	6.24	1.31	1.71
25	18.59	12.54	11.60	3.18	2.19	1.34
26	13.74	10.38	11.41	5.87	2.37	1.69
27	10.57	14.97	10.72	4.02	1.83	1.60
28	10.43	14.25	16.94	5.81	2.78	2.42
29	11.01	14.99	10.73	8.23	2.64	2.97
32	5.70	6.99	7.35	8.62	3.74	2.38
33	2.31	2.85	3.02	4.24	2.43	3.18
34	2.54	3.09	4.05	3.90	2.09	1.93
35	3.07	3.52	3.96	4.83	3.83	3.16
36	6.60	6.01	5.65	6.31	2.76	0.00
37	4.58	8.14	8.73	7.22	3.56	2.39
38	4.85	7.23	6.27	8.57	2.87	2.83
39	13.84	14.07	11.30	7.28	3.00	0.00
40	10.30	17.50	11.14	4.50	1.93	2.24
41	13.89	17.09	14.21	6.00	2.81	2.69
42	9.01	7.85	6.72	7.13	5.58	2.78
43	3.68	4.11	2.99	5.02	4.52	5.36
44	3.11	3.69	4.44	3.69	3.61	5.13
45	2.94	3.29	2.76	4.00	3.26	3.70
46	7.51	9.12	9.13	10.87	4.73	4.81
47	5.06	7.40	9.40	8.64	4.70	3.98
48	4.45	6.56	5.69	8.57	8.52	4.86
49	10.70	14.65	13.71	10.53	3.79	3.67
50	8.61	12.90	13.07	7.79	3.38	3.56
51	9.69	14.73	9.82	11.24	5.87	3.49
52	12.03	21.90	13.85	4.96	3.55	2.85
53	15.01	19.72	19.35	9.04	4.28	3.29
54	1.95	2.28	2.78	2.98	3.91	2.95

TABLE 8 (continued)

Root-Mean-Square Wave Height in (cm).

	STATION NUMBER					
TEST No.	#7	#6	#5A	#5	#4	#3
55	12.02	12.01	9.98	3.60	1.03	.51
56	15.27	8.40	7.57	3.67	1.48	.70
57	9.56	11.40	10.63	3.67	1.44	.72
58	9.30	9.30	7.63	3.44	.96	.55
59	9.88	9.36	6.00	3.18	.91	.61
60	9.88	7.70	7.45	3.79	1.56	.79
61	13.83	11.97	9.57	6.09	1.55	.86
62	11.55	13.59	10.38	5.72	1.50	.88
63	5.40	7.16	6.99	6.56	1.60	1.13
64	5.29	5.69	8.52	4.03	1.27	.96
65	6.04	6.97	5.89	5.83	1.86	1.17
66	2.65	3.06	2.73	1.79	1.43	1.13
67	10.53	8.22	6.76	5.82	2.24	.75
68	2.78	3.57	3.61	2.58	1.37	.83
70	7.24	6.08	5.45	4.68	2.96	1.84
71	3.39	3.56	3.39	3.28	1.94	1.56
72	2.53	2.70	3.02	2.92	2.15	1.78
73	2.72	2.79	2.84	3.19	1.91	1.34
74	6.01	6.50	6.29	6.14	3.11	2.44
75	5.33	7.27	7.82	6.19	2.89	1.84
76	5.05	4.95	5.50	6.29	2.39	1.59
77	12.42	13.84	13.57	7.13	2.38	1.73
78	10.91	16.03	8.55	3.90	1.62	1.39
79	9.59	14.80	10.42	3.82	1.97	1.70
80	15.59	14.55	9.72	8.76	3.45	2.27
81	11.42	15.42	13.28	7.43	2.11	1.76
82	16.88	10.37	6.24	5.03	2.31	1.92
83	14.70	9.48	6.31	3.82	1.72	1.76
84	12.82	15.46	11.95	4.40	2.10	1.73
85	13.71	19.44	18.04	6.65	3.00	2.79
86	14.66	12.15	7.75	4.61	3.08	2.36
87	16.58	12.69	10.75	5.05	2.58	2.57
88	7.93	13.42	12.00	12.40	3.97	3.69
89	9.60	14.89	16.41	6.05	3.06	2.31
90	15.75	16.62	13.07	8.49	3.15	4.04
91	10.81	12.00	11.26	10.70	5.05	3.32
92	5.12	6.34	5.77	6.07	5.37	4.19
93	6.03	9.07	9.06	7.15	4.17	2.53
94	2.95	3.27	2.89	3.34	2.00	1.61
95	5.56	5.60	5.19	5.62	4.78	3.66
96	2.69	3.10	2.96	3.39	2.55	1.99
97	7.94	7.14	6.13	4.83	3.54	2.55
98	2.65	2.69	2.42	2.57	2.33	1.80

TABLE 9

Wave Period Corresponding to Significant Wave Height in (sec.).

	STATION NUMBER					
TEST No.	#7	#6	#5A	#5	#4	#3
12	3.01	3.00	2.99	2.99	1.73	1.88
13	4.01	3.99	3.92	2.15	1.37	1.66
14	2.07	2.06	2.06	2.07	1.29	1.51
15	2.95	2.95	2.93	1.83	1.43	1.76
16	1.00	1.01	1.01	1.02	1.04	1.06
17	3.97	3.96	3.94	2.14	2.36	2.22
18	1.99	2.00	1.99	1.99	1.07	1.99
19	1.99	2.00	2.00	2.00	1.24	1.60
20	4.00	4.00	3.88	2.32	1.39	1.87
21	2.96	2.59	2.96	2.57	1.13	1.48
24	4.04	3.56	3.91	4.04	1.50	1.36
25	2.95	2.97	2.97	1.75	1.22	1.50
26	1.99	2.01	2.01	1.99	1.17	1.99
27	3.90	3.90	3.89	1.92	1.15	1.64
28	2.97	2.97	2.98	2.79	1.12	1.65
29	1.98	1.99	2.00	2.00	1.16	1.99
32	2.00	2.00	2.00	2.01	1.22	2.01
33	2.95	2.97	2.94	2.94	1.18	2.22
34	4.04	4.02	4.01	3.25	1.75	1.81
35	2.02	2.04	2.02	2.03	2.07	1.46
36	.99	1.00	.99	1.00	1.01	0.00
37	4.02	4.02	4.01	2.74	1.92	1.48
38	2.97	2.96	2.95	2.96	1.74	1.18
39	1.99	2.02	2.01	2.03	1.70	0.00
40	4.04	4.04	4.03	1.98	1.13	1.70
41	2.93	2.94	2.94	2.15	1.07	1.39
42	1.02	1.02	1.01	1.02	1.02	1.06
43	2.02	2.04	2.03	2.03	2.11	2.05
44	4.02	4.02	4.00	2.92	1.54	2.11
45	2.97	2.96	3.00	2.93	1.72	2.28
46	2.00	2.00	2.00	2.00	2.00	2.03
47	4.05	4.01	4.02	2.47	1.86	2.02
48	2.97	2.94	2.93	2.94	2.93	2.07
49	1.99	2.00	1.99	2.00	1.15	2.04
50	4.02	3.84	3.71	2.15	1.58	1.62
51	2.97	2.97	2.31	2.98	2.97	1.66
52	4.07	4.08	4.06	1.81	1.14	1.31
53	2.97	2.97	2.97	2.99	1.51	1.90
54	2.03	2.05	2.01	2.02	2.02	2.01

TABLE 9 (continued)

Wave Period Corresponding to Significant Wave Height in (sec.).

	STATION NUMBER					
TEST No.	#7	#6	#5A	#5	#4	#3
55	3.01	3.00	3.00	1.62	1.10	1.27
56	4.12	3.85	4.10	3.14	3.18	1.64
57	3.02	3.03	3.02	1.64	1.02	1.41
58	4.13	4.11	4.11	2.37	.84	1.26
59	4.31	3.12	3.05	2.52	1.35	1.23
60	3.63	2.91	3.62	1.62	1.38	1.20
61	1.99	2.01	2.01	2.01	1.28	2.01
62	1.99	1.99	2.00	2.00	1.16	1.63
63	3.02	3.00	3.00	3.00	1.64	1.52
64	4.14	3.37	4.12	2.50	1.65	1.66
65	1.99	2.00	1.99	1.99	1.99	2.03
66	2.99	2.98	2.96	1.71	1.18	2.05
67	1.01	1.01	1.01	1.01	1.01	1.06
68	4.13	4.12	4.11	2.37	2.80	2.37
70	1.00	1.01	1.00	1.00	1.00	1.01
71	2.03	2.04	2.02	2.02	1.36	2.04
72	4.21	4.16	4.16	4.14	2.42	1.55
73	3.01	2.99	2.98	2.97	1.82	1.58
74	2.00	2.00	1.99	1.99	2.01	1.60
75	4.06	4.05	4.05	2.74	1.69	1.33
76	2.99	2.97	2.97	2.97	1.61	1.38
77	1.98	1.98	1.99	1.99	1.08	1.99
78	4.12	4.11	3.75	2.20	1.64	1.55
79	4.58	4.55	4.11	2.86	2.29	1.64
80	2.00	2.01	2.00	2.01	1.19	1.79
81	3.05	3.06	3.05	3.05	1.38	1.22
82	4.16	3.70	2.70	3.34	1.86	1.75
83	3.72	3.35	2.68	1.61	1.57	2.15
84	3.05	3.02	3.02	2.33	1.11	1.66
85	2.99	2.99	2.99	2.70	1.47	1.53
86	3.69	3.50	2.34	2.27	2.11	2.35
87	4.16	4.15	4.14	2.32	1.76	1.77
88	3.01	3.03	3.02	3.02	1.72	1.56
89	4.07	4.06	4.07	2.05	1.65	1.41
90	1.99	2.00	2.00	2.00	1.60	2.01
91	1.99	1.99	2.00	2.00	1.13	1.99
92	3.03	3.01	3.00	3.00	1.71	2.36
93	4.06	4.04	4.02	2.59	2.16	1.70
94	3.06	3.03	3.00	3.00	1.87	1.92
95	2.00	1.99	1.99	1.99	1.99	2.00
96	4.12	4.12	4.09	4.09	3.10	1.54
97	1.01	1.01	1.00	1.01	1.01	1.03
98	2.03	2.03	2.02	2.02	2.02	2.05

TABLE 10

Mean Water Depth in (cm).

TEST No.	SWL ABOVE MLLW	STATION NUMBER #7	#6	#5A	#5	#4	#3
12	3.42	92.32	20.40	20.10	10.68	9.23	7.19
13	3.33	92.23	20.43	20.05	10.92	9.09	7.06
14	3.33	92.23	20.46	20.11	10.99	9.33	7.16
15	3.62	92.52	20.70	20.38	10.97	9.02	6.93
16	3.44	92.34	20.41	20.04	11.11	9.37	7.33
17	3.63	92.53	20.75	20.48	11.01	9.14	7.04
18	3.48	92.38	20.63	20.33	10.82	9.04	6.83
19	3.16	92.06	20.24	20.20	11.01	9.59	7.46
20	3.20	92.10	20.45	20.34	11.38	9.49	7.48
21	3.25	92.15	20.35	20.04	11.30	9.49	7.46
24	2.58	91.48	20.70	20.60	11.59	9.78	7.74
25	2.62	91.52	20.71	20.63	11.74	9.92	7.89
26	2.72	91.62	20.28	20.28	11.06	9.60	7.53
27	6.02	94.92	22.96	22.90	14.03	12.29	10.24
28	6.11	95.01	22.92	22.71	13.55	12.30	10.22
29	6.16	95.06	23.05	22.82	13.97	12.39	10.37
32	6.48	95.38	23.50	23.19	13.68	12.08	10.01
33	6.58	95.48	23.73	23.35	13.99	11.80	9.74
34	6.49	95.39	23.66	23.30	13.94	11.91	9.76
35	6.55	95.45	23.74	23.37	13.98	11.83	9.79
36	6.60	95.50	23.68	23.35	13.83	11.82	9.79
37	6.60	95.50	23.72	23.39	13.95	12.21	10.08
38	6.64	95.54	23.73	23.35	13.86	12.02	10.02
39	6.27	95.17	23.40	23.36	14.40	12.72	10.02
40	6.28	95.18	23.37	23.22	14.22	12.40	10.41
41	6.12	95.02	22.96	23.12	14.19	12.63	10.58
42	9.37	98.27	26.49	26.14	16.66	14.65	12.56
43	9.39	98.29	26.55	26.20	16.87	14.69	12.62
44	9.62	98.52	26.69	26.41	16.91	14.93	12.80
45	9.58	98.48	26.74	26.42	17.07	14.98	12.83
46	9.49	98.39	26.59	26.35	16.72	15.11	13.10
47	9.48	98.38	26.61	26.36	16.73	15.17	12.96
48	9.62	98.52	26.75	26.40	16.90	15.05	12.90
49	9.52	98.42	26.62	26.25	17.27	15.50	12.50
50	9.44	98.34	26.44	26.21	16.94	15.34	13.29
51	9.41	98.31	26.49	26.16	16.92	15.36	13.30
52	9.27	98.17	26.16	26.23	17.39	15.50	13.48
53	9.50	98.40	26.20	25.99	17.36	15.93	13.78
54	9.47	98.37	26.75	26.36	16.93	15.09	12.73

TABLE 10 (continued)

Mean Water Depth in (cm).

TEST No.	SWL ABOVE MLLW	STATION NUMBER #7	#6	#5A	#5	#4	#3
55	2.69	91.59	19.88	19.85	11.14	9.28	7.12
56	2.38	91.28	20.23	20.26	11.22	9.39	7.33
57	2.72	91.62	19.87	19.64	10.84	8.95	6.94
58	2.70	91.60	19.93	19.80	10.88	8.92	6.86
59	3.23	92.13	20.25	20.06	11.19	9.28	7.14
60	3.11	92.01	20.33	20.14	11.29	9.30	7.12
61	3.07	91.97	20.25	20.20	11.30	9.54	7.34
62	3.30	92.20	20.32	19.91	10.87	9.37	7.26
63	3.54	92.44	20.58	20.21	10.78	9.02	6.94
64	3.46	92.36	20.57	20.17	11.06	9.07	6.94
65	3.48	92.38	20.63	20.23	10.88	9.03	6.93
66	3.52	92.42	20.67	20.35	11.00	8.87	6.80
67	3.52	92.42	20.57	20.09	10.89	9.09	6.99
68	3.55	92.45	20.71	20.37	11.02	8.99	6.89
70	6.60	95.50	23.74	23.34	14.08	11.96	9.95
71	6.62	95.52	23.76	23.39	14.12	11.96	9.89
72	6.60	95.50	23.75	23.38	14.08	11.94	9.90
73	6.58	95.48	23.76	23.39	14.10	11.91	9.89
74	6.48	95.38	23.59	23.19	13.91	11.86	9.81
75	6.43	95.33	23.54	23.05	13.85	11.93	9.81
76	6.44	95.34	23.60	23.15	13.88	11.84	9.77
77	6.21	95.11	23.40	22.83	14.06	12.22	10.21
78	6.10	95.00	23.30	22.89	14.12	12.15	10.09
79	6.10	95.00	23.35	22.85	14.09	11.58	10.04
80	5.84	94.74	23.34	23.00	14.15	12.32	10.35
81	5.94	94.84	23.34	22.78	14.04	12.16	10.11
82	5.56	94.46	23.51	23.29	14.48	12.44	10.39
83	5.41	94.31	23.61	23.36	14.50	12.45	10.42
84	5.62	94.52	23.25	22.82	14.22	12.30	10.27
85	9.01	97.91	26.51	25.77	17.11	15.34	13.34
86	8.54	97.44	26.58	26.19	17.54	15.43	13.41
87	8.40	97.30	26.63	26.19	17.44	15.43	13.39
88	9.01	97.91	26.71	26.11	16.79	15.07	13.02
89	8.83	97.73	26.80	26.15	17.14	15.13	13.10
90	8.79	97.69	26.78	26.13	17.17	15.32	13.33
91	9.11	98.01	26.61	26.22	16.96	15.07	13.03
92	9.28	98.18	26.64	26.27	17.00	14.79	12.69
93	9.47	98.37	26.67	26.13	16.95	14.92	12.85
94	9.50	98.40	26.69	26.27	17.06	14.84	12.78
95	9.46	98.36	26.62	26.15	16.97	14.77	12.70
96	9.45	98.35	26.61	26.19	16.97	14.79	12.69
97	9.44	98.34	26.57	26.14	16.96	14.77	12.75
98	9.48	98.38	26.64	26.25	17.00	14.82	12.77

TABLE 11

Variance of Water Surface Elevation in (cm^2).

	STATION NUMBER					
TEST No.	#7	#6	#5A	#5	#4	#3
12	2.73	4.11	4.43	3.45	.44	.47
13	2.17	4.36	3.96	1.82	.28	.25
14	4.25	5.51	5.90	2.40	.29	.31
15	.71	1.35	1.09	1.14	.25	.19
16	13.14	9.46	8.78	1.52	.91	.27
17	.71	1.54	1.34	1.78	.33	.20
18	1.12	1.55	1.72	1.52	.45	.35
19	15.50	11.27	10.95	4.38	.53	.15
20	11.30	9.16	7.42	1.63	.24	.15
21	11.68	15.16	10.84	2.26	.37	.19
24	27.13	9.95	7.71	2.09	.27	.48
25	34.80	14.13	11.44	2.03	.67	.25
26	25.43	12.07	11.20	3.92	.60	.31
27	11.37	12.74	8.31	2.33	.46	.33
28	11.45	15.42	14.96	3.75	1.25	.90
29	15.23	16.64	10.61	5.66	1.06	1.02
32	4.21	5.02	5.98	5.63	1.64	.67
33	.55	.87	1.10	1.45	.83	1.01
34	.78	1.23	1.73	1.91	.70	.53
35	1.22	1.42	1.89	2.44	1.43	1.46
36	5.49	4.35	3.77	4.75	.88	0.00
37	2.38	4.88	5.03	5.20	1.73	.78
38	2.60	4.43	3.54	3.95	1.06	1.19
39	25.83	17.52	11.87	5.03	1.17	0.00
40	12.11	16.55	10.06	3.29	.68	.55
41	20.04	20.46	15.56	3.98	1.13	.88
42	9.05	7.66	5.85	5.76	3.68	.92
43	1.67	1.93	1.10	2.53	1.54	2.59
44	1.18	1.53	1.96	1.85	1.84	2.41
45	.92	1.24	.92	2.02	1.61	1.95
46	6.59	8.93	8.28	8.78	1.99	2.01
47	2.81	5.63	6.81	6.76	2.69	1.60
48	2.18	4.52	3.33	5.15	4.21	2.88
49	13.82	17.67	16.85	9.07	1.87	1.50
50	8.59	14.33	15.52	5.70	1.82	1.68
51	9.54	14.64	14.64	8.65	2.59	1.46
52	16.39	22.25	15.67	4.48	1.88	1.42
53	22.42	25.03	23.79	6.38	2.78	1.46
54	.44	.61	.93	.89	1.48	.88

TABLE 11 (continued)

Variance of Water Surface Elevation in (cm^2).

	STATION NUMBER					
TEST No.	#7	#6	#5A	#5	#4	#3
55	18.85	10.83	7.61	1.42	.17	.04
56	24.24	8.10	5.68	1.42	.26	.08
57	10.91	8.99	7.45	1.42	.33	.07
58	9.88	7.23	4.98	1.38	.17	.05
59	10.20	10.83	5.51	1.27	.12	.06
60	12.24	9.81	5.14	1.62	.27	.13
61	25.94	12.33	8.62	2.94	.34	.10
62	16.65	12.45	8.72	2.70	.38	.12
63	3.45	4.26	3.40	2.53	.42	.18
64	3.34	4.94	4.35	1.54	.25	.15
65	4.26	4.45	3.59	2.20	.32	.14
66	.77	1.08	.89	.60	.31	.14
67	13.71	8.46	5.50	3.39	.54	.06
68	.91	1.47	1.27	1.13	.20	.09
70	7.00	4.92	3.87	2.75	1.07	.43
71	1.41	1.45	1.49	1.20	.59	.33
72	.75	1.12	1.10	1.08	.60	.39
73	.78	1.04	.98	.93	.45	.32
74	4.50	4.46	4.28	3.01	.87	.76
75	3.40	4.78	4.53	3.47	.90	.53
76	2.89	3.45	3.10	2.48	.79	.51
77	17.86	14.07	13.50	4.49	.69	.40
78	13.55	15.67	8.59	2.61	.44	.31
79	10.68	13.16	9.50	2.20	.51	.49
80	28.07	17.47	9.34	5.32	1.53	.76
81	14.37	13.29	11.07	3.67	.77	.50
82	27.50	13.88	8.11	2.51	.78	.42
83	25.82	13.15	7.15	2.03	.46	.50
84	22.23	16.61	12.23	2.91	.66	.42
85	20.55	21.00	18.45	6.80	1.74	1.01
86	26.22	18.73	11.63	3.17	1.58	.78
87	25.43	17.71	13.04	3.99	1.11	.94
88	10.06	12.14	11.41	8.87	2.57	1.79
89	10.88	14.78	12.79	4.24	1.06	.77
90	26.21	21.52	15.69	7.22	1.54	1.59
91	13.86	13.51	12.02	9.64	3.01	1.43
92	3.06	3.78	3.54	3.01	3.21	2.12
93	4.52	6.28	6.05	4.72	1.68	.93
94	.89	1.20	1.00	1.14	.82	.45
95	3.72	3.71	3.16	3.18	1.91	1.35
96	.88	1.15	.92	1.11	.78	.56
97	7.92	6.04	4.62	3.00	1.60	.82
98	.82	.87	.76	.80	.57	.42

TABLE 12

Values of Wave Set-Up in (cm).

	MANOMETER NUMBER												
TEST No.	#13	#12	#11	#10	#9	#8	#7	#6	#5	#4	#3	#2	#1
12	0.00	-.06	-.09	-.17	-.15	-.18	-.25	-.26	.26	.45	.43	.48	.63
13	0.00	-.07	-.10	-.05	-.11	-.12	-.28	.06	.23	.40	.47	.44	.53
14	0.00	-.13	-.08	-.01	-.04	-.16	-.18	.15	.45	.64	.62	.54	.71
15	0.00	-.04	-.05	-.07	-.06	-.08	-.14	-.17	.01	.04	.03	.02	.14
16	0.00	-.04	-.16	-.18	-.23	-.18	-.08	.15	.51	.57	.56	.60	.59
17	0.00	-.01	-.01	-.02	.02	-.04	-.05	-.14	.08	.16	.12	.12	.13
18	0.00	-.00	.01	.00	.02	.00	-.08	-.17	.05	.20	.11	.06	.12
19	0.00	-.12	-.28	-.07	.21	.50	.47	.33	.95	1.07	1.05	1.01	.97
20	0.00	-.16	-.35	.09	.31	.55	.63	.66	.96	.93	1.00	.99	.94
21	0.00	-.13	-.31	-.05	-.04	.35	.44	.53	.80	.88	.89	.92	.97
24	0.00	-.29	-.67	.96	1.19	1.40	1.49	1.49	1.79	1.84	1.90	1.87	1.85
25	0.00	-.34	-.54	.95	1.18	1.57	1.54	1.60	2.06	1.95	2.00	1.99	2.02
26	0.00	-.22	-.46	.40	.72	1.00	1.02	.81	1.89	1.52	1.55	1.52	1.49
27	0.00	-.11	-.41	-.21	.05	.44	.51	.49	.85	.91	.93	.93	.93
28	0.00	-.21	-.44	-.34	-.23	-.02	.24	-.08	.72	.83	.90	.82	.93
29	0.00	-.11	-.44	-.26	-.16	.20	.27	.30	.79	.87	.96	.93	.95
32	0.00	-.06	-.10	-.13	-.12	-.04	-.22	-.32	.03	.24	.30	.24	.22
33	0.00	-.03	-.01	-.00	-.06	-.05	-.03	-.10	-.13	-.13	-.14	-.12	-.09
34	0.00	.04	.03	.03	-.02	-.03	.00	-.07	.06	.07	.00	-.02	.01
35	0.00	.02	.02	.04	-.01	.02	-.05	-.09	-.05	-.08	-.03	-.04	-.09
36	0.00	-.02	-.04	-.06	-.07	.01	-.14	-.29	-.02	-.14	-.06	.09	.09
37	0.00	-.00	.01	-.02	-.04	-.00	-.19	-.17	.11	.25	.23	.19	.19
38	0.00	.01	-.03	-.06	-.12	-.00	-.19	-.30	-.12	.02	.04	.09	.12
39	0.00	-.10	-.43	-.02	.25	.85	.69	.60	.92	1.09	1.14	1.18	1.17
40	0.00	.02	-.34	-.06	.11	.42	.44	.41	.65	.76	.82	.84	.85
41	0.00	-.12	-.37	-.31	.17	.67	.76	.55	1.11	1.15	1.18	1.17	1.31
42	0.00	.00	-.02	-.03	-.06	.01	-.13	-.23	-.03	-.07	-.01	-.10	.09
43	0.00	.01	-.02	.01	-.02	.02	-.09	-.04	-.03	-.06	-.08	-.06	.00
44	0.00	.00	.02	-.08	-.04	.00	-.14	-.23	-.20	-.05	-.06	-.10	-.04
45	0.00	.04	.01	.01	.01	.01	-.05	-.02	-.11	.04	.02	-.03	.00
46	0.00	.08	-.01	-.05	.04	.08	-.23	-.29	-.27	.27	.37	.32	.26
47	0.00	.06	.03	-.03	.05	.09	-.16	-.27	.03	.33	.27	.18	.21
48	0.00	.06	.04	-.02	-.05	.06	-.10	-.24	-.14	.07	.22	-.01	.07
49	0.00	.07	-.14	-.05	-.10	.02	-.29	.23	.58	.62	.88	-.31	.66
50	0.00	.07	-.14	-.15	-.06	.05	.03	-.02	.42	.54	.63	.56	.57
51	0.00	.12	-.17	-.07	-.08	.22	-.16	-.01	.32	.59	.78	.60	.64
52	0.00	.12	-.26	-.26	.13	.66	.50	.60	.74	.87	.96	.92	.88
53	0.00	-.24	-.39	-.45	-.34	.20	.31	.34	.58	1.07	.99	.99	1.02
54	0.00	.03	.03	.12	.05	.08	-.02	-.07	-.07	.25	-.04	-.03	-.05

TABLE 12 (continued)

Values of Wave Set-Up in (cm).

	MANOMETER NUMBER												
TEST No.	#13	#12	#11	#10	#9	#8	#7	#6	#5	#4	#3	#2	#1
55	0.00	-.59	-.03	.03	.32	.62	.87	.93	1.12	1.22	1.24	1.13	-
56	0.00	-.55	.04	.76	1.05	1.29	1.41	1.32	1.61	1.66	1.65	1.66	-
57	0.00	-.30	.23	.00	.09	.35	.58	.60	.85	.87	.90	.94	-
58	0.00	-.32	.24	.08	.27	.60	.70	.66	.80	.86	1.11	.87	-
59	0.00	-.21	-.09	-.13	.00	.34	.49	.43	.64	.69	.71	.62	-
60	0.00	-.15	-.07	.07	.20	.53	.60	.66	.82	.83	.82	.72	-
61	0.00	-.19	-.06	.03	.30	.79	.71	.71	1.04	1.11	1.10	.98	-
62	0.00	-.19	-.08	-.13	-.23	.18	.04	.05	.66	.70	.72	.67	-
63	0.00	-.03	-.00	-.11	-.16	-.05	-.17	-.29	.02	.11	.09	.10	-
64	0.00	-.01	-.02	-.05	-.12	-.00	-.10	.08	.23	.25	.28	.19	-
65	0.00	-.05	-.03	-.01	-.08	.00	-.09	-.12	.11	.19	.21	.16	-
66	0.00	.02	.02	.00	.00	.03	.00	-.04	-.04	-.00	-.01	-.00	-
67	0.00	-.04	-.08	-.10	-.26	-.07	-.12	-.15	.18	.21	.24	.18	-
68.	0.00	.01	.02	.02	-.01	.03	-.01	-.05	.05	.08	.10	.05	-
70	0.00	0.00	-.05	-.01	-.09	-.12	-.02	-.04	-.12	-.01	0.00	.06	-
71	0.00	-.00	-.01	-.01	-.06	-.07	-.03	-.02	-.04	-.01	-.01	-.01	-
72	0.00	.00	-.04	-.00	-.04	-.05	.00	-.04	-.06	-.02	-.04	.01	-
73	0.00	.03	-.00	.02	-.03	-.02	.01	-.01	-.04	-.03	-.01	.02	-
74	0.00	-.02	-.09	-.04	-.12	-.24	-.05	-.08	-.12	.02	.03	.04	-
75	0.00	-.02	-.10	-.04	-.20	-.23	-.11	-.10	.03	.14	.11	.09	-
76	0.00	-.02	-.05	.00	-.13	-.13	-.05	-.09	-.10	.03	-.01	.04	-
77	0.00	-.07	-.13	.04	-.21	-.42	-.08	.33	.61	.65	.69	.71	-
78	0.00	-.04	.01	.05	-.04	.24	.49	.50	.64	.69	.76	.70	-
79	0.00	.03	.03	.10	-.07	.18	.43	.47	.58	.12	.64	.65	-
80	0.00	-.04	.04	.34	.32	.61	.78	.79	.95	1.12	1.21	1.22	-
81	0.00	.05	.20	.26	.01	.09	.39	.59	.78	.87	.89	.88	-
82	0.00	.02	.22	.80	.89	.99	1.31	1.39	1.52	1.52	1.55	1.53	-
83	0.00	.10	.17	1.05	1.12	1.20	1.52	1.57	1.65	1.68	1.79	1.72	-
84	0.00	.07	.36	.48	.37	.57	.96	1.08	1.29	1.32	1.39	1.36	-
85	0.00	-.41	-.08	.35	-.07	-.32	.35	.58	.81	.97	1.01	1.04	-
86	0.00	-.22	.21	.89	.82	1.03	1.38	1.48	1.51	1.53	1.57	1.58	-
87	0.00	.13	.47	1.08	.96	1.01	1.46	1.52	1.62	1.67	1.80	1.70	-
88	0.00	.18	.26	.55	.27	-.16	.24	.26	.35	.70	.79	.72	-
89	0.00	.20	.43	.82	.49	.14	.69	.80	.84	.94	1.02	.98	-
90	0.00	.03	.24	.84	.51	.15	.69	.86	.93	1.17	1.25	1.25	-
91	0.00	.04	.11	.34	.27	-.38	.18	.33	.41	.59	.55	.62	-
92	0.00	.04	.08	.21	.16	-.13	.19	.20	.07	.15	.26	.12	-
93	0.00	-.09	-.05	.05	-.17	-.11	-.10	-.04	-.03	.09	.03	.09	-
94	0.00	-.02	.03	.03	-.06	-.06	.00	.04	-.06	-.02	-.06	-.01	-
95	0.00	-.02	-.02	.01	-.13	-.11	-.03	-.00	-.11	-.04	.09	-.05	-
96	0.00	.01	.04	.01	-.08	-.03	.00	.00	-.06	-.02	.04	-.05	-
97	0.00	-.01	-.02	-.02	-.12	-.09	-.00	.01	-.10	-.02	.04	.02	-
98	0.00	-.05	-.05	.00	-.06	-.06	.02	0.00	-.04	-.02	.02	0.00	-

TABLE 13

Wave Particle Amplitude, Amplitude Reynolds Number, Friction Factor, Mean Shear Stress and Energy Dissipation due to Bed Shear Stress at Station 5.

TEST No.	K_s (cm)	a_δ (cm)	RE	C_f	$\overline{\tau}$ ($g/cm \cdot sec^2$)	E_d (g/sec^3)
12	.14	9.41	21473	-	-	-
13	.14	7.24	9523	.005	-.05	4.6
14	.14	6.02	12936	-	-	-
15	.14	6.04	8671	-	-	-
16	.14	3.25	7458	-	-	-
17	.14	7.78	10965	.004	.11	7.1
18	.14	4.93	8627	-	-	-
19	.14	7.95	22489	.081	4.03	360.2
20	.14	6.94	8410	-	-	-
21	.14	7.06	11777	-	-	-
24	.14	7.76	10516	.070	-1.81	39.3
25	.14	6.83	10985	-	-	-
26	.14	7.11	17581	-	-	-
27	.14	8.10	11563	-	-	-
28	.14	8.62	17305	.035	-2.76	61.8
29	.14	7.63	20556	.010	-.26	43.9
32	.14	7.42	19155	.055	5.51	264.6
33	.14	7.27	12241	-	-	-
34	.14	7.70	10057	.005	.15	8.4
35	.14	6.49	14293	-	-	-
36	.14	3.38	7725	-	-	-
37	.14	6.85	7833	.031	-.16	44.7
38	.14	8.52	16444	-	-	-
39	.14	9.24	28905	-	-	-
40	.14	8.23	11254	-	-	-
41	.14	6.03	7952	.041	-2.52	33.3
42	.14	3.84	9363	-	-	-
43	.14	6.08	11833	-	-	-
44	.14	11.09	21237	-	-	-
45	.14	7.33	12685	-	-	-
46	.14	9.56	31929	.066	3.96	537.6
48	.14	10.24	24453	-	-	-
49	.14	7.99	22044	.037	-.29	135.6
50	.14	-	-	-	-	-
51	.14	11.94	33030	-	-	-
52	.14	9.36	14848	-	-	-
53	.14	9.45	20591	-	-	-
54	.14	3.88	5179	-	-	-

TABLE 13 (continued)

Wave Particle Amplitude, Amplitude Reynolds Number, Friction Factor, Mean Shear Stress and Energy Dissipation due to Bed Shear Stress at Station 5.

TEST No.	K_s (cm)	a_δ (cm)	RE	C_f	$\overline{\tau}$ ($g/cm \cdot sec^2$)	E_d (g/sec^3)
55	3.12	-	-	-	-	-
56	3.12	-	-	-	-	-
57	3.12	-	-	-	-	-
58	3.12	-	-	-	-	-
59	3.12	-	-	-	-	-
60	3.12	-	-	-	-	-
61	3.12	-	-	-	-	-
62	3.12	-	-	-	-	-
63	3.12	-	-	-	-	-
64	3.12	-	-	-	-	-
65	3.12	-	-	-	-	-
66	3.12	-	-	-	-	-
67	3.12	-	-	-	-	-
68	3.12	-	-	-	-	-
70	3.12	2.78	5324	-	-	-
71	3.12	4.58	7292	-	-	-
72	3.12	8.16	11204	.190	1.46	128.1
73	3.12	6.06	8626	.121	.80	71.0
74	3.12	5.90	12557	.181	4.27	420.7
75	3.12	6.57	7796	.125	4.37	423.6
76	3.12	7.76	14806	.171	4.94	398.9
77	3.12	6.92	17715	.098	-1.48	301.1
78	3.12	7.89	11151	.160	2.61	259.9
79	3.12	9.40	14218	.198	.72	202.9
80	3.12	7.63	21543	.202	11.76	982.5
81	3.12	7.85	14926	.207	1.32	308.3
82	3.12	9.08	14599	.188	-.81	240.0
83	3.12	5.79	6625	.194	3.13	233.5
84	3.12	6.32	9753	.221	.99	303.3
85	3.12	10.25	25628	-	-	-
86	3.12	5.65	6330	.256	1.25	251.8
87	3.12	9.34	15357	.212	-1.03	332.1
88	3.12	11.26	30722	.146	7.71	1026.0
89	3.12	10.23	18952	.157	2.46	410.3
90	3.12	6.37	14933	.263	6.43	673.9
91	3.12	9.35	32345	.232	9.96	1796.2
92	3.12	8.64	18338	.168	3.97	396.0
93	3.12	9.23	15165	.148	5.23	512.1
94	3.12	6.01	8710	.209	.96	98.7
95	3.12	5.88	12623	.245	2.94	428.5
96	3.12	8.45	12606	.203	.53	111.8
97	3.12	2.81	5670	-	-	-
98	3.12	3.83	5284	-	-	-

TABLE 14

Wave Particle Amplitude, Amplitude Reynolds Number, Friction Factor, Mean Shear Stress and Energy Dissipation due to Bed Shear Stress at Station 5A.

TEST No.	K_s (cm)	a_δ (cm)	RE	C_f	$\overline{\tau}$ ($g/cm \cdot sec^2$)	E_d (g/sec^3)
12	.14	7.77	14624	-	-	-
13	.14	11.12	22463	.045	1.36	82.2
14	.14	6.19	13686	.122	5.05	236.3
15	.14	5.48	7143	-	-	-
16	.14	4.08	11732	-	-	-
17	.14	8.16	12084	.070	1.07	37.1
18	.14	4.00	5664	-	-	-
19	.14	6.42	14650	.043	-5.89	105.3
20	.14	11.99	25126	-	-	-
21	.14	9.29	20387	.035	-1.07	111.4
24	.14	12.11	25638	.061	-2.48	153.0
25	.14	10.58	26343	-	-	-
26	.14	7.09	17474	.074	-6.23	206.3
27	.14	13.01	29805	-	-	-
28	.14	11.22	29325	.066	6.15	511.8
29	.14	7.71	20979	.008	.50	31.4
32	.14	6.30	13815	.025	1.40	44.7
33	.14	5.10	6022	.020	.21	5.6
34	.14	7.19	8778	.029	.35	9.2
35	.14	4.04	5548	-	-	-
36	.14	2.63	4682	-	-	-
37	.14	10.97	20106	.077	2.93	130.6
38	.14	6.86	10661	.009	.34	9.5
39	.14	6.64	14931	-	-	-
40	.14	12.41	25604	-	-	-
41	.14	10.63	24668	.025	-1.83	119.7
42	.14	2.62	4355	-	-	-
43	.14	4.90	7680	-	-	-
44	.14	9.06	14163	-	-	-
45	.14	5.28	6578	-	-	-
46	.14	6.44	14517	.083	3.74	183.6
48	.14	8.08	15204	-	-	-
49	.14	8.06	22422	-	-	-
50	.14	14.09	33981	-	-	-
51	.14	10.99	27949	.015	.87	72.4
52	.14	14.11	33750	-	-	-
53	.14	12.20	34368	.046	1.58	334.5
54	.14	2.93	2942	-	-	-

TABLE 14 (continued)

Wave Particle Amplitude, Amplitude Reynolds Number, Friction Factor, Mean Shear Stress and Energy Dissipation due to Bed Shear Stress at Station 5A.

TEST No.	K_s (cm)	a_δ (cm)	RE	C_f	$\overline{\tau}$ ($g/cm.sec^2$)	E_d (g/sec^3)
55	3.12	11.70	32875	.190	-6.89	844.4
56	3.12	12.56	27578	.211	-5.83	606.5
57	3.12	10.64	27080	.175	.96	783.1
58	3.12	11.60	23459	.229	-6.21	635.5
59	3.12	12.50	24962	.204	-5.16	580.5
60	3.12	10.44	20757	.224	-11.41	609.0
61	3.12	7.70	21349	.260	-29.86	1008.1
62	3.12	7.48	20243	.306	.41	1239.5
63	3.12	8.28	16513	.156	1.19	290.4
64	3.12	11.99	25231	.175	1.55	417.6
65	3.12	6.16	13835	.277	-1.13	487.7
66	3.12	5.57	7566	.319	-1.83	117.4
67	3.12	3.67	9695	-	-	-
68	3.12	8.48	12586	.245	.60	134.7
70	3.12	-	-	-	-	-
71	3.12	-	-	-	-	-
72	3.12	-	-	-	-	-
73	3.12	-	-	-	-	-
74	3.12	-	-	-	-	-
75	3.12	-	-	-	-	-
76	3.12	-	-	-	-	-
77	3.12	-	-	-	-	-
78	3.12	-	-	-	-	-
79	3.12	-	-	-	-	-
80	3.12	-	-	-	-	-
81	3.12	-	-	-	-	-
82	3.12	-	-	-	-	-
83	3.12	-	-	-	-	-
84	3.12	-	-	-	-	-
85	3.12	-	-	-	-	-
86	3.12	-	-	-	-	-
87	3.12	-	-	-	-	-
88	3.12	-	-	-	-	-
89	3.12	-	-	-	-	-
90	3.12	-	-	-	-	-
91	3.12	-	-	-	-	-
92	3.12	-	-	-	-	-
93	3.12	-	-	-	-	-
94	3.12	-	-	-	-	-
95	3.12	-	-	-	-	-
96	3.12	-	-	-	-	-
97	3.12	-	-	-	-	-
98	3.12	-	-	-	-	-

TABLE 15

Values of Nonlinearity Parameter, P_n.

	STATION NUMBER					
TEST No.	#7	#6	#5A	#5	#4	#3
12	.48	7.63	8.63	20.77	6.98	16.32
13	.58	10.43	11.57	18.35	8.02	13.20
14	.38	5.27	5.67	9.38	3.73	7.77
15	.24	3.40	3.23	8.99	6.69	8.29
16	.25	2.78	2.87	3.51	3.67	3.05
17	.34	4.94	5.13	17.16	12.01	13.86
18	.19	2.55	2.79	7.73	5.94	7.66
19	.68	7.99	7.95	14.15	5.98	4.81
20	1.36	16.81	15.42	15.16	7.69	9.63
21	1.05	14.38	13.45	14.67	7.23	7.70
24	2.27	14.85	14.03	21.75	6.59	13.06
25	1.86	13.40	12.34	8.90	8.46	7.58
26	.86	8.33	8.23	12.50	6.59	6.39
27	1.38	17.75	13.95	13.49	7.49	8.04
28	.99	13.20	14.72	14.20	8.13	8.94
29	.64	8.39	6.27	10.44	4.51	7.15
32	.34	3.84	4.15	10.85	6.79	5.67
33	.23	2.36	2.47	7.70	8.79	12.76
34	.35	3.86	4.60	12.71	9.95	11.26
35	.19	2.14	2.34	6.29	6.90	8.67
36	.14	1.43	1.35	3.54	2.13	0.00
37	.61	8.98	9.70	24.25	15.15	14.10
38	.46	5.84	5.38	15.72	8.55	11.92
39	.80	7.97	6.56	8.63	5.01	0.00
40	1.37	21.53	15.21	16.25	7.97	11.73
41	1.35	15.18	13.13	14.48	8.11	9.52
42	.19	1.59	1.42	3.13	3.51	2.28
43	.21	1.94	1.41	4.62	5.46	7.82
44	.39	3.56	4.17	9.08	12.25	17.84
45	.27	2.34	1.91	6.16	7.02	9.75
46	.42	4.11	4.13	10.16	6.08	6.80
47	.64	8.03	8.71	22.70	14.19	17.24
48	.40	4.41	3.83	11.56	14.02	13.59
49	.59	6.50	6.22	9.56	5.59	5.62
50	1.10	15.83	16.12	18.96	9.90	13.60
51	.88	10.05	8.88	15.84	10.82	8.12
52	1.53	21.85	15.87	13.54	10.37	10.87
53	1.36	14.71	13.96	13.97	9.30	9.25
54	.12	1.06	1.26	2.73	4.15	4.19

TABLE 15 (continued)

Values of Nonlinearity Parameter, P_n.

TEST No.	STATION NUMBER #7	#6	#5A	#5	#4	#3
55	1.23	13.50	11.18	12.33	5.29	3.25
56	2.22	16.41	14.19	16.55	7.52	5.81
57	1.00	13.91	11.98	12.99	7.28	4.51
58	1.35	17.16	14.34	19.51	6.47	5.29
59	1.48	19.35	12.64	18.13	5.30	5.23
60	1.23	12.87	11.99	18.03	8.58	5.89
61	.86	8.73	6.74	11.17	3.98	3.42
62	.70	9.18	7.50	10.82	4.26	3.57
63	.54	7.24	7.19	17.90	7.45	7.17
64	.76	10.48	12.73	19.00	7.36	8.67
65	.37	4.61	3.96	10.18	4.71	4.18
66	.27	3.11	2.75	6.35	7.80	7.36
67	.24	2.49	2.12	5.03	2.76	1.52
68	.40	5.39	5.07	13.42	8.62	7.02
70	.16	1.46	1.33	2.61	2.13	1.81
71	.20	1.93	1.84	3.86	3.91	3.29
72	.36	3.80	3.52	9.67	10.24	9.29
73	.27	2.49	2.32	5.68	5.75	5.28
74	.35	3.50	3.43	7.37	5.31	6.47
75	.71	8.91	9.11	20.32	12.34	10.96
76	.48	4.93	4.58	11.83	8.55	7.34
77	.73	7.57	7.69	9.18	4.75	4.14
78	1.50	22.57	13.36	14.75	7.51	7.58
79	1.48	23.79	18.53	14.93	10.84	10.64
80	.92	8.35	5.66	10.54	6.37	5.52
81	1.12	13.52	12.06	14.85	6.70	7.16
82	2.35	16.16	9.82	16.28	10.16	9.97
83	1.81	12.43	8.53	12.53	6.67	9.77
84	1.32	13.82	11.36	10.52	7.05	6.51
85	1.26	14.82	12.98	11.85	6.24	6.95
86	1.71	13.57	8.67	10.96	9.38	8.80
87	2.19	16.02	14.03	13.40	8.27	9.84
88	.85	9.23	8.43	18.34	9.03	9.87
89	1.23	15.82	16.38	14.41	9.98	9.20
90	.88	7.50	6.14	8.49	4.47	5.75
91	.60	5.32	5.07	9.44	6.71	5.21
92	.47	4.34	3.97	8.87	12.10	11.91
93	.76	8.47	8.87	17.68	13.51	10.89
94	.28	2.31	1.99	4.44	4.23	4.19
95	.31	2.49	2.36	4.94	5.21	5.22
96	.37	3.13	2.86	6.65	7.46	7.90
97	.17	1.42	1.24	2.01	1.82	1.71
98	.15	1.24	1.11	2.32	2.54	2.59

REFERENCES

1. Battjes, J.A., 1972, "Set-up due to Irregular Waves," Proc. 13th Conf. on Coastal Engineering, vol. 3, ASCE, pp. 1993-2004.

2. Battjes, J.A., 1974, "Surf Similarity," Proc. 14th Conf. on Coastal Engineering, vol. 1, ASCE.

3. Battjes, J.A. and Jassen, J.P.F.M., 1978, "Energy Loss and Set-up due to Breaking of Random Waves," 1978, Proc. 16th Conf. on Coastal Engineering, vol. 1, ASCE, pp. 569-587.

4. Black, K.P., 1978, "Wave Transformation over Shallow Reef," Tech. Rep. No. 42, J.K.K. Look Lab., Univ. of Hawaii.

5. Bowen, A.J., Inman, D.L. and Simmon, V.P., 1968, "Wave Set-Down and Set-Up," J. of Geoph. Res., vol. 73, No. 8.

6. Bretschneider, C.L., 1960, "Selection of Design Wave for Offshore Structures," Trans. of ASCE, vol. 125.

7. Christoffersen, J.B., 1982, "Current Depth Refraction of Dissipative Water Waves," Series Paper 30, Inst. of Hydrodynamics and Hydraulic Engineering, Technical Univ. of Denmark.

8. Eagleson, P.S., 1962, "Laminar Damping of Oscillatory Waves," J. of Hydraulic Div., vol. 88, HY3, ASCE.

9. Eagleson, P.S., 1956, "Properties of Shoaling Waves by Theory and Experiment," Trans. Am. Geophysical Union, vol. 37, No. 5, pp. 565-572.

10. Fan, Loh-Nien and Le Méhauté, B. 1969, "Coastal Movable Bed Scale Model Technology," Tetra Tech No. TC-131, Tetra Tech, Inc.

11. Galvin, C.J., 1969, "Breaker Travel and Choice of Design Wave Height," J. of Waterways and Harbors Div., vol. 95, WW2, ASCE, pp. 175-200.

12. Gerritsen, F., 1981, "Wave Attenuation and Wave Set-Up on a Coastal Reef," Tech. Rep. No. 48, J.K.K. Look Lab., Univ. of Hawaii.

13. Goda,Y., 1983, "A Unified Nonlinearity Parameter of Waves," Report of the Port and Harbor Res. Inst., Japan, vol. 22, No. 3.

14. Hansen, J.B. and Svendsen, I.A., 1979, "Regular Waves in Shoaling Water Experimental Data," Series Paper 21, Inst. of Hydrodynamics and Hydraulic Engineering, Technical Univ. of Denmark.

15. Hansen, U.A., 1978, "Wave Set-up in the Surf Zone," Proc. 16th Conf. on Coastal Engineering, vol. 1, ASCE, pp. 1071-1084.

16. Horikawa, K. and Kuo, C., 1966, "A Study on Wave Transformation Inside Surf Zone," Proc. 10th Conf. on Coastal Engineering, vol. 1, ASCE, pp. 217-233.

17. Hudson, R.Y. and Keulegan, G.H., 1979, "Principles of Similarity, Dimensional Analysis and Scale Model," Coastal Hydraulics Model, Special Rep. No. 5, Coastal Engineering Res. Center, U.S. Army Corps of Engineers, pp. 24-47.

18. Hunt, J.N., 1952, "Viscous Damping of Waves over an Inclined Bed in a Channel of Finite Width," La Houille Blanche, pp. 836-842.

19. Hwang, Li-San and Divoky, D., 1970, "Breaking Wave Setup and Decay on Gentle Slopes," Proc. 12th Conf. on Coastal Engineering, vol. 1, ASCE.

20. Iversen, H.W., 1952, "Laboratory Study of Breakers," Gravity Waves, National Bureau of Standards, U.S. Dept. of Commerce, Circular 521, pp. 9-32.

21. Iwagaki, Y. and Sakai, T., 1972, "Shoaling of Finite Amplitude Long Waves on a Beach of Constant Slope," Proc. 13th Conf. on Coastal Engineering, vol. 1, ASCE, pp. 347-364.

22. James, I.D., 1974, "Non-linear Waves in the Nearshore Region: Shoaling and Set-up," Estuarine and Coastal Marine Science, vol. 2, No. 3.

23. Jonsson, I.G., 1966, "Wave Boundary Layers and Friction Factors," Proc. 109th Conf. on Coastal Engineering, vol. 1, ASCE, pp. 127-148.

24. Jonsson, I.G., 1976, "Experimental and Theoretical Investigations in an Oscillatory Turbulent Boundary Layer," J. of Hydraulic Res., vol. 14, No. 1, pp. 45-60.

25. Jonsson, I.G., 1980, "A New Approach to Oscillatory Rough Turbulent Boundary Layers," Ocean Engineering, vol. 7, pp. 109-152.

26. Kajiura, K., 1968, "A Model of the Bottom Boundary Layer," Balletine of the Earthquake Res. Inst., Tokyo Univ., vol. 46, pp. 75-123.

27. Kamphuis, J.W., 1974, "Determination of Sand Roughness for Fixed Beds," J. of Hydraulic Res., vol. 12, No. 2.

28. Kamphuis, J.W., 1975, "Friction Factor under Oscillatory Waves," J. of Waterways, Harbors and Coastal Engineering Div., vol. 101, WW2, ASCE, pp. 135-144.

29. Le Méhauté, B. and Koh, R.C.Y., 1967, "On the Breaking of Waves Arriving at an Angle to the Shore," J. of Hydraulic Res., vol. 5, pp 67-88.

30. Le Méhauté, B., 1976, "An Introduction to Hydrodynamics and Water Waves," Springer-Verlag, New York.

31. Longuet-Higgins, M.S. and Stewart, R.W., 1964, "Radiation Stress in Water Waves; A Physical Discussion with Applications," Deep-Sea Res., vol. 11, pp. 529-562.

32. Longuet-Higgins, M.S., 1974, "On the Mass, Momentum, Energy and Circulation of a Solitary Wave," Proc. Royal Society, London, Series A, vol. 337, pp. 1-13.

33. McCowan, J., 1894, "On the Highest Wave of Permanent Type," Phil. Mag. J. Sci., vol. 38, No. 5.

34. Michell, J.H., 1893, "On the Highest Waves in Water," Phil. Mag. J. Sci., vol. 36, No. 5.

35. Nadaoka, K., Kondoh, T. and Tanaka, N., 1982, "The Structure of Velocity Field within the Surf Zone Revealed by Means of Laser-Doppler Anemometry," Report of the Port and Harbor Res. Inst., Japan, vol. 21, No.2, pp. 49-106.

36. Riedel, P.H., Kamphius, J.W. and Brebner, A., 1972, "Measurement of Bed Shear Stress under Waves," Proc. 13th Conf. on Coastal Engineering, vol. 1, ASCE, pp. 587-603.

37. Riedel, P.H. and Kamphius, J.W., 1973, "A Shear Plate for Use in Oscillatory Flow," J. of Hydraulic Res., vol. 11, No.2.

38. Rouse, H., Siao, T.T. and Nagaratnam, S., 1958, "Turbulence Characteristics of the Hydraulic Jump," J. of Hydraulic Div., vol. 84, HYI, ASCE.

39. Sakai, T. and Battjes, J.A., 1980, "Wave Shoaling Calculated from Cokelet's Theory," Proc. 17th Conf. on Coastal Engineering, vol. 1, ASCE, pp. 121-134.

40. Sawaragi, T. and Iwata, K., 1974, "On wave Deformation after Breaking," Proc. 14th Conf. on Coastal Engineering, vol. 1, ASCE.

41. Shuto, N., 1974, "Nonlinear Long waves in a Channel of Variable Section," Coastal Engineering in Japan, vol. 17, pp. 1-12.

42. Sleath, J.F.A., 1974, "Stability of Laminar Flow at Seabed," J. of Waterways and Harbor Div., vol. 100, WW2, ASCE, pp. 105-122.

43. Stive, M.J.F., 1980, "Velocity and Pressure Field of spilling Breakers," Proc. 17th Conf. on Coastal Engineering, vol. 1, ASCE, pp. 547-566.

44. Stive, M.J.F. and Wind, H.G., 1982, "A Study of Radiation Stress and Set-up in the Nearshore Region," Coastal Engineering, No. 6, pp. 1-25.

45. Stive, M.J.F., 1984, "Energy Dissipation in Waves Breaking on Gentle Slopes," Coastal Engineering, No. 8, pp. 99-127.

46. Svendsen, I.A. and Brink-Kjaer, O., 1972, "Shoaling of Cnoidal Waves," Proc. 13th Conf. on Coastal Engineering, ASCE, pp. 365-384.

47. Svendsen, I.A. and Hansen, J.B., 1976, "Deformation up to Breaking of Periodic Waves on a Beach," Proc. 15th Conf. on Coastal Engineering, ASCE, pp. 477-496.

48. Svendsen, I.A. and Hansen, J.B., 1976, "Wave Set-Down near Breaking," Prog. Rep. 41, Inst. of Hydrodynamics and Hydraulic Engineering, Technical Univ. of Denmark.

49. Svendsen, I.A., Madsen, P.A., and Hansen, J.B., 1978, "Wave Characteristics in the Surf Zone," Proc. 16th Conf. on Coastal Engineering, ASCE, pp. 520-539.

50. Thse Committee of the Hydraulics Division on Hydraulic Research, 1942, "Hydraulic Models," Manuals of Engineering Practice No. 25, ASCE.

51. Van Dorn, W.G., 1976, "Set-up and Run-up in Shoaling Breakers," Proc. 15th Conf. on Coastal Engineering, vol. 1, ASCE, pp. 738-751.

52. Van Dorn, W.G., 1978, "Breaking Invariants in Shoaling Waves," J. of Geophysical Res., vol. 83, No. C6, pp. 2981-2987.

53. Walker, J.R., 1974, "Wave Transformations over a Sloping Bottom and over a Three-Dimensional Shoal," Miscellaneous Rep. No. 11, J.K.K. Look Lab., Univ. of Hawaii.

54. Weggel, J.R., 1972, "Maximum Breaker Height for Design," Proc. 13th Conf. on Coastal Engineering, ASCE, pp. 419-431.